RESEARCH REPORT

VTT-R-04407-16

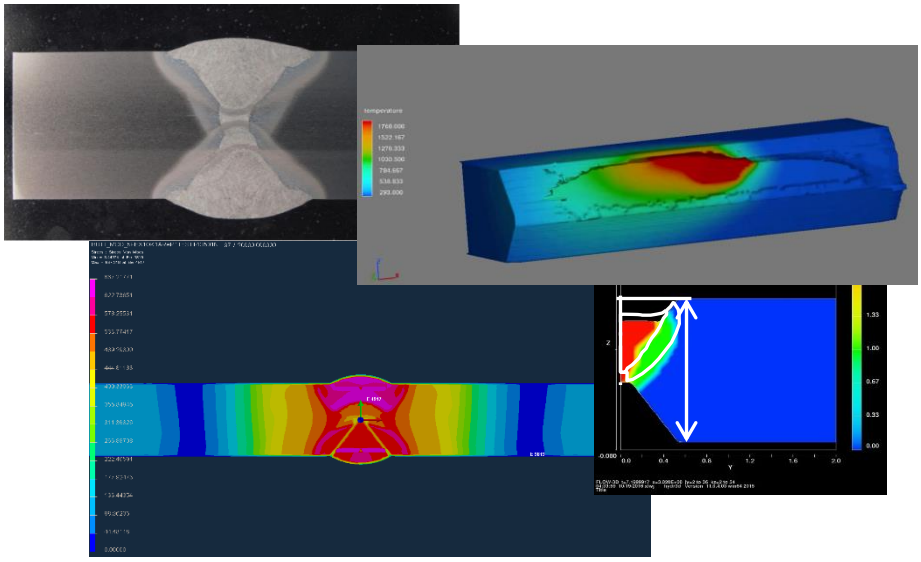

Digital materials engineering and modelling of mass and heat flow for optimisation of joining of materials (FIDIPRO NA)

Final Report

Authors: Mika Sirén, Timo Niemi, Suck-joo Na, Hannu Martikainen, Veli Kujanpää

Confidentiality: Public

Report's title Digital materials engineering and modelling of mass and heat flow for optimisation of joining of materials (FIDIPRO NA) - Final Report	
Customer, contact person, address Tekes, Sisko Sipilä, PL 69, 00101 Helsinki Companies (5 pcs)	**Order reference** Tekes funding decision 40300/13
Project name Digital materials engineering and modelling of mass and heat flow for optimisation of joining of materials	**Project number/Short name** 100976 / FIDIPRO NA
Author(s) Mika Sirén, Timo Niemi, Suck-joo Na, Hannu Martikainen, Veli Kujanpää	**Pages** 69/13 p. app.
Keywords welding, simulation, CFD, deformations, residual stresses	**Report identification code** VTT-R-04407-16

Summary

This report describes the research work carried out and technical results achieved in the Tekes FiDiPro project FIDIPRO NA in 2014 - 2016, executed in close co-operation with the top Korean technical university, Korea Advanced Institute of Science and Technology KAIST

The final goal of the project was to bring the Finnish welding simulation capabilities, expertise and tools to international level at all scales and phases of the welding processes: (i) molten weld pool behaviour prediction and control, (ii) weld metallurgical and microstructural optimisation during molten stage, solidification and cooling, and (iii) macroscopic behaviour of the welded product or component with respect to residual stress state and/or welding deformations.

The project research work focused on the true industrial simulation cases provided by the funding company partners of the consortium: **Posiva**´s FSW closure welding of the 50 mm wall thickness copper canisters for nuclear fuel waste repository, **Outotec Turula**´s stainless steel assemblies and components for metal ore processing and refinement and **Technip Offshore Finland**´s fatigue loaded offshore structural detail of the Spar hull first frame ring section. In addition to welding process simulation, an effort was put in the use of simulation results for FE deformation analysis source data.

Confidentiality	Public

Espoo 9.11.2017

Written by	**Reviewed by**	**Accepted by**
Mika Sirén, Senior Scientist	Veli Kujanpää, Principal Scientist	Tarja Laitinen, Vice President

VTT's contact address
VTT Ltd, POB 1000, FI-02044 VTT

Distribution (customer and VTT)
VTT: 1 original + pdf
Steering group members: pdf

Preface

This report describes the research work carried out and results achieved in the Tekes FiDiPro (Finland Distinguished Professor) programme project “Digital materials engineering and modelling of mass and heat flow for optimisation of joining of materials (FIDIPRO NA)” in 2014 - 2016. Accoring to the FiDiPro rules, the project included a minimum of 4 person-months per year researcher exchange from one of the top Korean technical university, the Korea Advanced Institute of Science and Technology KAIST. This was realised by inviting professor Suck-Joo Na of KAIST, Division of Mechanical Engineering, for a visiting professorship to VTT. Professor Na is one of the leading scientists in the field of process simulation of arc and laser beam welding, most notably of laser hybrid welding. Apart from prof. Na´s visits, the researcher exchange was further strengthened by VTT scintists´ visits to KAIST for a total of almost eleven months.

The project was supported by and executed in collaboration with five Finnish companies, Posiva Oy, Outotec Oy, Technip Offshore Finland Oy, Outokumpu Stainless Oy and SSAB Europe. The project work was supervised by the steering group including a representative from each company, Fimecc Oy (currently Dimecc Oy), VTT and Tekes, as well as two external academic experts:

Rauno Kakkola, Antti Nykänen	Outotec Turula Oy
Timo Salonen (chairman)	Posiva Oy
Marko Pennanen, Ari Ahto	Technip Offshore Finland Oy
Hannu-Pekka Heikkinen	Outokumpu Stainless Oy
Jukka Siltanen	SSAB Europe
Sisko Sipilä	TEKES
Prof. David Porter	University of Oulu
Prof. Reijo Karvinen	Tampere Unversity of Technology
Dr Kalle Kantola	Fimecc Ltd
Prof. Veli Kujanpää	VTT Ltd

The authors wish to acknowledge the contribution of all the steerong group members during the whole project.

Espoo 9.11.2017

Authors

Contents

1. Background and introduction of the project

The success of Finnish machinery industry companies is the prerequisite for the improvement of national employment rate and thus the well-being and growth of the whole society. Technology industries represent a major role in the Finnish exports. Mechanical engineering branch – metal goods, machinery and transport equipment – contribution is in the 20% range of the total Finnish exports. Hence, machinery industry plays a determining role for the prosperity of the Finnish economy and society. Fusion welding processes – including arc, beam and hybrid welding methods – are key enabling technologies in virtually all the exported machinery products. Therefore, welding technologies have an extremely strong indirect influence on the nation´s welfare.

Utilisation of weld simulation provides excellent means for shortening the development cycle and hence the time-to-market or profit of new products. The importance and benefits of efficient simulation are emphasised when applying emerging new and advanced material developments, e.g. (ultra) high strength steels: they typically require careful pre-planning of their joining processes, too. Furthermore, optimal material usage, i.e. right material in right location or component, inevitably introduces an increasing number of dissimilar material joints, including fusion welds between different grades or even types of steels or metals. Efficient use of latest material developments – in this case metals – in machinery products substantially increases the competitive edge of Finnish industry and plays a vital role in its survival in the globally competed markets.

During the past decade(s) the Finnish metal and especially steel industry has been profiling in high-end products instead of bulk production. In order to maximise the added value achievable with these high-quality products, their welding processes have to be optimised order to exploit their full potential in the service properties of the end products. Simulation is a powerful tool in designing the welding procedure for advanced steel structures. However, the challenges with weld pool modelling and simulation are being multiplied when introducing a combination of two different types of processes, as is the case in laser-arc hybrid welding for improved welding productivity.

Furthermore, the high energy density in beam welding processes, e.g. laser or electron beam welding, emphasizes the importance of governing the weld pool and keyhole phenomena on multiphase level: although liquid-gas and solid-gas interactions take place in arc welding, too, the high energy density in beam processes emphasizes the role of metal vapour in the weld pool behaviour. Obviously, the complexity is further increased when combining these two processes in one weld pool, as is the case in hybrid welding. Compared to welding simulation utilising the thermal analysis by conduction only, welding processes can be effectively optimized by introducing the computational fluid dynamics (CFD) in weld pool behaviour, where the recognition of interaction between heat source and workpiece is an essential prerequisite for precise simulations. Apart from the simulation of molten weld pool, the welding deformations and distortion, originating from the thermal effects and phase changes during the solid-phase cooling stage, play an important role in the design of large and medium-sized machine parts. Furthermore, such deformations – or their avoidance – have a marked effect on welding productivity through the possible need for excessive fixturing and clamping during welding, or even post-welding rectifying procedures.

Currently, the thermal-elasto-plastic behaviour of weld cannot be properly implemented in the elastic design process of welded structures, since the thermal-elasto-plastic analysis of a complete structure typically requires too complicated a preparation and too long a computation time due to the need of fine meshes in the whole structure. Instead, an effective way to handle this thermal-elasto-plastic behaviour of weld and elastic behaviour of ambient structure is to separate the weld from the structure, since the former is only a small fraction of the latter, so that the thermal-elasto-plastic behaviour of the weld can be simulated precisely with very fine meshes.

The weld thermal-elasto-plastic behaviour is influenced not only by the size of weld bead and heat affected zone, but also by the temperature distribution, thermal history at every weld point, and phase transformation characteristics of the weldment. Compared to the thermal analysis by conduction only, the simulation results of CFD analysis will give much more reasonable results of temperature distribution and thermal history of the weld, and hence will result in a more accurate estimation of thermal-elasto-plastic behaviour. The deformation of welded structures can in turn be estimated and controlled accurately once the result of proper thermal-elasto-plastic analysis of welds with CFD simu lations is calculated and applied. Consequently, the welded structures can be effectively designed through the elastic analysis of complete structures by adopting the inherent strains in welds obtained after CFD simulations of welding processes and thermal-elasto-plastic analysis of the weldment.

2. Welding simulation State-of-the-Art and project goals

The arc plasma simulations normally describe the process to form arc plasma from welding parameters such as current, voltage, arc length, shielding gas, and tip angle. These simulations can provide the distributions of temperature, velocity, and pressure in the arc plasma. Many studies have adopted the Finite Differential Method (FDM) to analyse the arc.

Arc heat flux, current density and arc pressure should be described properly to simulate the arc welding processes accurately. There are several arc heat flux models proposed and applied for simulations of heat and mass transfer in arc welding. The arc heat flux distribution could also be measured by using a special type of calorimeter or thermocouples. The same arc characteristic of heat flux distribution can be adopted for arc pressure and current density. The irradiance distribution of welding arc next above the anode workpiece is obtained by applying Abel inversion algorithm to the CCD arc image, and then used to determine the distribution of arc heat flux, arc pressure and current density from the physical relations of arc irradiance, temperature and current density in gas tungsten arc welding.

The basic theory of heat flow developed by Fourier and applied to moving heat sources by Rosenthal (1946) is still the most popular analytical method for calculating the thermal history of welds. However, Rosenthal's analysis which assumes a point, line, or plane source of heat, is subject to serious error for temperatures in or near the fusion zone and HAZ. To overcome such limitations, several authors have used Finite Element Method (FEM) to analyse the heat flow in welds. To simulate the FEM model of heat transfer in welding processes, an appropriate heat source model is crucial because it decides the size of both the molten zone and HAZ. Goldak et al. (1984) proposed a new mathematical model for weld heat sources based on a Gaussian distribution of power density. After this model was released, many studies have used the model to predict the fusion zone, HAZ, welding residual stresses, and distortions from various welding processes.

While FEM considers only the heat conduction transfer, FDM can describe the convective molten pool flows in the welding process. Considering the significant effects of weld pool convection on the microstructure and properties of the resultant weld, numerous investigators have attempted to calculate the heat transfer and fluid flow in the weld pool. The transporting phenomena from the welding arc to the molten pool have been taken from the simulation results of the corresponding welding arc, and the driving forces responsible for the weld pool convection were considered in FDM simulation.

To estimate the laser keyhole shape, Kaplan (1994) used an energy balance equation with a simple multiple reflection model. Multiple reflections were considered in a conical shape with an average angle of the keyhole wall; thus, only rough predictions could be made of the keyhole shape. In addition, a laser model based on the optical geometry of a laser system and the theoretical laser- and material-dependent value which affects the reflectivity in the simplified Fresnel's reflection model was recently used by Cho et al. (2010) for simulations of the laser-arc hybrid welding process and laser welding process.

2.1 Project scientific goals

The scientific and the technical goals for the project were set as:

- To develop weld simulation skills, collect source data, validate the simulation procedure and demonstrate the simulation of chosen industrial structures and details welded using advanced high-productivity welding techniques, including laser and hybrid welding
- To develop modelling and simulation techniques for optimisation of weld geometrical and metallurgical quality according to the demands of practical issues in both arc and beam-based welding processes
- To develop modelling and simulation techniques of welding procedure and solidification process to define the dependence between metallurgical phenomena and associated material parameters.

2.2 Expected project results

The expected research results, their significance and practical applicability were defined as:

- Feasible simulation toolbox for novel welding process and procedure development. Efficient and reliable design of welded structures using tailored computational fluid dynamics (CFD) tool applications and methodologies. Utilisation of simulation for process development for improved efficiency and productivity. Model for mechanical property distribution of welds in e.g. high strength steels.
- Multi-phase CFD modelling tools and procedures/methodologies for utilisation in the study and consequent development of welding processes, including beam based and hybrid processes. At VTT models for selected sub-processes will be developed in collaboration with KAIST. Moreover, through the application of the welding model entity based on the FLOW3D program a good expertise for the utilization of CFD in practical application studies will be achieved. It should be noted, however, that although the software tools as such will be completed and tested during the project, the full industrial implementation will have to be carried out after the shortened project time frame
- Most potential novel materials and/or structures for the industrial applications can be tested for improving and shortening the procedures of their welding procedure specification process.
- Intermediate results will be transferred to industry already during the project for utilisation in specific production sub-processes in the participating industrial partner companies. Feedback from such application experiments and tests will be returned to the project research partners for further simulation toolbox development and optimisation

- Strong linking and connections between welding CFD simulation results – weld pool behaviour and phenomena – and welding residual stress and welding deformation/distortion prediction will be established, i.e. link from CFD to FEM packages (FLOW3D and related subroutines to e.g. Ansys and/or Abaqus)

- Mastering the simulation, prediction and control of weld pool behaviour in thick section position welding using arc and/or beam techniques, as well as predicting and tailoring the dilution behaviour in novel stainless steel grade or ultra-high strength structural steel (UHSS) welding, either in dissimilar joints or when using dissimilar welding filler metal in homogenous joints

The final goal at the end of the project was to bring the Finnish welding simulation capabilities, expertise and tools to international level at all scales and phases of the welding processes: (i) molten weld pool behaviour prediction and control, (ii) weld metallurgical and microstructural optimisation during molten stage, solidification and cooling, and (iii) macroscopic behaviour of the welded product or component with respect to residual stress state and/or welding deformations. The scientific aspects of welding simulation were fostered and developed further at VTT together with top national and international RTD partners. The practical production environment expertise and industrial implementation were led by the industrial partner companies, supported by VTT. However, due to the requested project schedule and respective budget cuts, it was foreseen that this industrial implementation phase cannot be completed within the project frame, but will have to be continued after the project utilising other external funding, if appropriate.

Since the project kick-off some adjustments had to be made in the project contents and hence goals. The most important ones of these originated from Posiva´s strategic decision to select Friction Stir Welding (FSW) as the welding process for the nuclear repository canister closure instead of Electron Beam Welding (EBW), and from the changes in the project personnel in both VTT and companies.

2.3 References

Cho, W. I., Na, S. J., Cho, M. H., Lee, J. S., 2010. Numerical study of alloying element distribution in CO2 laser-GMA hybrid welding. Comput. Mater. Sci., 49, 792-800

Goldak J., Chakravarti A., Bibby, M. A New Finite element model for welding heat source, Metall. Mater. Trans. B. 15 (1984) 299-305.

Kaplan, A., 1994. A model of deep penetration laser welding based on calculation of the keyhole profile. J. Phys. D-Appl. Phys., 27, 1805-1814

Rosenthal, D. The theory of moving sources of heat and its application to metal treatments, Trans. ASME, 68 (1946) 849-865.

3. Background and KAIST experience in welding simulation

3.1 Background for weld modelling and simulation

The arc plasma simulations normally describe the process to form arc plasma from welding parameters such as current, voltage, arc length, shielding gas, and tip angle. These simulations can provide the distributions of temperature, velocity, and pressure in the arc plasma. Many studies have adopted the finite differential method (FDM) to analyze the arc by Lee & Na (1995), McKelliget & Szekely (1986), Ushio & Matsuda (1988) and Lee et al. (2002).

Arc heat flux, current density and arc pressure should be described properly to simulate the arc welding processes accurately. There are several arc heat flux models proposed and applied for simulations of heat and mass transfer in arc welding, such as Gaussian surface flux distribution, hemispherical power density distribution and double ellipsoidal power density distribution. The arc heat flux distribution could also be measured by using a special type of calorimeter or thermocouples. The same arc characteristic of heat flux distribution can be adopted for arc pressure and current density. The irradiance distribution of welding arc next above the anode workpiece is obtained by applying Abel inversion algorithm to the CCD arc image, and then used to determine the distribution of arc heat flux, arc pressure and current density from the physical relations of arc irradiance, temperature and current density in gas tungsten arc welding, Cho et al. (2013).

The basic theory of heat flow developed by Fourier and applied to moving heat sources by Rosenthal (1946) is still the most popular analytical method for calculating the thermal history of welds. As many researchers have shown, Rosenthal's analysis which assumes a point, line, or plane source of heat, is subject to serious error for temperatures in or near the fusion and HAZ. In regions of the workpiece where the temperature is less than about 20 percent of the melting point, Rosenthal's solution can give quite accurate results. However, the infinite temperature at the heat source assumed in this model and the temperature sensitivity of the material thermal properties – a temperature independent mean value is assumed – increases the error in the area close to the heat source.

To overcome most of these limitations, several authors have used FEM to analyze the heat flow in welds. To simulate the FEM model of heat transfer in welding processes, a heat source model is crucial because it decides the size of both the molten zone and HAZ. Pavelic et al. (1969) first suggested that the heat source should be distributed. He proposed a Gaussian distribution of flux (W/m) deposited on the surface of the workpiece. While Pavelic's model is certainly a significant step forward, some authors like Paley & Hibbert (1975) have suggested that the heat should be distributed throughout the molten zone to reflect the digging action of the arc more accurately.

Goldak et al. (1984) suggested a new mathematical model for weld heat sources based on a Gaussian distribution of power density. He modified an axisymmetry Gaussian distribution heat source model to a double ellipsoidal volumetric Gaussian heat source model which can predict a more realistic fusion zone and HAZ by adjusting the heat source parameters. After Goldak's model was released, many studies by, e.g. Lee & Na (1991), Geru et al. (2005) and Kong et al. (2011), have used the model to predict the fusion zone, HAZ, welding residual stresses, and distortions from various welding processes.

While FEM considers only the heat conduction transfer, FDM can describe the convective molten pool flows in the welding process. Considering the significant effects of weld pool convection on the microstructure and properties of the resultant weld, numerous investigators, e.g. Fan et al. (2001), Kim & Na (1994) and Kumar & Debroy (2007), have attempted to calculate the heat transfer and fluid flow in the weld pool. Most of these investigators have used either the rigid-lid assumption like Lei & Shi (1994) or the stepwise approximation for the weld pool surface by Choo et al. (1990). The transporting phenomena from the welding arc to the molten pool, such as the heat flux, current density, and shear stress acting on the surface of molten pool, were taken from the simulation results of the corresponding welding arc. The driving forces responsible to the weld pool convection, i.e., the self-induced electromagnetic force, surface tension due to the temperature gradient at the surface of molten pool, the effect of surface depression due to the arc pressure and drag force by the arc plasma flow, were considered in FDM simulation.

To estimate the laser keyhole shape, Kaplan (1994) used an energy balance equation with a simple multiple reflection model. Multiple reflections were considered in a conical shape with an average angle of the keyhole wall; thus, only rough predictions could be made of the keyhole shape. Since then various numerical techniques have been used to track the free surface

so that the precise keyhole shape can be calculated. Ki et al. (2001) used a level-set method by Osher & Sethian (1988) to calculate the free surface of the keyhole for the purpose of realizing the multiple reflections inside the calculated keyhole shape. Lee et al. (2002) used a volume-of-fluid (VOF) method by Hirt & Nichols (1981) to understand the mechanism of keyhole instability. Cho and Na (2006) also used the VOF method in conjunction with a ray-tracing algorithm to calculate the keyhole shape and realize the real-time multiple reflections. The same algorithm was used by Cho & Na (2007) to estimate the results of the drilling process vis-à-vis the polarization of the laser beam as well as the results of laser-arc hybrid welding, Cho & Na (2009). In addition, a laser model based on the optical geometry of a laser system and the theoretical laser- and material-dependent value which affects the reflectivity in the simplified Fresnel's reflection model was recently used in simulations of the laser-arc hybrid welding process by Cho et al. (2010) and laser welding process by Cho et al (2012).

3.2 KAIST simulation activities and experience

Prof. Suck-Joo Na at KAIST has been working on welding simulation from various aspects for more than 20 years and his group is at the very top on the subject globally. The research topics have covered all major welding processes, both arc - MAG, TIG, SAW and PAW - and beam ones - laser (LBW) and electron beam (EBW) - as well as combinations, such as laser-arc hybrid welding (LAHW). The simulation activities have included CFD based melt pool and flow behavior, FE based residual stress and distortion prediction and control, as well as metallurgical models for phase distribution prediction. Furthermore, KAIST has adopted a comprehensive simulation approach in combining some or all of these simulation fields in single individual cases. In the following, an outline of KAIST activities is drafted based on selected recent publications by the group. Further details can be found in the referred papers and prof. Na and his students´ other published works.

Prof. Na and his group at KAIST have conducted three-dimensional transient numerical simulations for MAG welding on true weld grooves in various welding positions. They adopted the Abel inversion method to form the resultant asymmetric arc models, such as arc heat flux, electromagnetic force and arc pressure. Due to the different position specific gravity effects, it became possible to obtain the different molten pool flow patterns, solidification times, temperature distributions and bead shapes along the welding positions by numerical simulations. The formation process of convex and concave weld bead can then be analyzed in detail for different welding positions. By comparing the fusion zone simulation results with the experimental ones, the various models used can be also be reliably validated as concluded in Cho & Na (2015).

The concept of three-dimensional numerical heat transfer and fluid flow model has also been developed to examine the temperature profiles, velocity fields, weld pool shape and size in a two-wire tandem submerged arc welding process by Cho et al. (2014). The developed model solves the equations of the conservation of mass, momentum, and energy alongwith the volume of fluid (VOF) method. The VOF method is used to track the shape of the free surface. Further, they proposed a novel scheme to handle the arc interaction between the two wires and its influence on the molten droplet transfer direction. The use of the computational fluid dynamics simulations revealed that the droplet movement and arc forces from the leading electrode affect strongly the molten pool flow patterns and the resultant bead shapes, even though the applied heat inputs remain the same. The calculated weld width and penetration could be validated fairly well by experimental results.

An example of KAIST metallurgical simulation research is presented by Cheon et al. (2015). A numerical approach is required for the investigation of the welding procedure with respect to phase fraction changes because of the difficulties related to experimental observation. The temporal combination of CFD mass and heat transfer and FEM conductive heat transfer thermal analysis can be used for temperature history simulation. In the case of mild steel welds the phase distribution can be predicted, compared to and validated with experimental results. The numerical phase fraction estimation can be carried out using critical austenite temperature

model in the heating process as a function of heating rate. The CCT information based transformation starting and finishing temperature model, as well as maximum fraction model are utilised with the instant cooling rate in the cooling process. The thermal analysis results show good agreement with measured temperature history. The hardness estimation based on the numerical phase fraction distribution result is slightly overestimated as compared to measured hardness.

From industrial production point of view, one of the most important and most immediately exploitable result from welding simulation is the prediction of welding residual stresses and deformations. Reliable deformation estimates are a key tool for weld sequence optimisation to further minimise these distortions and, consequently, the required corrective actions. Cheon et al. (2014) have developed a welding deformation predicting technique and and accumulated it with previous studies. As the most recent and general method, numerical estimation of welding deformations has been proposed in Finite Element Method (FEM) base with Conduction Heat Transfer (CHT) model. Instead of that, KAIST is employs a more practical temperature history approach from Computational Fluid Dynamics (CFD) based thermal and mass flow analysis. Additionally, an improved phase fraction estimation model and element activation and deactivation (EAD) technique are being used. These will help to estimate welding deformation more accurately. However, CFD temperature history result was different from CHT analysis and further, the resultant volumetric strains were also different by difference of temperature history in phase transformation effected model, and shrunk bead effect was realised by EAD technique. The outcome of this study needs yet to be validated with experimental results, accompanied by employment of more accurate thermal and mechanical properties in the analysis and simulation work.

The CFD simulations alone can be used to evaluate the molten pool behavior and the internal flow patterns in the melt. This can be further utilised in, e.g. the mixing and dilution behavior of varius elements during welding, which is of particular interest in, e.g. dissimilar metal welds of power generation applications. The study by Han et al. (2014) covers the numerical analysis of high power laser keyhole welding with varying laser power by using Volume-Of-Fluid (VOF) method to analyze fluid flow and flow patterns in the molten pool. The analyses of flow and flow patterns are performed with streamline formed by reconstructing the value of the velocity vector in simulation results. The general flow patterns can be estimated in all phases of welding, including keyhole formation period, partial penetration state and after full penetration keyhole with varying laser power. Effects such as leakage of laser through full penetration keyhole, recoil pressure, surface tension and keyhole collapse frequency, etc. can be observed and taken into account in simulations. Although laser beam welding is not a dominant production process in, e.g. Finnish manufacturing industries, a similar kind of approach can be used and utilized in arc or laser-arc hybrid welding, too. Obviously, particular attention will have to be paid on the inclusion of arc-related phenomena in the simulation models, e.g. electromagnetic forces, arc shape, pressure and other properties, etc., as well as the combined effects of and interactions between arc and laser beam in hybrid welding.

3.3 References

Lee, J. Y., Ko, S. H., Farson, D. F., Yoo, C. D., 2002. Mechanism of keyhole formation and sta-bility in stationary laser welding. J. Phys. D-Appl. Phys., 35, 1570-1576

Lee, S.Y., Na, S.J. Analysis of TIG welding arc using boundary-fitted coordinates, Proc. Inst. Mech. Eng., B J. Eng. Manuf. 209 (1995) 153-164.

Lei, Y.P., Shi, Y.W. Numerical treatment of the boundary conditions and source terms on a spot welding process with combining buoyancy-Marangoni-driven flow, Numer. Heat. Tr. B-Fund. 26 (1994) 455-471.

McKelliget, J., Szekely, J. Heat transfer and fluid flow in the welding arc, Metall. Mater. Trans. A. 17 (1986) 1139-1148.

Osher, S., Sethian, J. A., 1988. Fronts propagating with curvature-dependent speed: algorithms based on Hamilton-Jacobi formulations. J. Comput. Phys., 79, 12-49

Paley, Z., Hibbert, P.D. Computation of temperatures in actual weld designs, Weld. J. 54 (1975) 385s-392s.

Pavelic, V., Tanbakuchi, R., Uyehara, O.A., Myers, P.S. Experimental and computed temperature histories in gas tungsten-arc welding of thin plates, Weld. J. 48 (1969) 295s-305s.

Rosenthal, D. The theory of moving sources of heat and its application to metal treatments, Trans. ASME, 68 (1946) 849-865.

Ushio, M., Matsuda, F. A mathematical modeling of flow and temperature flow and temperature fields in gas-tungsten-arc, Journal of JWS. 6 (1988) 91-98.

4. Simulation methods used in the project

According to the original goals of the project, the simulation work was heavily concentrated on CFD based simulations for GMAW and FSW, in order to adopt both the simulation approach and the tools for work at VTT. Furthermore, FE based simulation was conducted for evaluation of GMAW butt weld deformations and residual stresses. It should be noted that the KAIST customisation for FLOW-3D was used as such for the reference case simulations. More detailed simulation information can be found in the appropriate simulation case descriptions, as well as in the project scientific publication in the attachments.

4.1 Governing equations and models for CFD simulation of GMAW

The framework for gas metal arc welding simulations has been implemented on top of the commercial CFD software FLOW-3D. FLOW-3D is a multipurpose CFD code based on the volume of fluid (VOF) simulation approach. The VOF method is a well known technique for free-surface modelling. In the VOF method it is assumed that there exists two or more immiscible fluids and between them a sharp interface is formed. In addition to solving the fundamental equations for the fluids, a separate procedure is used to track the location and evolution of the interface. The typical uses for the VOF method include cases such as prediction of jet breakup or solving the motion of large bubbles in a liquid. However, the approach itself is very flexible and it has been used in many different applications. In the case of GMAW, the modelled fluids are the welded material and the gas atmosphere that surrounds the welded piece.

Large part of the capability and physical models required for arc welding simulations are readily available in FLOW-3D, but several additional models related to the welding arc are needed. These additional models include the arc heat flux and pressure, electromagnetic and drag forces and volumetric sources that represent the addition of filler material. The FLOW-3D allows to compile custom versions of the solver which can have these kinds of user defined source terms and boundary conditions. The implementation language of FLOW-3D is Fortran. The models that are described here have been successfully implemented in FLOW-3D and they have been tested to work with FLOW-3D versions up to v11.

The fundamental equations of motion and heat transfer are solved by the FLOW-3D and the exact details of these equations and their implementation can be found in the FLOW-3D user manual. The equations presented here follow the notation given in Cho and Na (2015). For incompressible flow the mass conservation equation can be written as

$$\nabla \cdot \vec{V} = \frac{\dot{m}_s}{\rho} \quad (1)$$

where $\vec{V}$ is the velocity of the material and ρ is the density. Here $\dot{m}_s$ represents mass sources due to droplets created when the filler metal melts. In the simulation model, the location of the welding electrode is determined based on the given initial position and the welding speed. The actual electrode geometry is not included in the simulation, but the location of the electrode tip is used to calculate the sources created by the welding arc. The mass source $\dot{m}_s$ is only active when a filler material droplet is created at the location of the welding electrode tip and otherwise it is zero. In the current implementation the material droplets are created as spheres but other shapes would be also technically possible.

The momentum equation can be written as

$$\frac{\partial \vec{V}}{\partial t} + \vec{V} \cdot \nabla \vec{V} = -\frac{\nabla p}{\rho} + \frac{\mu}{\rho}\nabla^2 \vec{V} + \frac{\dot{m}_s}{\rho}\left(\vec{V}_s - \vec{V}\right) + f_b \quad (2)$$

where p is pressure, μ viscosity, $\vec{V}_s$ velocity of the created filler material droplets and f_b represents additional body forces. Similarly as the mass source, the velocity source is only active during the creation of the droplets. The initial velocity of the droplets is given as input and as it is a vector value, different welding angles can be taken into account.

The enthalpy equation can be written as

$$\frac{\partial \mathrm{h}}{\partial t} + \vec{V} \cdot \nabla h = \frac{1}{\rho}\nabla \cdot (k \nabla T) + \dot{h_s} \quad (3)$$

where k is the thermal conductivity and $\dot{h_s}$ enthalpy source due to droplets. To capture the full range from fully liquid to fully solid state, the enthalpy for the welded material is defined in the simulations as

$$h = \begin{cases} \rho_S C_s T_s & (T \le T_s) \\ h(T_s) + h_{sl}\dfrac{T - T_s}{T_l - T_s} & (T_s < T \le T_l) \\ h(T_l) + \rho_l C_l (T - T_l) & \end{cases} \quad (4)$$

where T_l and T_s are the liquidus and solidus temperatures, C_s and C_l are the specific heat capacities of liquid and solid material and h_{sl} is the enthalpy of fusion. The various parameters are specific to the material in question and are given as input.

Being a volume of fluid code, the FLOW-3D also needs to keep track of the volume fraction of the welded material. The equations for the volume fraction can be expressed as a transport equation

$$\frac{\partial F}{\partial t} + \nabla \cdot \left(\vec{V} F\right) = \dot{F_s} \quad (5)$$

where F is the volume fraction of the welded material and $\dot{F_s}$ is volume fraction source from the filler metal droplets. The algorithms used for the volume fraction and surface interface tracking are key components to any VOF code and the exact details of the FLOW-3D methods can be found in the user manual. However, one key feature of FLOW-3D is that the fundamental equations are only solved in those mesh cells where there is a positive volume fraction of the primary fluid, ie. in this case the welded material. The cells which contain only gas are treated as voids with uniform values for temperature and pressure, and no equations are solved there.

Similarly, for fully solidified regions the momentum equation is not solved. The interface between the gas and welded material is treated as a boundary condition in the solution of the equations.

Following the FLOW-3D approach, apart from the volumetric source terms due to droplets, the other effects caused by the welding arc are modelled through boundary conditions. Starting with the heat flux due to the arc, the boundary condition for energy at the top surface can be expressed as

$$k\frac{\partial T}{\partial n} = q_A - q_{conv} - q_{rad} - q_{evap} \tag{6}$$

where q_A is the heat source from the arc and the other terms are heat losses from convection, radiation and evaporation. For the convection, radiation and evaporation the standard models available in FLOW-3D can be used, but for the arc heat source a custom model is required. For accurate simulations it is important to have a good estimation for the shape of the arc. In the present implementation the heat source is expressed as

$$\mathrm{q_A(x,y)} = \eta_\mathrm{A}\frac{\mathrm{VI}}{2\pi\sigma_{x\_ave}\sigma_{y\_ave}}\exp\left(-\frac{\mathrm{x}^2}{2\sigma_{x_{1,2}}^2}-\frac{\mathrm{y}^2}{2\sigma_{y_{1,2}}^2}\right) \tag{7}$$

where η_A is the efficiency of the arc, V and I are the welding voltage and current and σ refer to the effective radiuses of the arc. The effective radii are defined as

$$\sigma_{\mathrm{x}_{1,2}} = \begin{cases}\sigma_{x_1}, & x < 0\\ \sigma_{x_2}, & x \geq 0\end{cases} \tag{8}$$

and

$$\sigma_{\mathrm{y}_{1,2}} = \begin{cases}\sigma_{y_1}, & y < 0\\ \sigma_{y_2}, & y \geq 0\end{cases} \tag{9}$$

where (x,y) are the coordinates relative to the center of the arc and the σ_{x_ave} and σ_{y_ave} are defined as

$$\sigma_{x\_ave} = \frac{(\sigma_{X1} + \sigma_{x2})}{2} \tag{10}$$

$$\sigma_{y\_ave} = \frac{(\sigma_{y1} + \sigma_{y2})}{2} \tag{11}$$

Ideally the effective radii should be determined from experiments as they are affected by the arc parameters and also by the welding geometry. However, if experimental data is not available, reasonable estimates can be used instead. Although the equation (7) allows to have 4 different effective radii, quite often either fully symmetrical or elliptical arc shapes are assumed.

It should be noted that part of the heat output of the arc is used to melt the filler material and thus the efficiency of the arc η_A in equation (7) is expressed as

$$\mathrm{n_A} = \eta - \eta_d \tag{12}$$

where η is the overall efficiency (eg. 0.8) and η_d represents the energy used to melt the filler material. The heat loss due to melting of filler material droplets of size r_d is calculated as

$$\mathrm{q_d} = \frac{4}{3}\pi r_d^3 \rho[C_s(T_s - T_0) + C_l(T_d - T_s) + h_{sl}]f_d \quad (13)$$

where T_d is the temperature of the droplet, T_0 the ambient temperature and f_d the frequency of the creation of the filler material droplets. In the simulation model a droplet is assumed to detach when the volume of exposed wire equals the volume of the droplet. Based on this assumption, the frequency of the droplets can be expressed as

$$\mathrm{f_d} = \frac{3r_w^2 \mathrm{WFR}}{4r_d^3} \quad (14)$$

where r_W is the radius of the wire and WFR is the feed rate of the filler wire. The radius of the created droplet is a user definable parameter and typically it is assumed to be similar to the wire radius, $r_d \approx r_w$.

From $\mathrm{q_d}$ the expression for droplet efficiency is obtained as

$$\mathrm{n_d} = \frac{q_d}{VI} \quad (15)$$

The overall efficiency η is required as user input. When specifying the efficiency it is important to notice that a significant part of the energy losses is already taken into account in the boundary conditions for the enthalpy equation. For this reason, the efficiency η that is used in the simulations should likely be higher than a typical rule of thumb value from literature. The values presented in literature are often given for total overall efficiency that assumes no other losses.

On the free surface the pressure is expressed as

$$p = p_A + \frac{\gamma}{R_c} \quad (16)$$

where p_A is arc pressure, γ surface tension and R_c the radius of the surface curvature. The surface tension is modelled using the built in model of FLOW-3D. For the arc pressure it is assumed that it has the same area of effect as the arc heat source model and thus

$$\mathrm{P_{arc}(x,y)} = \frac{\mu_0 I}{4\pi^2 \sigma_{x\_ave}\sigma_{y\_ave}} \exp\left(-\frac{\mathrm{x}^2}{2\sigma_{x1,2}^2} - \frac{\mathrm{y}^2}{2\sigma_{y_{1,2}}^2}\right) \quad (17)$$

where μ_0 is permeability of vacuum. To account for the electromagnetic force, in the present implementation the model of Kou and Sun (1985) is applied. In the model the axial and radial current densities of the arc are calculated as

$$J_z = \frac{1}{2\,\pi}\int_0^\infty \lambda J_0(\lambda r_a)\exp(-\lambda^2\sigma_r^2/12)\frac{\sinh[\lambda(c-z)]}{\sinh(\lambda c)}\mathrm{d}\lambda \quad (18)$$

and

$$J_r = \frac{1}{2\,\pi}\int_0^\infty \lambda J_1(\lambda r_a)\exp(-\lambda^2\sigma_r^2/12)\frac{\cosh[\lambda(c-z)]}{\cosh(\lambda c)}\mathrm{d}\lambda \quad (19)$$

and the angular component of the magnetic field as

$$B_\theta = \frac{\mu_m I}{2\,\pi}\int_0^\infty J_1(\lambda r_a)\exp(-\lambda^2\sigma_r^2/12)\frac{\sinh[\lambda(c-z)]}{\sinh(\lambda c)}\,\mathrm{d}\lambda \tag{20}$$

The terms J_0 and J_1 in the above expressions refer to the first kind of Bessel functions of zero and first order. When the current densities and magnetic fields have been solved, the electromagnetic force (EMF) affecting the flow can be expressed as

$$F = \vec{J} \times \vec{B} \tag{21}$$

which can be presented in the Cartesian coordinate system as

$$F_x = -J_z B_\theta \frac{x}{r_a} \tag{22}$$

$$F_y = -J_z B_\theta \frac{x}{r_a} \tag{23}$$

$$F_z = J_r B_\theta \tag{24}$$

In addition to EMF, the simulation model also takes in to account the shearing drag force caused by the impingement of the arc plasma jet flow to the material surface. The drag force model follows the expressions presented by Phares et al. (2000). Other physical models such as the gravity, buoyancy and surface tension are calculated using the built-in models of FLOW-3D.

4.2 Governing equations and models for CFD simulation of FSW

4.2.1 Overview of FSW process from the simulation point of view

Friction Stir Welding (FSW) is joining method where a rotating, non-consumable cylindrical tool is used to mechanically weld two workpieces together. A schematic of a typical FSW process is shown in Figure 1. In the process heat is generated both by friction and by plastic deformation of the workpiece, which softens the material in the region near the tool. The tool moves along the welding line and the rotating motion mechanically stirs the softened material of the two workpieces together. The process is solid-state and the material does not melt during the welding. FSW is especially suitable for joining materials that are difficult to weld by using conventional welding methods and for processes requiring high quality welds. The most common workpiece material for FSW is aluminium, but the process can be used for a wide range of materials. FSW can be also used for joining different types of materials together.

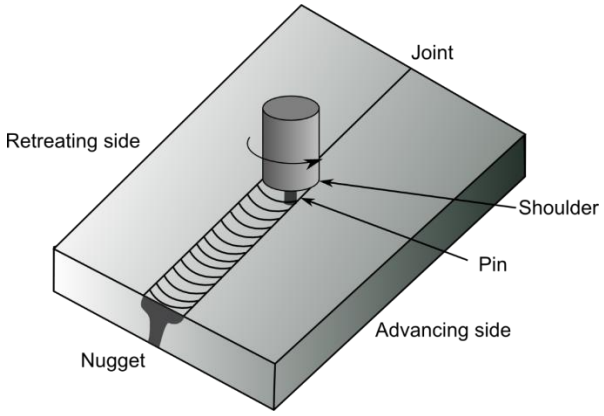

Figure 1 Schematic drawing of FSW process with the common terminology.

From the simulation point of view, the FSW process is quite a challenging topic. The process is dominated by highly non-linear and coupled physical phenomena, such as large plastic deformation, rapid material flow, mechanical stirring and surface interaction between the tool material and the work piece. In addition, as the material properties in the visco-plastic flow regime are typically highly dependent on the temperature, modelling thermal effects such as frictional heating and plastic dissipation are key requirements for successful FSW simulation.

He et al. (2014) gives a recent and comprehensive review of the different simulation approaches and aspects for the FSW process. According to He et al., a large variety of simulation methods have been applied to FSW simulation ranging from simplified semi-analytical heat source models to more comprehensive 3D finite difference, finite element and finite volume methods. When discussing the more comprehensive simulation methods, one difficulty that is pointed out is the large deformations in the FSW process. The modelling of deformations can pose difficulties to finite element or finite difference codes that are designed for rigid structures with small deformations from the reference configuration. For practical FSW simulation, the simulation method has to be able to handle arbitrary large deformations.

One way to deal with the large deformations is to use CFD-like approaches, where no fixed configuration is assumed, and large deformations and material flow are natural. One of the earliest authors in CFD modelling of FSW were Colegrove and Shercliff (2005), who presented a fully 3D CFD simulation framework for simulating a raked tool. The model took into account strain rate dependent flow stress and heat transfer modelling in addition to tool tilt angle. Shercliff and Colegrove were able to produce qualitatively reasonable results, although quantitatively there were problems such as the predicted heat generation was too high, deformation zone was too large and the welding forces were not accurately predicted. However, guidelines for improving the simulation models were given and subsequent authors, such as Pal and Phaniraj 2015, Chen et. al 2013 and Atharifar et al. 2009 have reported also quantitatively valid results. Based on these reports, CFD seems to be a reasonable approach for FSW simulation.

Typically in the literature the CFD simulation has been done for aluminum FSW. To investigate more thoroughly the CFD approach and to evaluate its applicability to FSW simulations of copper, implementation and testing of the proposed CFD models was conducted. The models presented by Colegrove and Shercliff and several other authors were implemented as a user defined functionality to a commercial CFD code Ansys Fluent. However, instead of Ansys Fluent, in this project the implementation was done to open source CFD code OpenFOAM.

4.2.2 CFD simulation models for FSW

The simulation approach presented by Colegrove and Shercliff (2005) uses an Eulerian approach, where the tool is stationary and the linear motion is emulated by using an inlet velocity

boundary condition for the workpiece material, as shown in Figure 2. The approach used steady state modelling and the rotation of the raked tool was taken into account by using Multiple Reference Frame (MRF) technique. In MRF the mesh is stationary and the rotation is modelled by using a rotating reference frame in the vicinity of the tool, which gives a steady-state approximation of the rotating motion with the tool locked in one orientation. In principle the same modelling structure can be also applied to fully transient analysis by using a sliding mesh approach, where the mesh rotates along the tool. However, in that case the computational requirements would be much higher due to transient time stepping and there may be numerical issues due to the sliding mesh interface.

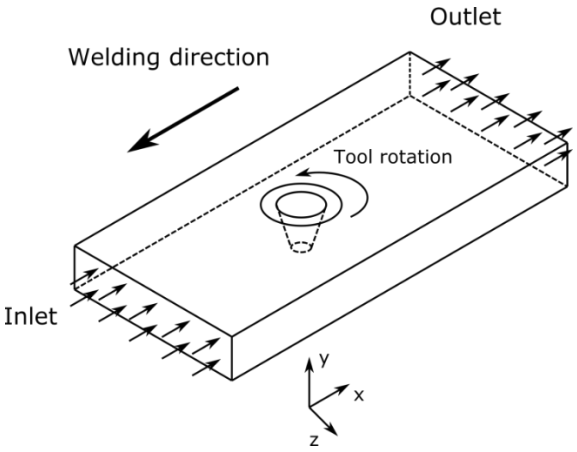

Figure 2 Example of a typical simulation setup for FSW process.

Following the notation of Pal and Phaniraj (2015), assuming incompressible flow, the steady state continuity equation can be written as

$$\frac{\partial \rho u_i}{\partial x_i} = 0 \tag{25}$$

where u is the velocity and ρ the density of the (base) material. The steady state momentum balance equation is

$$\frac{\partial \rho u_i u_j}{\partial x_i} = -\frac{\partial p}{\partial x_i} + \frac{\partial}{\partial x_i}\mu\left(\frac{\partial u_j}{\partial x_i} + \frac{\partial u_i}{\partial x_j}\right) \tag{26}$$

where p is the pressure and μ is the viscosity. As the material flow in FSW is highly non-Newtonian, the treatment of viscosity is a key part of the simulation approach. Following the approach presented by Colegrove and Shercliff (2005), the viscosity can be expressed as

$$\mu = \frac{\sigma_e}{3\bar{\dot{\epsilon}}} \tag{27}$$

where σ_e is the effective stress and $\bar{\dot{\epsilon}}$ is the effective strain-rate of the material. The effective strain-rate is given by

$$\bar{\dot{\epsilon}} = \sqrt{\frac{2}{3}\dot{\epsilon}_{ij}\dot{\epsilon}_{ij}} \tag{28}$$

where $\dot{\epsilon}_{ij}$ is the strain-rate tensor

$$\dot{\epsilon}_{ij} = \frac{1}{2}\left(\frac{\partial u_i}{\partial x_j} + \frac{\partial u_j}{\partial x_i}\right) \quad (29)$$

In order to use the expression (27) for viscosity, a constitutive law, also known as flow stress model, is required. The flow stress model forms the connection between the strain rate and stress of the material. There are several well know flow stress models available for visco-plastic flows, but a common approach that is used for CFD FSW modelling is the so called Sellars and Tegart constitutive law. A typical form for this model can be expressed as

$$Z = \bar{\dot{\epsilon}} \exp\left(\frac{Q}{RT}\right) = A(\sinh \alpha\sigma_e)^n \quad (30)$$

where Q is the activation energy, R is universal gas constant, T temperature, A, α and n are material constants and the parameter Z is known as Zener-Hollomon parameter. If the material parameters are known for the given workpiece material, the effective stress can then be solved from equation (30) giving

$$\sigma_e = \frac{1}{\alpha}\sinh^{-1}\left(\left[\frac{Z}{A}\right]^{1/n}\right) \quad (31)$$

For many materials, the Zener-Hollomon parameter has a strong dependency on temperature and as such, in addition to equations for the material motion, equations for heat transfer are also needed. The thermal energy equation can be expressed as

$$\frac{\partial \rho C_p u_i T}{\partial x_i} = \frac{\partial}{\partial x_i}\left(k\frac{\partial T}{\partial x_i}\right) + \dot{q} + Q \quad (32)$$

where C_p is the specific heat capacity, T is the temperature, k is the thermal conductivity, $\dot{q}$ is the heat source due to the friction at the tool/workpiece interface and Q represents heat source terms due to plastic deformation of the base material. A suitable boundary condition for the free surfaces can be expressed as

$$-k\frac{\partial T}{\partial z} = \sigma_{SB}\epsilon(T_s^4 - T_a^4) + h_t(T_s - T_a) \quad (33)$$

where k is the thermal conductivity of the material, σ_{SB} the Stephan-Boltzmann constant, ϵ emissivity, T_s and T_a the surface and ambient temperatures and h_t the heat transfer coefficient.

In principle the modelling structure is quite straightforward up to this point provided that there is valid experimental data available for the parameters in the flow-stress model. However, there are still several difficulties which have to be overcome. Perhaps the most important question is the treatment of the velocity boundary condition between the tool and the workpiece. A common choice in CFD is to assume no slip boundary condition for wall-like boundaries, but as demonstrated by Colergrove and Shercliff (2005), this leads to excessive deformation and heat generation. To alleviate this, a slip condition can be assumed, but this brings the difficulty of determining what the correct amount of slip is. Most of the works in literature use simple approximations, where the slip is treated as a modeling parameter and adjusted so that reasonable results are obtained.

In addition to the slip boundary condition, the models for heat generation due to friction and plastic deformation have to be provided. Unfortunately, there is no clear consensus on the relative importance of these mechanisms in the literature and varying assumptions have been proposed. For instance, Colegrove and Shercliff (2005) assumed only plastic heat generation indicating negligible contribution from frictional heating. On the other hand, Nandand et al. (2007) refer to experimental measurements, where it was shown that only 4.4 % of the total heat generation for the FSW of aluminum alloy was due to viscous dissipation. A straightforward approach is to include both forms of heating to the model and provide adjustable parameters. In the work by Pal and Phaniraj (2015), the frictional heat source at the interface is modeled as

$$\dot{q} = v_{slip} m \tau \tag{34}$$

where v_{slip} is the slip velocity, τ the shear stress and m a friction factor. The heat generation by plastic deformation is taken to be proportional to flow stress and strain rate

$$Q = n\sigma\bar{\dot{\epsilon}} \tag{35}$$

The values of n and m are fitting parameters that have to be tuned.

One further difficulty is related to the flow-stress model and the solution procedure as a whole. Because the viscosity depends on the strain-rate, which in turn depends on the viscosity and both are strongly coupled to temperature, the convergence of the solution can be difficult. Also from the numerical point of view the expression (27) for viscosity is somewhat challenging as the value of viscosity can vary a great deal within the simulation domain and when the strain rate tends to zero, the viscosity tends to infinity. In practice some numerical maximum and minimum limits are therefore required to stabilize the computations.

4.2.3 Implementation in OpenFOAM

The modelling framework presented by Colegrove and Shercliff (2005) was implemented in commercial CFD solver Ansys Fluent. Similar approach was also followed by other authors, such as Pal and Phaniraj 2015, Chen et. al 2013 and Atharifar et al. 2009. However, whenever a new modelling approach is implemented or investigated, it is a large benefit that the full source of the solver is available, because it is then easier to diagnose what is happening in the code. With closed source software it can be sometimes difficult to know if a certain result is due to the implemented model or due to something happening within the black box. For these reasons, in this project it was decided to test the implementation of FSW modelling framework using an open source code.

In recent years, an open-source CFD-library called OpenFOAM has been gaining popularity. The code originated in Imperial College London during the late 1980's and was published as open-source in 2004. At the present the management and distribution of the OpenFOAM source code is handled by a not-for-profit organization OpenFOAM Foundation Ltd. Active developers of the code include CFD Direct, which is a company led by the original authors of the code, and OpenCFD Ltd, a company owned by the ESI Group. In addition to these companies, there are several other contributors from different organizations and individuals and there also exists active forks of the codebase. Compared to other open source CFD codes, the benefits of OpenFOAM are a large and active user base, involvement of several companies, modern approach to mesh handling with unstructured meshes and an extensible, object oriented code structure.

OpenFOAM is organized as a general-purpose C++ toolbox for numerical solvers mainly intended for CFD use. It comes pre built with several different types of CFD solvers, which can

be either used as-is or tailored to suit the specific needs of the application in question. In case of FSW modelling, a suitable solver that is included in the OpenFOAM distribution is chtMultiRegionFoam. The chtMultiRegionFoam is a general purpose solver for fluid flow, but it also supports conjugate heat transfer between solid and fluid regions. This allows solving heat transfer between the tool and the workpiece and heat conduction within the tool. In addition, chtMultiRegionFoam supports the MRF approach.

A viscosity model following the Sellars and Tegart constitutive law was successfully implemented to OpenFOAM version 3.0.x. and a custom version of chtMultiRegionFoam was created which supports the frictional and plastic heat source models presented in equations (34) and (35). In addition, the thermal boundary condition with radiative heat loss was implemented and the solver was used to simulate several test cases.

4.3 Finite element analysis overview

Numerical and analytical methods can be used for optimization of welding process parameters. The aim of the studies in this project was to evaluate the possibilities to use numerical methods for welding process optimization. The simulations were carried out by the Sysweld-program which is based on Finite Element Method (FEM). Sysweld has several different modules. In the current study, programs of Visual Environment (pre- and post-processing programs) and Sysweld solver were used (single CPU-version). Material data was defined on the basis of Sysweld material database that includes some of the most common materials. The thermo-mechanical simulations were carried out as uncoupled: thermal simulation is followed by mechanical one - no backward coupling.

Finite element analyses (FEA) were carried out for double side butt-welded GMAW experiments simulated using Sysweld solver. The problem was described by means of a 2D-model and two-dimensional generalized plane strain elements were used.

Heat input was described by Goldak's Double ellipsoidal heat source. Thermal boundary conditions used are as follows: emissivity 0.7, free air cooling: convective losses 8 $W/m^2 K$ for all boundaries, ambient temperature 22 °C and initial temperature of the plate 22 °C.

4.4 References

Atharifar, H., Lin, D. and Kovacevic, R. 2009. Numerical and Experimental Investigations on the Loads Carried by the Tool During Friction Stir Welding, Journal of Materials Engineering and Performance, vol. 18, no 4., pp. 339-350

Chen, G.-Q., Shi, Q.-Y., Li, Y.-J., Sun, Y.-J., Dai, Q.-L., Jia, J.-Y., Zhu, Y.-C. and Wu, J.-J. 2013. Computational fluid dynamics studies on heat generation during friction stir welding of aluminum alloy, Computational Materials Science, vol. 79, pp. 540–546

Cho, D-W., Na, S. J. 2015. Molten pool behaviors for second pass V-groove GMAW, International Journal of Heat and Mass Transfer, vol. 88, pp. 945-956.

Colegrove, P. A. and Shercliff, H. R. 2005. 3-Dimensional CFD modelling of flow round a threaded friction stir welding tool profile, Journal of Materials Processing Technology, vol. 169, iss. 2, pp. 320–327

Garcia Fernández, V.G. 2004. Constitutive relations to model hot flow of commercial purity copper, PhD thesis, Barcelona Technical Univ.

He, X., Gu F. and Ball, A. 2014. A review of numerical analysis of friction stir welding, Progress in Materials Science, vol. 65, pp. 1–66

Kou, S., Sun, D.K. 1985. Fluid flow and weld penetration in stationary arc welds, Metallurgical Transactions A 16 (1), pp. 203–213.

Nandan, R., Roy, G.G. Lienert T.J. and Debroy, T. 2007. Three-dimensional heat and material flow during friction stir welding of mild steel. Acta Materialia 55, pp. 883–895

OpenCFD Ltd, https://openfoam.com/

OpenFOAM Foundation Ltd, https://openfoam.org/.

Pal, S. and Phaniraj, M. P. 2015. Determination of heat partition between tool and workpiece during FSW of SS304 using 3D CFD modeling, Journal of Materials Processing Technology, vol. 222, pp. 280–286

Phares, D. J., Smedley, G. T. and Flagan R. C. 2000. The wall shear stress produced by the normal impingement of a jet on a flat surface. J. Fluid Mech., 2000, 418, 351-375

5. Project simulation cases

According to the original project proposal, the adoption of the welding simulation software at VTT was carried out through industrially relevant case studies from the participating companies. Each of the funding partners selected a suitable example together with VTT experts that was further refined for simulation purposes, i.e. simplified, scaled down and/or reduced to a suitable mock-up. Additionally, a well documented scientific reference case was selected to be able to commence with the simulation excercises soonest possible, well before the experimental validation cases were available within the project.

5.1 Company specific cases

Posiva is interested in the simulation of the closure welding of the copper canisters (~ ø 1 m × 4 – 5 m, t = 50 mm) for nuclear fuel waste repository. During the first project year they made the choice between two candidate welding methods, namely friction stir and electron beam welding (FSW and EBW) that guided Posiva´s interests and goals in the project. With FSW, the key issues are the heat transfer during and residual stresses after welding. Posiva had been and will be working in close collaboration with the Swedish counterpart Svensk Kärnbränslehantering SKB in the FSW research.

Posiva had already started carrying out comprehensive residual stress analysis for the FSW solution. Residual stress modelling is important to avoid the stress corrosion cracking risk during the 100 000 years´ repository time. In this project the emphasis was on the modelling of the welding process.

Outotec Turula fabricates mainly stainless assemblies and components for metal ore processing and refinement. Apart from stainless grades, also some structural steel and titanium is welded, too. Outotec´s company case dealed with FCAW of fatigue critical welds in duplex stainless steels. The main driving force is increasing robot welding application rate in production for improved productivity. The material selection covered all basic duplex grades from lean to super duplex steels (LDX 2101, 2205 and 2507). These fatigue critical structures are typically manufactured using multipass fillet welding. Since weld geometry is critical for fatigue life, simulation was to be targeted at the last (top) bead and its surface topology.

Technip Offshore Finland´s key interest was fatigue in offshore structures operating in harsh ocean environments. In the future, the service conditions will become even more demanding as the importance of the Arctic increases. The planned platform service life is about 30 years and site repairs are expensive, so the structural reliability is vital.

From productivity and cost competitiveness point of view, the welding distortion management plays a key role. Typical structures are SAW or FCAW welded heavy (t = 30 – 200 mm) structural steel assemblies. Technip´s case study covers the initial steps of a Spar hull ring section production. The main object of the simulation work is a structural detail of the first frame ring, but it was expected that the previous stages would have to be modelled on some accuracy level, too, in order to determine the initial conditions for frame ring welding.

5.2 Reference simulation case

For the validation of the very first simulation excercises using the Flow 3D software together with the KAIST customisations, a simple yet well documented and characterized experimental case was searched for in the literature. A suitable case was found in the doctoral thesis of Dr Olaf Voß (2001) prepared in the Technische Universität Braunschweig.

In the experimental part of the thesis, well controlled and monitored bead-on-plate welding experiments were carried out to produce validation data for the welding simulations. The experiments comprised of laser and TIG welding on several materials, e.g. S355 structural steel and austenitic and ferritic stainless steels in 1 to 15 mm thickness. The welding was monitored with respect to temperature evolution on both top and root side, as well as displacement changes during welding in both XY direction at the plate edges, and Z direction at the plate surface. In order to have clearly defined boundary conditions with repect to the workpiece to substrate contact, the plates were supported by three points contacts only. The overall welding arrangements are described in detail in the thesis, as weld as characterization as macrographs and hardness testing results, too. A sketch of the experimental arrangement of the thesis is presented in Figure 33.

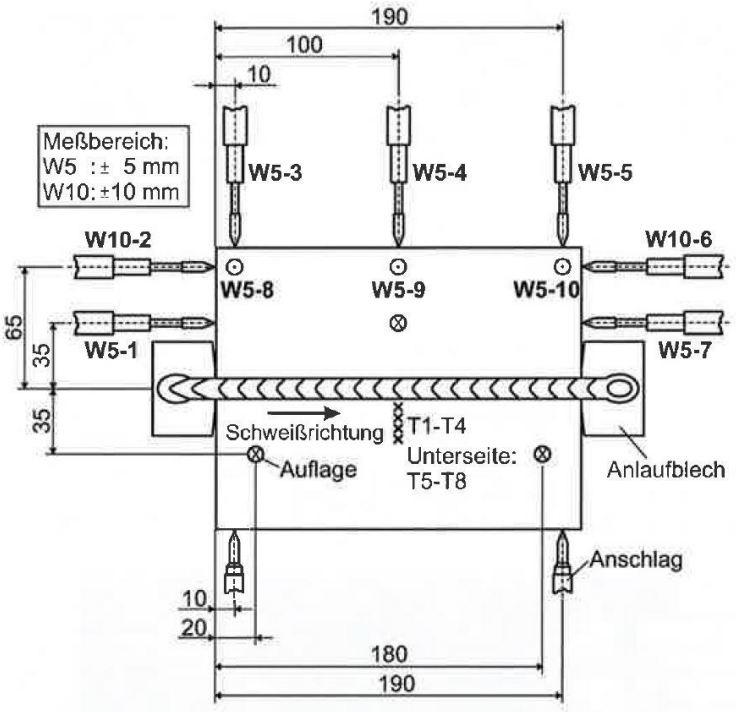

Figure 3 A sketch of the experimental welding arrangements of Voß (2001)

Based on the reference experiments of the thesis, the experimental validation programme was designed for the project, too. However, it should be noted that the experimental matrix was expanded to cover true welds in addition to bead-on-plate ones, too, section B of *Table* 1. These were intended to serve the simulation of the industrial cases, particularly the 15 mm MAG welds were aimed at serving the Technip company case.

Originally, the structural steel S355 as an in-kind contribution of SSAB Europe was selected for the base material in 5 and 15 mm thickness and laser, laser-arc hybrid, TIG and MAG welding were used as welding processes. Also SSAB S500 grade was planned for a reference to S355, mainly because of the availability of the comprehensive material properties, but due to the production scheme, no material was available for experiments in due time for the project validation schedule. The experimental validation matrix is presented in *Table* 1 below. It should be noted that not all the experimental results were produced for the project, particularly the 5 mm thickness was found not relevant from industrial needs viewpoint, and the 15 mm laser-arc hybrid welds could not be realised in one pass as intended.

Table 1. The original experimental matrix based on Voß (2001). The welding tests indicated with red font were not realised in the project. LBW = laser welding and LAHW = laser-arc hybrid welding, i.e. LBW + MAG welding; X = X-groove, I = I-groove.

Experiment	Welding	Material	Filler metal
A. Bead-on-plate welds			
A1. Surface tension forces			
	MAG	S355	ø 1 mm G 19 9 LSi
	LAHW		(OK 308LSi)
A2. Autogenous welding, pool size			
	TIG	S355	-
	LBW	S355	-
B. True butt welds			
B1. True MAG welding			
	MAG 70° X groove	S355	ø 1.2 mm G3Si1
		S500	(OK 12.50)
B2. True hybrid welding (optional)			
	LAHW I groove*)	S355	ø 1.2 mm G3Si1
		S500	(OK 12.50)

*) No acceptable single-pass LAHW welds were realised in the 15 mm base material

5.2.1 Reference case experimental validation

Some changes were made in the experimental arrangements described in Voß (2001) for the project purposes. The most significant difference was the rejection of the continuous displacement measurement in XYZ direction with extensometers. Apart from having been difficult to arrange in practice, i.e. lack of space, complicated attachment og gauges, etc., this would have also extended and probably delayed the validation experiments extensively due to the need of limited personnel and equipment resources. Instead, a combination of a 3D measuring arm and a laser scanner was used to document the sample dimensions in all phases of the welding experiments: dimensions of the individual plate(s), after eventual tack welding, and after cooling down to 50 °C of each weld pass. In this manner, the final result of deformation evolution could be measured after all stages, but the changes in displacement during welding could not be monitored.

Another difference was the use of MAG and hybrid welding together with laser and TIG processes, because they were regarded more relevant in the Finnish industry, and particularly in the true joint welds of the company cases. Furthermore, the filler metal selected for the bead-on-plate weld was not of matching composition to the base material, but an austenitic stainless steel one. The motivation was to enable the study of the mixing and dilution behavior better in

macro and micrographs. However, this change showed to be futile. Instead, the use of non-matching filler metal was usable in thick-section austenitic stainless steel joints, see 5.3.

As for monitoring of the welding experiments, KAIST experience showed that the recording of the true arc geometry is essential for reliable simulation results. Therefore, an attempt was made to use CCD camera to monitor the arc from both in front and from the side direction of the welding torch. There were several prblems with the recording, the most severe ones being the inadequacy of direct visual cvontact from both directions, as well as the control of suitable filtering of the arc light - the arc details tended to be oversaturated. In the case of the true butt welds, the weld groove sides shaded the arc details, i.e. no valid recording of root passes could be made from the side direction - which is the more important one. In addtition to attempts for arc imaging, observations of the melt pool bevaviour were done using high-speed imaging with laser stroboscope lighting, too.

5.2.2 Reference case simulation results

The reference case simulation results were analysed in collaboration with Mikko Kuitunen´s MSc. Thesis prepared simultaneously but with separate funding. The complete results were reported in Kuitunen (2016), so only a brief review is done here. The comparison between the published reference data, experimental work characterisation and simulation results concentrated on weld fusion zone and HAZ dimensions and cooling times $t_{8/5}$.

The TIG bead on plate experiments used for comparisons were carried out for 5 and 15 mm S355 plates, see also Table 1. The welding parameters are listed in Table 2. As can be seen in the parameter values, three different heat inputs were used for each thickness according to Voß (2001), and the main variable was the traverse speed. Slight changes in voltage are due to power source synergy curves.

Table 2. Welding parameters used for the TIG bead-on-plate experiments.

Experiment		Welding parameters				
type	s (mm)	I (A)	U (V)	v (m/min)	k	Q (kJ/cm)
TIG_5_1	5	250	10.5	0.13	0.8	9.42
TIG_5_2	5	250	10.9	0.28	0.8	4.66
TIG_5_3	5	250	10.2	0.43	0.8	2.88
TIG_15_1	15	250	10.0	0.13	0.8	9.17
TIG_15_2	15	250	10.0	0.28	0.8	4.27
TIG_15_3	15	250	10.0	0.43	0.8	2.81

The principle of the simulated weld dimension measurements is shown in Figure 4. The most convenient way of measuring was calculating the number of simulation mesh grid cells for both fusion zone and the HAZ, for this is also the simulation resolution. Both in Voß (2001) and Kuitunen (2016) the measurements were made from weld macrographs.

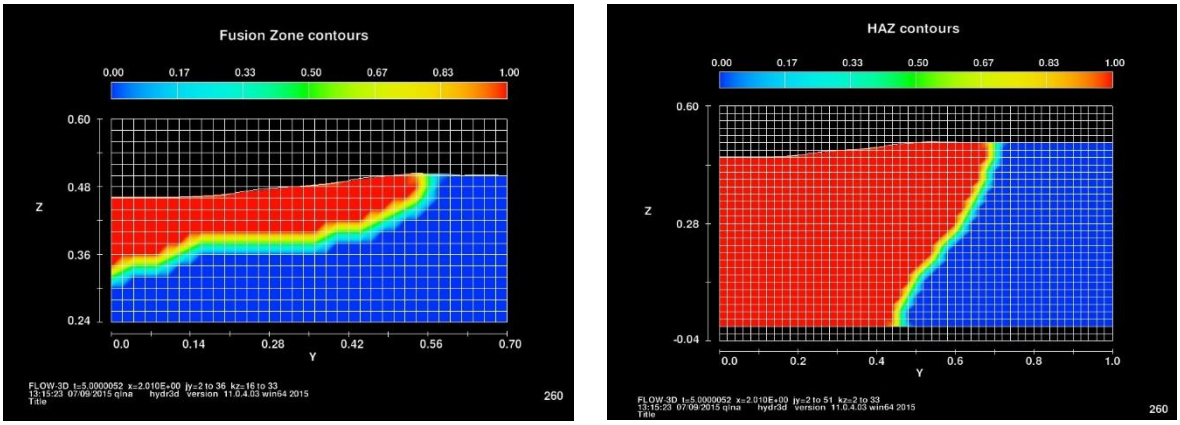

a) b)

Figure 4. The principle of measuring the simulated weld width: a) fusion zone with zooming and b) the HAZ.

It should be noted that the arc efficiency k was changed from the typically used value 0.8 to 1.0 for the simulation of the 15 mm specimens: the simulated melt pool and HAZ dimensions were unrealistically small with k = 0.8. This was corrected in the software customisation code for the later weld joint simulations.

Table 3. Comparison of TIG bead-on-plate weld penetration results, sim = simulated, OV = measured in Voß (2001) and MK = measured in Kuitunen (2016). Full = full through-thickness penetration.

Experiment type	Welding			Simulation		Penetration					
						fusion zone			HAZ		
	s	k	E	Q	mesh	symm.	sim	OV	MK	sim	OV	MK
	(mm)		(kJ/cm)	(kJ/cm)	(cm)		(mm)	(mm)	(mm)	(mm)	(mm)	(mm)
TIG_5_1	5	0.8	11.78	9.42	0.02	on	1.8	full	3.2	full	-	full
					0.04	on	4.6	full	3.2	full	-	full
TIG_5_2	5	0.8	5.83	4.66	0.04	off	1.4	2.4	1.7	full	-	full
					0.04	on	1.8	2.4	1.7	full	-	full
					0.02	on	1.2	2.4	1.7	full	-	full
TIG_5_3	5	0.8	3.60	2.88	0.04	on	1.0	1.8	1.7	3.8	-	3.7
TIG_15_1	15	1.0	11.46	11.46	0.04	on	2.6	2.8	3.3	4.6	-	5.2
TIG_15_2	15	1.0	5.34	5.34	0.04	on	1.8	2.3	2.5	3.8	-	3.8
TIG_15_3	15	1.0	3.51	3.51	0.04	on	1.4	1.7	1.4	3.4	-	2.7

It can be seen in the results that there is a reasonable agreement between the simulated and those measured by Kuitunen (2016). However, the results by Voß (2001) typically show larger penetration values that simulation or VTT experiments. The effect of simulation mesh size - 0.02 cm vs. 0.04 cm - is most dramatic in the in the first 5 mm thick sample with the highest heat input of 9.42 kJ/cm with the resulting penetration values of 1.8 vs. 4.6 mm, respectively. Noteworthy is that, unlike what could be expected, the coarser mesh actually estimates the penetration better wehen compared to Voß (2001). The tendency is similar with smaller heat input of 4.66 kJ/cm, although not as pronounced. Furthermore, the overall agreement with both with Voß (2001) and Kuitunen (2016) is clearly better with the thicker 15 mm welds with all the heat input values. However, the arc efficiency value of k = 1.0 may have an impact here, too.

The results in Table 3 also show that, using the same mesh size of 0.04 cm, the simulation results with symmetry, ie. simulating only half of the joint cross section, and without are very close to each other. This together with the mesh size effect is important when simulating more demanding cases, eg. true welds: using simulation with symmetry condition and/or a coarse mesh can reduce the simulation times quite drastically while still retaining reasonable accuracy.

A comparison between the siumulated and measured bead-on-plate weld geometries was done for the weld widths, too. The simulation cases were the same as in Table 3, and similarly, both fusion zone FZ and heat affected zone HAZ values were compared, Table 4.

Table 4. Comparison of TIG bead-on-plate weld width results, sim = simulated, OV = measured in Voß (2001) and MK = measured in Kuitunen (2016).

Experiment type	Welding				Simulation		Width					
	s	k	E	Q	mesh	symm.	fusion zone			HAZ		
							sim	OV	MK	sim	OV	MK
	(mm)		(kJ/cm)	(kJ/cm)	(cm)		(mm)	(mm)	(mm)	(mm)	(mm)	(mm)
TIG_5_1	5	0.8	11.78	9.42	0.02	on	11.4	13.4	10.6	14.0	17.9	19.3
					0.04	on	10.0	13.4	10.6	12.8	17.9	19.3
TIG_5_2	5	0.8	5.83	4.66	0.04	off	8.2	9.5	9.3	11.0	11.4	11.3
					0.04	on	8.0	9.5	9.3	11.2	11.4	11.3
					0.02	on	9.0	9.5	9.3	11.6	11.4	11.3
TIG_5_3	5	0.8	3.60	2.88	0.04	on	6.4	7.4	7.6	9.2	8.9	9.6
TIG_15_1	15	1.0	11.46	11.46	0.04	on	10.0	9.7	9.0	13.6	12.6	12.5
TIG_15_2	15	1.0	5.34	5.34	0.04	on	6.0	8.1	8.1	9.2	9.9	10.8
TIG_15_3	15	1.0	3.51	3.51	0.04	on	8.0	7.0	7.2	10.4	8.6	9.5

Generally, it can be said that the simulation results are more consistent with both the measured ones than was the case with penetration values. The only more pronounced difference can be seen in the HAZ width of the 5 mm specimen with the largest 9.42 kJ/cm heat input, where the simulation clearly underestimaes the width compared to both Voß (2001) and Kuitunen (2016). In this case, the Voß (2001) measured fusion zone width values are also larger than those of Kuitunen (2016) or simulation, regardless of the mesh size.

The $t_{8/5}$ cooling times from 800 to 500°C were calculated using the analytical formular given in the standard SFS-EN 1011-2, and defined from the thermoelement measurement data in the welding experiments in Kuitunen (2016). The $t_{8/5}$ cooling times were calculated in both two and three dimensional cases, but for comparison purposes the two dimensional one was selected for 5 mm plates and the three dimensional for thicker 15 mm cases.

The analytical and measured results from closest to the fusion line are compared to the simulated thermal history of a corresponding cell on the specimen surface. However, the original weld simulation runs had to be continued, because they did not always cover the cooling phase down below 500 °C - this was to keep the simulation times reasonable. This was also the reason for restricting the comparison the measurements closest to the weld. The results of the comparison are presented in Table 5.

Table 5. Comparison of calculated, measured and simulated $t_{8/5}$ cooling times from Kuitunen (2016). FL = weld fusion line.

Process	Thickness (mm)	Heat input (kJ/cm)	Cooling time $t_{8/5}$ calculated (s)	measured (s)	simulated FL (s)
LAHW	5	-	2.0	4.9	-
	15	-	1.2	4.9	
LBW	5	-	0.7	-	-
	15	-	1.1	1.0	-
TIG	5	9.42	25.7	9.8	12.5
	5	4.66	2.5	3.7	-
	5	2.88	6.6	-	12.5
	15	11.46	4.0	3.6	5.1
	15	5.43	2.0	1.6	4.5
	15	3.51	1.2	-	-

The results are very confusing with respect to calculations, measurements and simulations. The measurement results are always somewhat uncertain due to the experimental errors, especially with surface-mounted thermocouples as was the case in these experiments. From simulation point of view, the procedure of defining the cooling temperature cycle for a particular location, ie. simulation cell, needs refining. Firstly, the $t_{8/5}$ cooling time of the 5 mm specimen cannot be the same for two so different heat inputs of 9.42 and 2.88 kJ/cm. Secondly, the difference between the simulated cooling times of the 15 mm specimen with 11.46 and 5.43 kJ/cm of 5.1 and 4.5 s, respectively, is suspiciously small compared to both calculated 4.0 and 2.0 s and and measured 3.6 and 1.6 s ones, respectively. Finally, there are too many missing simulation cases and successful measurement points to draw any solid conclusions of the consistency of the results.

5.3 Stainless steel hybrid welding simulation

The background of the stainless steel welding simulation is twofold: firstly, there was plenty of existing experimental data at VTT on laser MAG hybrid welding of thick section austenitic 316L stainless steel that was immediately available for simulation results validation, and even more so with some complimentary experimental and characterisation results form the project. Secondly, stainless steels are a vital material group for Outotec, too, and it was foreseen that combining the industrial applications from Outotec and the more research oriented supplementary work would provide a fruitful combination.

The austenitic stainless steel welding experiments were started in collaboration with Outokumpu Stainless who promised to supply the materials and conduct SEM EDS characterisation work as their project in-kind contribution. Outotec, in turn, connected the project work to their welding production renewal, ie. automation of a major part of their Outokumpu production work. For a practical case, a large duplex stainless steel rotor structure was selected as their simulation case, with the aim of studying the optimising the top pass geometry of a multipass fillet weld for improved fatigue performance.

Unfortunately, both these research lines were prematurely terminated due to restructuring and consequent loss of key personnel at both VTT and Outotec. However, based on the austenitic

stainless steel experiments and characterisation work at Outokumpu Stainless Tornio Research Centre during the first project year, a considerable number of publications could be prepared for the project, see also chapter Project pulications at the end of this report. As for the simulation of duplex stainless steel welding, additional hindrances on top of personnel changes were created by the lack of sufficient and comprehensive base material source data.

5.3.1 Austenitic stainless steel case simulation and experimental results

The processes laser welding and MAG welding alone possess quite complex multiphysics phenomena, and the situation becomes even more complex when they are combined together. Laser welding in partial penetration and full penetration mode show different characteristics and the addition of MAG in leading or trailing configuration can also affect the flow behavior, which in turn can affect the mixing of MAG wire in weld pool. It was found that mixing is incomplete in laser and hybrid welding (Karhu et al. 2013). Laser-arc hybrid welding is better in terms of mixing as compared to laser-cold wire welding, and near top surface mixing is higher as compared to lower surface.

To study these interaction effects further, experimental studies are costly and give very little insight of flow behavior. Therefore, simulation studies are preferred. Modelling of the process involves complex multiphysics phenomena which include multiple reflection inside keyhole, arc heat source, recoil pressure, Marangoni flow, bubble pressure model, etc. In order to validate the simulation results, some partial penetration welding studies were carried out in the project using laser, MAG and hybrid welding. The experimental and simulation details are described in detail in Sohail et al. (2015, 2017) and Na et al. (2015), so only a brief review of the main findings is given here.

Experiments were carried out on AISI 316L austenitic stainless steel using a combination of pulsed MAG welding and 10 kW fiber laser welding. The compositions of filler wire and base metal were slightly dif-ferent in terms of Cr and Ni concentration, in order to provide a sufficient concentration of alloying ele-ments in the fusion zone. The 10 mm thick plate was welded in both laser trailing and leading configurations, as shown in Figure 5.

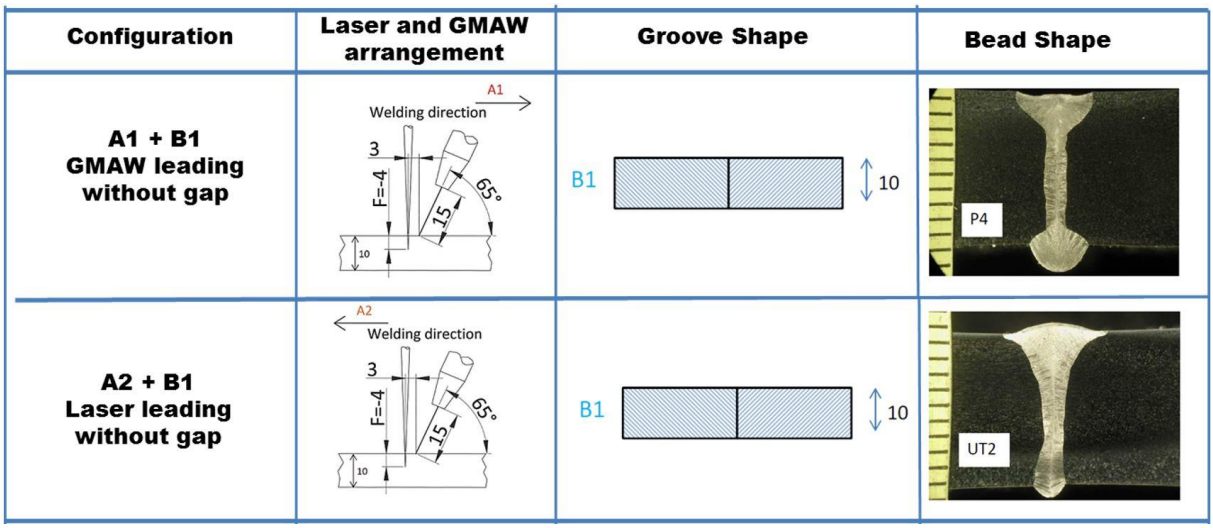

Figure 5. The laser-MAG welding experiment configurations.

Simulations were made for the both cases to show the behaviour in different steps of welding process. In Figure 6we can see longitudinal cuts of laser-arc hybrid welds (arc leading).

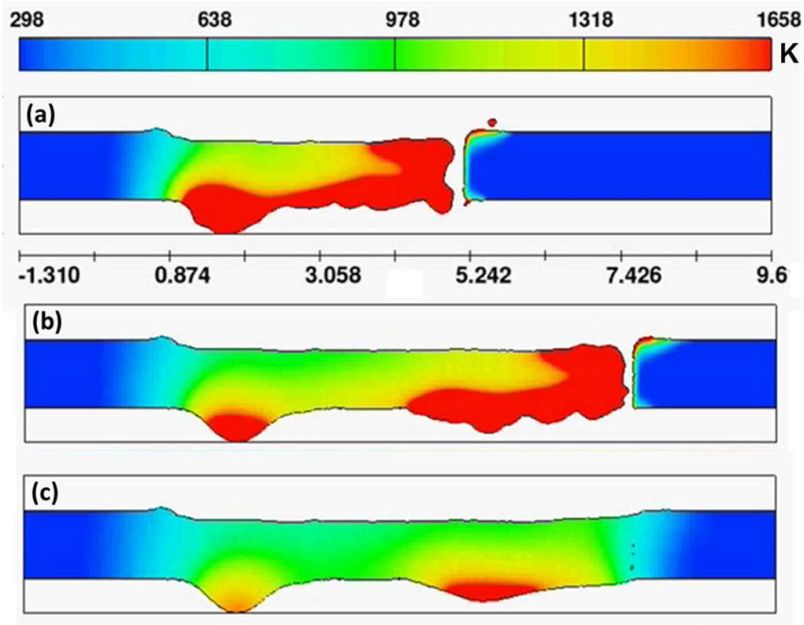

Figure 6. Simulated longitudinal cuts of laser hybrid welding with GMAW leading. Welding direction from left to right. Flow patterns and temperature contours of the simulated weld in the same location at different times. (a) 1.9 sec. after switch-on the laser beam, (b) 3 sec. (at the time of switch-off the laser beam) and (c) 4.3 sec. (1.3 seconds after switch-off the laser beam). The colours describe temperature in Kelvins as shown in ruler at the top.

Apart from metallography, the weld cross sections were characterised using EDS line scans at four different depths from the specimen top surface to study the chromium mixing behaviour in different welding configurations. The Cr EDS results were compared to the simulated chromium content at corresponding depths. The EDS analyses were carried out by Outokumpu Stainless Tornio Research Centre as their project in-kind contribution.

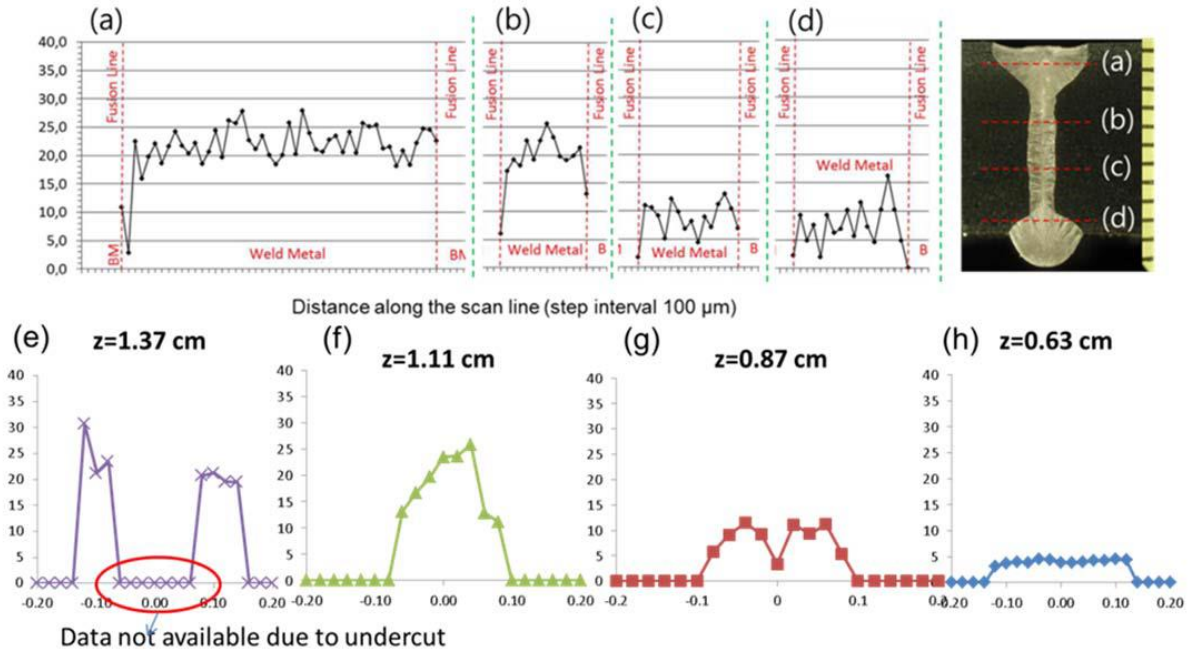

Figure 7. Experimental (a-d) and simulation (e-h) of mixing profiles for laser-arc hybrid welds, arc leading. Vertical axis shows mixing values as per cent. The locations in micrograph a-d are the same as e-h, respectively.

As for numerical analysis of the hybrid welding process, mainly three-dimensional transient simulations were carried out for laser-MAG welding. Here, the mass conservation equation, the momentum conservation equation, referred to here as the Navier-Stokes equation, the energy conservation equation and the VOF equation were used as governing equations to execute the molten metal flow analysis. An additional equation for alloying element conservation was used to investigate the mixing of Cr. The molten metal was treated as a Newtonian flow, considering the fluid to be an incompressible laminar flow. Based on these assumptions, the aforementioned governing equations were solved. An example of the EDS experiments and the corresponding simulation results are seen in Figure 7. The simulations give quite a good consistence with the experimental ones.

The conclusions from the simulation results and corresponding experimental validation tests and their characterization can be summarized as follows:

- Laser-MAG hybrid welding in full penetration configuration is studied by simulation and experimental means using MAG leading and MAG trailing configuration. Experimental results of full penetration hybrid welding show the bead shape for both configurations, GMA-leading and MAG trailing, are quite different. The same cases are simulated in order to study the mixing behavior and flow characteristics.

- In hybrid welding for both configurations, it is found that laser is dominant in defining flow pattern. Two recirculating flows are found, one on top surface and second on root surface. The molten pool is longer in bottom surface as compared to upper surface, this is also a characteristic of full penetration laser welding.

- The filler wire used in MAG contains an additional amount of Cr as a mark for mixing measurements. It is found that MAG leading configuration is showing more concentration of Cr in upper half of bead while in MAG trailing a more uniform mixing is observed even if it is not complete.

- Five sets of Tungsten (W) particles were introduced in simulation to study the flow behaviour, which reveals that in MAG leading configuration, once the particles reach the bottom recirculation they are unable to return back to the upper one. In MAG trailing configuration the particles introduced in upper part were able to reach the bottom recirculation and then return towards the upper recirculation; this phenomenon helps in mixing of Cr in MAG trailing.

5.3.2 Duplex stainless steel case simulation

The Outotec simulation case was related to the welding production automation development of their Outokumpu production work, as described in chapter 5.1 Company specific cases. Their simulation case was a duplex stainless steel rotor and the aim was to optimise the top fillet pass geometries for improved fatigue performance. Unfortunately, the simulation of duplex stainless steel welding was hindered by both personnel changes and the lack of sufficient base material source data.

5.4 Friction Stir Welding simulation

The motivation for the FSW simulations came from the decision of Posiva to use FSW for the encapsulation of spent nuclear fuel. The spent nuclear fuel will be encapsulated to canisters consisting of an inner cast iron container and of an outer copper tube, as shown in the full size demonstration of the canister in Figure 8. The bottom of the copper tube can be integrated, but the top will be closed with a lid that is welded in the encapsulation plant after the spent fuel has been assembled into the canister. As the copper canister is a very important barrier in the safety concept for nuclear waste storage, the quality requirements for the welding are very

high. Ideally, the properties of the weld should not deviate from the properties of the copper in other parts of the canister. Even though it has been concluded that with the FSW approach it is possible to reach the quality targets, there is still much to be studied in the FSW process. To further develop the understanding of the phenomena in FSW, the capability for detailed simulation of the welding process would be useful.

Figure 8. Copper canister used to store spent nuclear fuel. The lid will be joined to the canister using FSW.

Within this project, the aim of the FSW simulations was to test the implemented CFD model and evaluate the possibilities of CFD for simulation of FSW of copper. With this aim, a series of simplified concept test simulations were made. In the simulations a simple flat plate geometry was assumed and a simplified, cylindrical tool shape, as shown in Figure 9, was used. The size of the simplified tool was chosen to roughly match the actual tool that will be used to weld the canisters but without any of the complex threads and grooves of the actual tool.

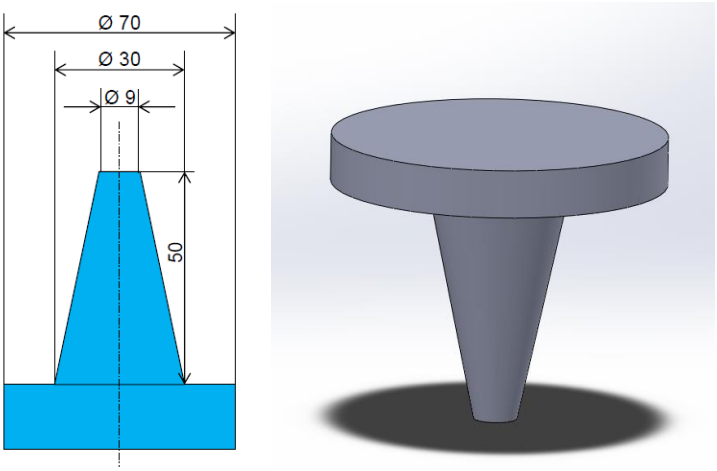

Figure 9. Simplified tool used in the concept test simulations, the dimensions are in mm.

5.4.1 Material properties for copper

The first task before any actual simulations was to obtain suitable material parameters for the flow stress model of copper. Unfortunately, reliable material properties at high temperatures, strains and strain rates present in FSW are difficult to obtain experimentally and thus the amount of experimental data available is quite scarce for many materials (Tello et al. 2010). This issue is even more profound for copper than eg. for aluminium, as copper is more uncommon material for FSW. However, for the simulations suitable material properties for copper were found in the PhD thesis of García (2004). García expresses the flow stress for copper as

$$\frac{\dot{\bar{\epsilon}}}{D_{sd}(T)} = \left\{A_{ss}\sinh\left(\frac{\alpha_{ss}(\sigma_e - \sigma_0)}{E(T)}\right)\right\}^n \quad (36)$$

where $A_{ss} = 687$, $\alpha_{ss} = 1209$, n=5, $D_{sd}(T)$ is the diffusion coefficient, $E(T)$ the elastic modulus and σ_0 corresponds to back stress. The diffusion coefficient for copper is given as

$$D_{sd}(T) = D_{ov}\exp\left(-\frac{Q_{sd}}{RT}\right) \quad (37)$$

where $D_{ov} = 2\cdot 10^{-5}\mathrm{m}^2/\mathrm{s}$ and $Q_{sd} = 197\ \mathrm{kJ/mol}$. The elastic modulus is

$$E(T) = 2.66\mu_0\left(1 + \left(\frac{T-300}{T_m}\right)\left(\frac{T_m}{\mu_0}\frac{d\mu}{dT}\right)\right) \quad (38)$$

where $\mu_0 = 4.21\cdot 10^4\mathrm{MN/m}^2$, $T_m = 1356\ \mathrm{K}$ and $\left(\frac{T_m}{\mu_0}\frac{d\mu}{dT}\right) = -0.54$.

To simplify the expressions for flow stress, it was assumed that the back stresses are zero in the simulations. In addition, as the dependence of the flow stress to elasticity is not very high, a constant value of $E(T) = 0.8\cdot 10^{11}\mathrm{N/m\text{^}2}$ was assumed. With these assumptions, the flow stress expression (36) can be cast into the more common form of Sellars and Tegart law and the corresponding parameters used in the simulations are given in Table 9. The flow stress at different strain rates is illustrated in Figure 10. Flow stress of copper as a function of temperature and with different rates of strain.

Table 6 Flow stress parameters for pure copper.

Parameter	Value
A	1.19×10^{10} 1/s
Q	$197\frac{\mathrm{kJ}}{\mathrm{mol}}$
α	$0.0151\frac{1}{\mathrm{MPa}}$
n	5

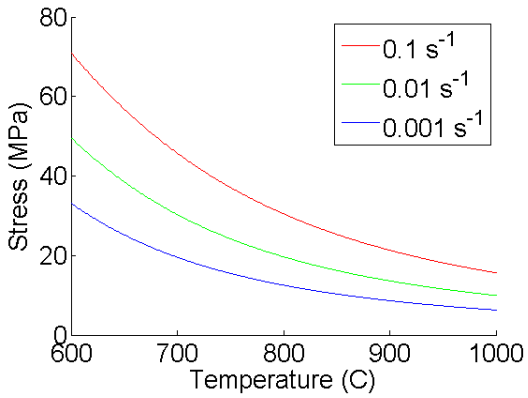

Figure 10. Flow stress of copper as a function of temperature and with different rates of strain.

5.4.2 Simulation results

The simulation model was tested both on isothermal cases and on cases with heat transfer enabled. In the initial state, a passive scalar s1 is used to mark the different sides of the plate: 1 = advancing side,0 = retreating side of the tool of the FSW process,

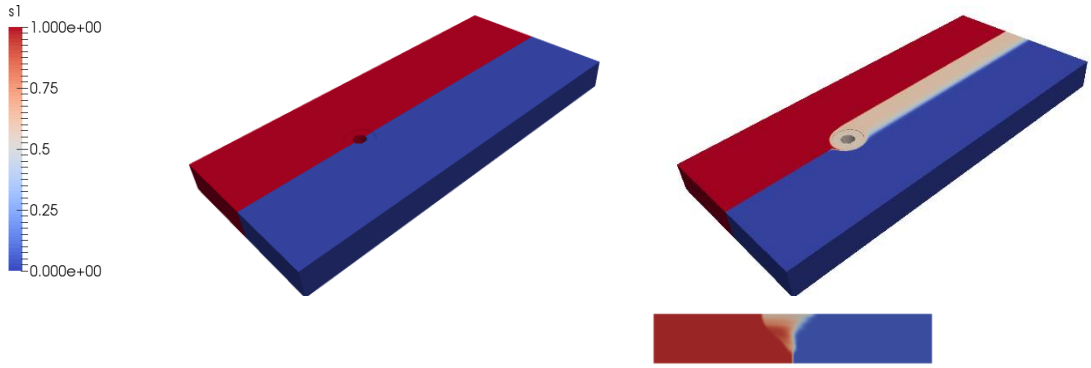

Figure 11. Scalar variable s1 indicates the extent of mixing of the workpiece. Initial condition on the left, steady state solution on the right.

Velocity vectors were simulated illustrating the material flow around the tool, Figure 12. Also the velocity magnitude could be simulated in the near field of the tool.

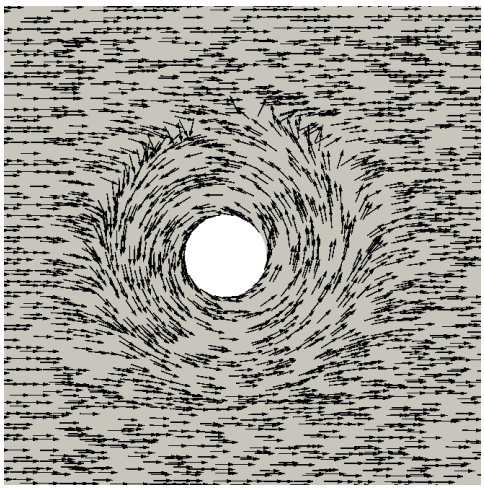

Figure 12. Velocity arrows at the middle of the tool, horizontal plane.

The simulated temperature distributions were simulated, as can be seen in Figure 13 and Figure 14. However, an experimental validation would have been essential for these si mulaitons. As opposed to velocity vectors and magnitudes, the temperature distributions could have been compared to experimental values within a reasonable accuracy using the standard experimental arrangements, ie. without extra instrumentation.

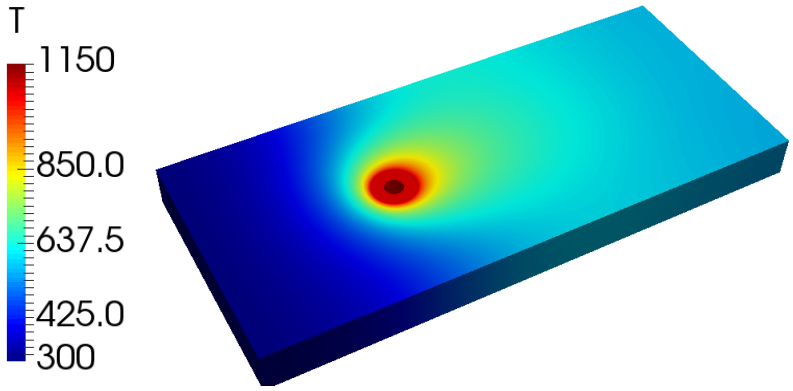

Figure 13. Temperature field around the tool.

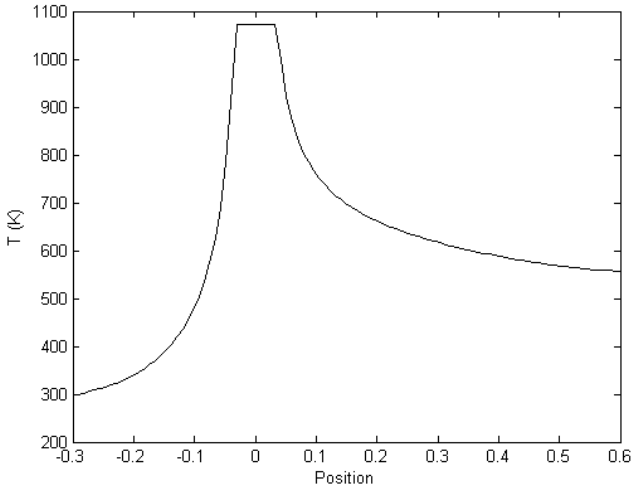

Figure 14. Temperature distribution along the welding line in the middle of the workpiece.

5.4.3 Summary

The simulation of FSW process is a difficult topic due to high strain rates and high temperature viscoplastic flow with frictional and plastic heat generation involved. So far, many different approaches have been used to simulate FSW, eg. analytical methods, Finite Element Methods (FEM), Computational fluid dynamics (CFD), Arbitrary Lagrangian Eulerian methods (ALE) and Smoothed-particle hydrodynamics (SPH). Within this project CFD approach was chosen, for it has the advantage of being able to naturally handle the high strain rates present in FSW.

Generally, there are several challenges are present in CFD simulation. Firstly, accurate simulations also require accurate models for flow stress/viscosity of the base material. However, experimental data for stress/strain relation under high temperature, high strain rate conditions is not abundant, and the flow stress is usually only a function of temperature and strain rate because dynamic effects and strain state are ignored.

Secondly, modelling of friction and frictional/plastic heating is challenging because no universal consensus exists on the importance of frictional vs. plastic heating. Therefore, calibration of the models would be required since the models are not fully predictive.

Thirdly, modelling of complex tool shapes is challenging. Cylindrically symmetric tools are easy to model but real tools usually have threads, flutes and other small details that require a very fine mesh to be resolved. On ther other hand, simulation of a non-axisymmetric rotating tools

is complicated: transient simulation with sliding mesh is computationally expensive, therefore simplifications, such as Multiple Reference Frame (MRF) approach are needed.

Many published papers have used commercial CFD codes such as ANSYS Fluent or CFX. However, the required constitutive models are not readily available and have to be implemented using customization. The aim of the current project was to test methods presented in literature and estimate their feasibility for copper FSW by implementing in OpenFOAM, which is a free, open source code. This means it is easily extendable and modifiable and the full source code is available, ie. there is no ”black box” between customization and results

The simulation framework implemented in OpenFOAM platform was tested in this project. It can be concluded that qualitatively reasonable results were obtained considering the simplifications used. However, the results are quite sensitive to modelling assumptions. In order to progress further with the CFD simulation of the FSW process, comprehensive experimental validation would be needed ideally starting with simple tool shapes and progressing towards more realistic and detailed tools.

5.5 Mild steel arc welding simulation

The the mild steel welding simulation case, ie. Technip industrial application, was started by defining the case and design of the corresponding validation experiments. The aim was that the case would be as realistic as possible, including not only true materials and dimensions, but also on-site welding by Technip at their premises. However, as controlled conditions are difficult to achieve in a production environment, preliminary tests were carried out in laboratory conditions at LUT, too. The purpose on these lab experiments was twofold: firstly, to provide a simplified and well controlled validation case for practising the simulation of true MAG weld joints, and secondly, to allow the recording of the arc shape and behaviour during welding.

Technip selected their case from the early stages of a typical Spar hull construction: the two-sided multipass submerged arc welding (SAW) of a wide hull sheet from individual plates, and the consequent fillet welding of bulb stiffener profiles to this widened plate using SAW with double wires (twin-SAW) and manual flux-cored arc welding (FCAW). The twin-SAW weld were done simulateneously on both sides of the bulb profile. The material was A420 shipbuilding steel for both the plate and bulb profile and sketches of the case are in Figure 15.

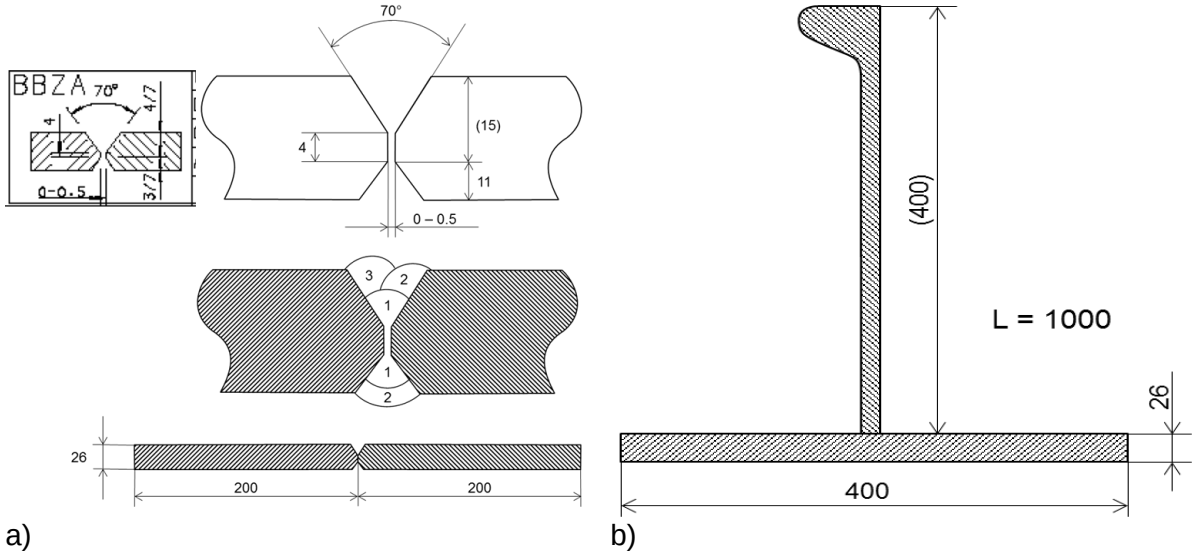

a) b)

Figure 15. Sketches of the Technip company case welds, a) multi-pass butt weld in a non-symmetric X groove in 25 mm A420 steel and b) 14 mm thick bulb stiffener fillet welding to 25 mm hull plate using twin-SAW and manual FCAW. (Note: the 26 mm plate thickness of the sketch is not correct.)

5.5.1 Laboratory scale mild steel arc welding experiments at LUT

The preliminary experiments for the Technip case were welded in LUT welding laboratory. The welding arrangement was partially the same as in the reference case welds in chapter 5.2 Reference simulation case, page 23, ie. the workpieces were welded without any fixturing on a three point support to allow free deformation. Obviously, the specimen halves had to be tack welded first. The welding was intended as three-pass per side, but after the first trials, it become evident that two passes per side was enough to fill the groove. Hence, the welds were also laterally symmetric, Figure 16. The welding parameters we not set beforehands but were selected based on initial experiments. The parameters are listed in Table 8 on page 52.

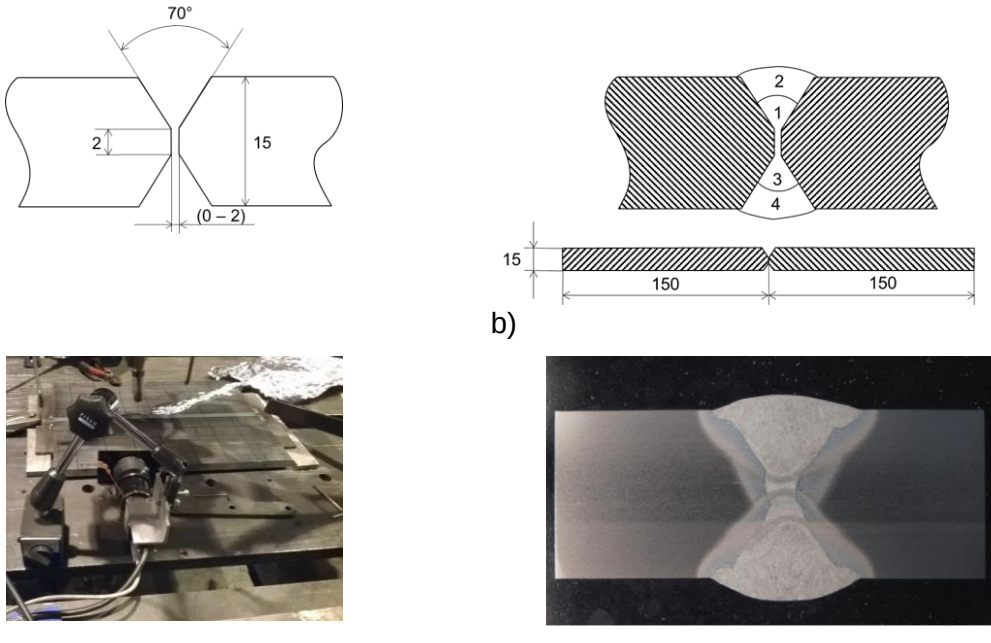

a) b)

c) d)

Figure 16. Laboratory MAG welding tests at LUT: a) groove geometry, b) welding sequence, c) welding arrangements with arc monitoring and d) weld macrograph.

It should be noted that, according to Table 1 on page 24, laser-arc hybrid welds were included in the experimental programme, too. However, 15 mm is at the very upper limit of the capability of the available 10 kW laser for a single pass weld and a satisfactory weld was reached for only a major distance in the 400 mm workpiece. Since multi-pass hybrid welding is not a viable solution in production, this alternative was excluded from the future experiments as well as from the simulation programme. Some analysis data on this hybrid weld can be found in Kuitunen (2016).

5.5.2 Mild steel arc welding experiments at Technip

The SAW butt welds in 25 mm A420 plate were carried on Technip site in Mäntyluoto using two ø 4 mm OK Autrod 13.27 (EN 756: S2Ni2) filler metal wire and OK 10.71 (EN 760: SA AB 1 67 AC H5) flux. Prior to welding in PA position (AWS 1G), the specimen halves were tack welded with about 120 mm long tacks at both ends and in the middle. This is a standard procedure in the plate end seam welding at Technip and is needed to prevent the air gap from closing because of the large heat input of SAW process. Furthermore, run-on and run-off tabs were used, too, and finally the plates were lightly tacked on a steel rail on the shop floor as well, Figure 17. All these precautions are necessary to ensure proper weld and are also standard Technip procedures. However, from especially FEM simulation point of view, they make the definition of the mechanical boundary conditions, ie. fixturing, impossible and thus make these simulations so uncertain that they were neglected in the end. Therefore, they were not prioritised for the CFD simulations either. Still, the samples were subjected to contour residual stress measurements, and the welding distortions were measured after the cooling down of each pass down to 50 °C.

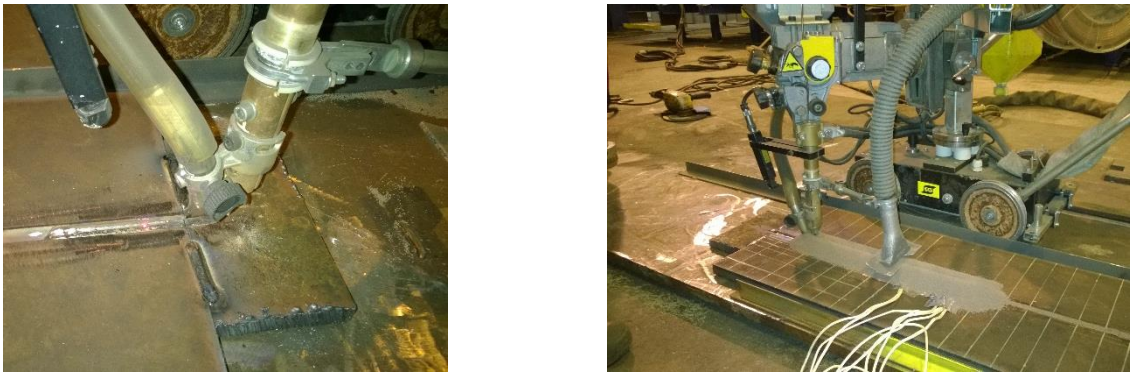

a) b)

Figure 17. Welding of a 25 mm butt joint with single wire SAW at Technip. a) Run-on tab and a tack weld, b) welding in progress with continuous temperature measuerement.

Similarly to the butt joint, the plate-to-bulb profile fillet specimens were also tack welded using about 120 mm tacks at the ends and in the middle on the both sides of the 14 mm bulb web. Run-on and run-off tabs were only used for the twin-SAW specimen and both specimens were welded in PB position (AWS 2F), the twin SAW one from both sides simultaneously using two ø 2 mm OK Autrod 13.27 (EN 756: S2Ni2) filler metal wires and OK 10.71 (EN 760: SA AB 1 67 AC H5) flux and the manual FCAW using ø 1.2 mm Filarc 6138 (EN ISO 17632-A: T 50 6 1Ni P M 1 H5) wire, Figure 18.

a) b) c)

Figure 18. Mild steel fillet welding experiments at Technip. a) Tack welded specimen with run-on and run-off tabs for SAW ready for welding, b) manual FCAW of the second weld and c) twin-SAW of both sides simultaneously, the twin-SAW head can be seen on the back side.

5.5.3 Mild steel arc welding simulation results at KAIST

The Technip SAW case was simulated at both VTT and KAIST. At KAIST the work concentrated on the double-sided fillet weld and was related to Mr Ligang Wu´s MSc. thesis work. A summary of his work is in Appendix 1. The values of each welding parameter were taken as the average of the maximum and the minimum in the Technip WPS No. 76/B03. Hence, the welding current was 675 A, voltage 29 V and speed 1.3 cm/s (780 mm/min). The torch angle is specified as 55 - 60° in the WPS; in simulation, 60° was used.

The wire feeding rate is not readily given in the WPS so it was approximated by fitting data from Chandel et al. (1997) data, resulting in the value 1.88 m/min. Similarly, the effective wire radius needed for the simulation was calculated using the equations given in Cho et al. (2014). With the welding current being I = 675A, the effective radius of σ_r=1.8936 mm can be calculated for an axisymmetric shape. In this case the surface heat flux model, arc pressure model, and EMF model were assumed to be axisymmetric. The flux consumption rate for the slag heat flux model was fitted with the flux consumption data available from ESAB website (2017). With a 29 V arc voltage the flux consumption is estimated at 0.7882 kg flux/kg wire, equalling to 2.41 g/s. The slag heat flux model considers flux consumption rate, flux specific heat and flux melting temperature for the calculation of slag efficiency. Since the flux OK Flux 10.71 indicated in WPS belongs to the same classification AWS A5.17 as the flux used in Cho et al. (2014), the same material properties of the flux were used;

For the simulation, the following parameters had to be assumed:

- Total arc efficiency was assumed to be 0.95;
- The droplet radius was assumed to be same with the welding wire radius, ie. 0.2 cm;
- The droplet speed was assumed to be 100 cm/s;
- The slag thickness for modeling the slag heat flux was assumed to be 0.3 cm (same as Cho et al. (2014) case)

Due to the difficulties to find the material properties of A420, which is rarely used for welding simulation research, properties of AH36 were used in the simulation instead. Drag force is a shear stress induced by the shielding gas, but flux is used instead of shielding gas in submerged arc welding, therefore, the drag force model is not used in the current simulation. Image captures from Mr Wu´s simulation are in Figure 19.

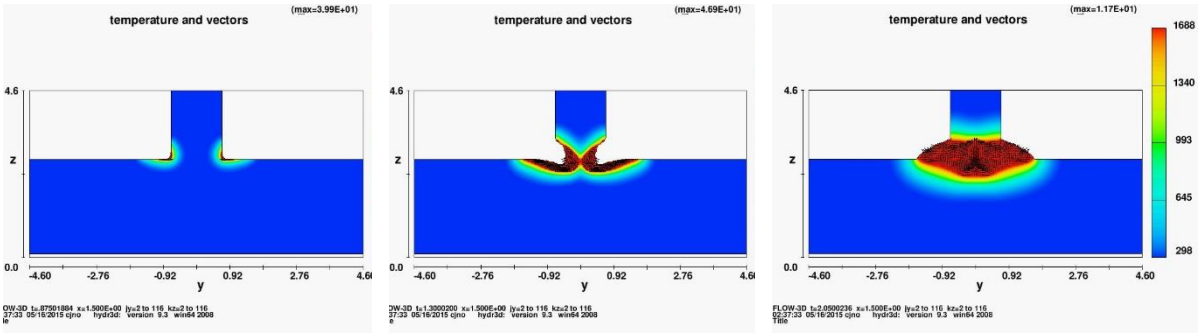

a) b) c)

Figure 19. Simulation of double-side SAW welding: a) initial melting, b) full penetration reached and c) final result.

It can be concluded from these initial simulations that full penetration may be possible because the thickness of the vertical plate is only 14 mm, and the welding was performed from both sides of the joint with high welding current. According to e. g. TWI (2017) and Lincoln Electric (2017), full penetration welding from both sides of T-butt joint is an economical way used to improve the joint strength.

5.5.4 Mild steel arc welding simulation results at VTT

As mentioned earlier in chapter 5.5.2 Mild steel arc welding experiments at Technip, the mild steel arc welding simulations were focused on the laboratory welding experiments using 15 mm S355 MAG welded specimens described in chapter 5.5.1. The simulations were started by modifying the KAIST Flow 3D customisation in order to solve the problems with excessive spatter and verifying that welding in X groove can be simulated correctly. The initial results appeared to be qualitatively reasonable, Figure 20.

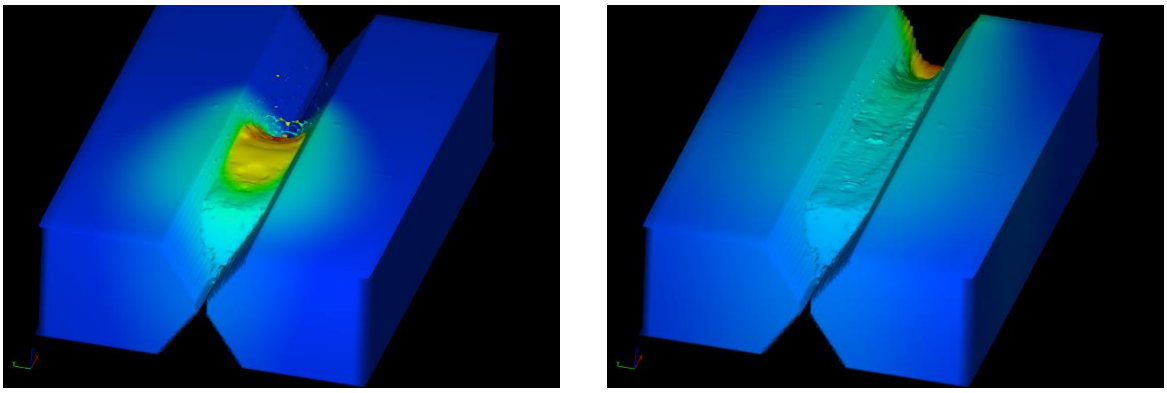

a) b)

Figure 20. Initial simulation results of the 15 mm mild steel weld in an X groove. a) In the middle and b) at the end of the weld.

Already the qualitative result appeared to be well in line with the true weld first pass filling. This was also confirmed by the very encouraging results from the comparison of the simulation results to the weld macrosection, Figure 21.

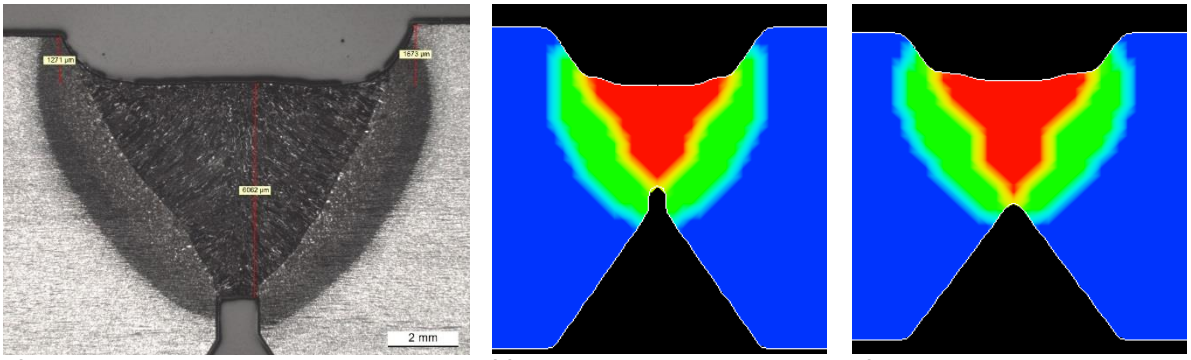

a) b) c)

Figure 21. Comparison of the simulation results with experimental results. a) Weld macrosection of the first weld pass, b) simulation in the middle of the weld and c) simulation at the end of the weld. Red = fusion zone, green = HAZ.

Based on these initial experiments with modified KAIST customisation, the simulation plan was constructed. As described above, the simulation case was preliminary experimental work for Technip company case, ie. a multi-pass butt joint in 15 mm S355 using ø 1 mm G3Si1 filler metal. The specimen was welded in a 70° X-groove from both sides (2 + 2 passes) at LUT. However, for simulations only two first passes, ie. the first side welds were simulated. The measurements and monitoring during and after different welding stages are described in 5.5.1 Laboratory scale mild steel arc welding experiments at LUT and 6 Thermo-mechanical FE analyses using Sysweld software.

The basic simulation case was constructed based on the LUT experimental values and previous simulation experience with respect to simulation specimen dimensions. Hence, the welding speed v_w = 300 mm/min and torch angle α = 0°. For the root pass the welding current I = 201 A, the voltage U = 25.6 V and the wire feed v_f = 9.6 m/min; for the filling pass I = 229 A, U = 29.2 V and v_f = 10.5 m/min

The Flow 3D simulation initial conditions, including the arc parameters (pressure, EMF, heat flux) and material data, were used from the KAIST customisation as such. Base on the previous simulations, the simulation specimen length l_p = 60 mm and width w_p = 20 mm. The mesh was 0.4 mm to achieve reasonable simulation times and symmetry condition was in use, ie. only one half of the specimen was simulated, again in order to keep the time reasonable.

The simulation procedure was tested for the first pass of this basic case and compared to the corresponding macrosection. As can be seen in Figure 22, the simulation result is qualitatively in reasonable agreement with the experimental result.

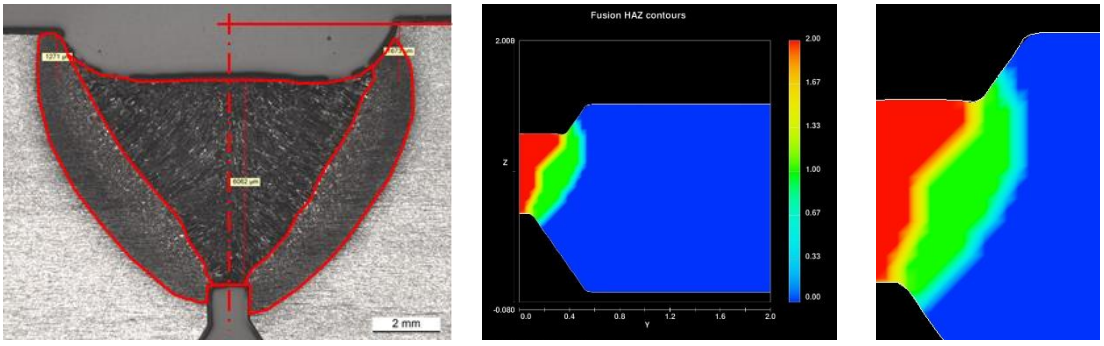

a) b) c)

Figure 22. a) Macrosection of the test weld first pass with fusion zone and HAZ indicated with red lines, b) corresponding simulation image and c) weld detail from the simulation. Red = fusion zone, green = HAZ.

Consequently, a simulation matrix was constructed to study the effects of various welding and simulation parameters on the results. The final simulation plan is presented in Figure 23. It should be noted that the weld current values for various wire feed speed were tested experimentally and recorded at LUT.

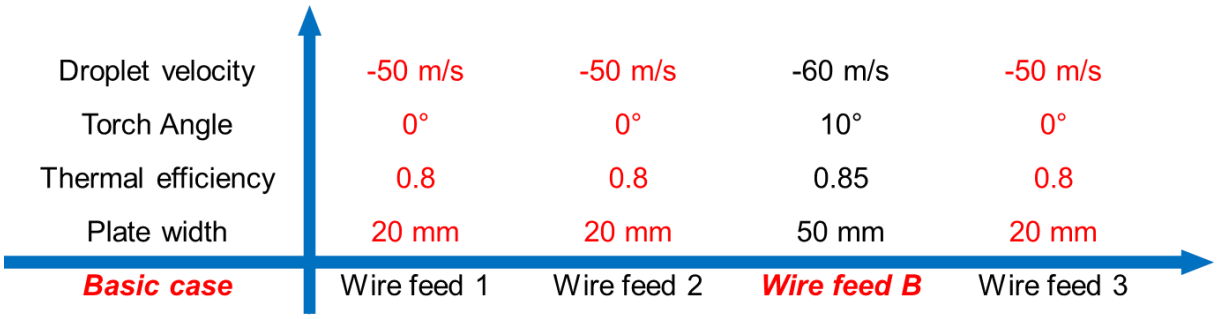

Figure 23. The simulation test scheme. Red indicates the "basic case", ie. test weld case.

The purpose of the presented simulation work was firstly to compare the simulation results of the basic case to validation test results. Secondly, the qualitative effect and sensitivity of welding variables on especially the root pass quality was studied. Thirdly, the CFD (Flow 3D) result data transfer to FE analysis (Sysweld) for deformation simulations was demonstrated.

Unless otherwise stated, all the following simulation images presented in this chapter have been captured at simulation time t_s = 6 s. This corresponds to a weld length of 30 mm at the welding speed of 300 mm/min. In reality, the total simulation time t_{tot} =10 s and the simulated weld length l_s = 30 mm, ie. the simulations covered the deposition of a 30 mm weld plus 4 s of consequent solidification and cooling.

Simulation results: the effect of simulated plate width

The simulations were started by comparing the differences of the basic case when using two simulation specimen widths, namely the "standard" 20 mm and the wider 50 mm. It should be noted that because the symmetry condition was used, the widths refer to one half of the joint. Furthermore, as opposed in the future simulations, the heat input of both passes were equal in this case.

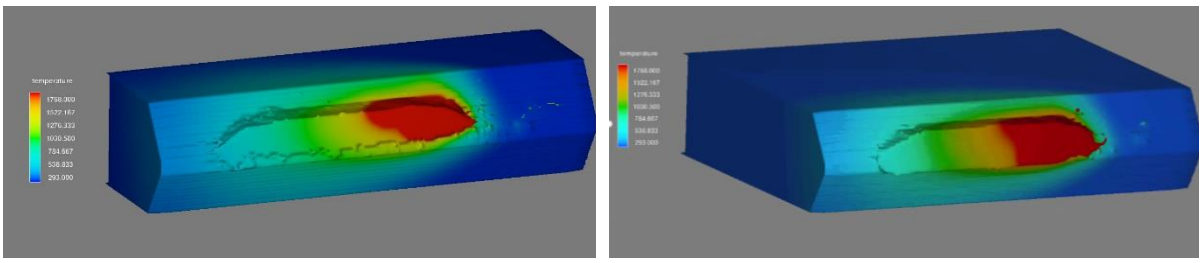

a) b)

Figure 24. The basic case root pass with a) "standard" 20 mm (t_w = 8 s) and b) wide 50 mm plate width. The heat input Q = 0.82 kJ/mm (201 A, 25.6 V, 9.6 m/min feed, 0° torch angle, cf. Figure 23).

As can be seen in Figure 24, the narrower specimen shows smaller and more irregular penetration as compared to the 50 mm wide. This corresponds well to the differences in the weld pool size, which is indicated by the red colour in the temperature chart: this highest chart value of 1768 K is the upper end of the steel melting range T_{liq} used in the customisation. However, less obvious is the fact that the root pass fill height does not change correspondingly but is more or less the same for both the plate widths. Some spatter can be noted in both the cases.

The root pass simulation results were also compared using specimen cross sections. These 2D Y-Z sections were taken from x = 30 mm, ie. 20 mm from the weld start position, where the welding process had stabilised sufficiently. The experimental root pass macrograph of Figure 22a was used as a reference and the fusion zone and HAZ borders are marked in the simulation images, Figure 25.

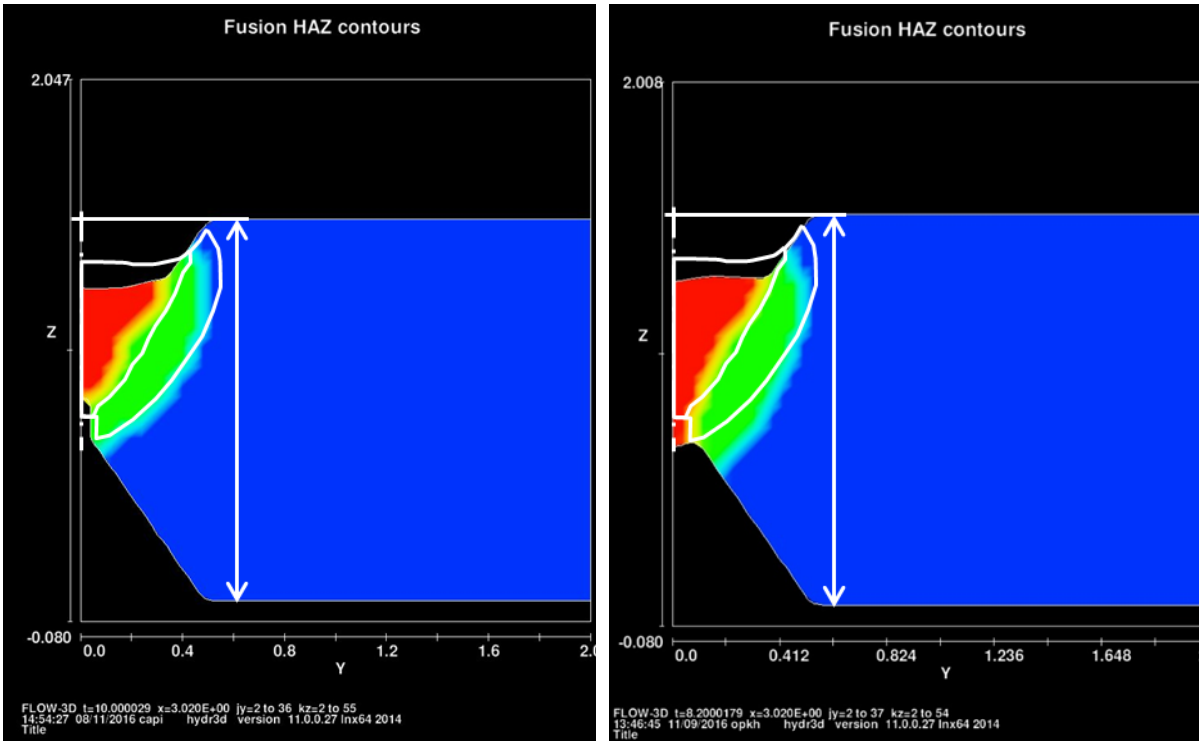

a) b)

Figure 25. Comparison of simulated and true weld geometries. a) XMAG-1_3_5c: w_p = 20 mm and b) XMAG-2_1b: w_p = 50 mm. Red = fusion zone, green = HAZ and white = macrograph borders.

It can be seen clearly in Figure 25 that there are two noticeable differences between the true weld and both the different plate width simulations. First of all, the simulations appear to underestimate the root pass groove filling. With the true reference weld was filled about 1.2 to 1.6 mm short of plate top surface, whereas the simulations show clearly more, about 50 to 70% underfilling with both plate widths. The reason for this remained unclear, but one explanation could be the indications of material loss in simulations for some cases. However, this phenomenon could not be studied systematically and in detail within this project frame. Secondly, plate width affects clearly the root pass penetration result. With the 20 mm plate the root gap penetration is clearly underestimated to almost zero, whereas for the wider plate the simulation overestimates a full root gap penetration for the root pass.

As for the HAZ dimensions, the simulation results show better agreement with the true weld. The wider root side HAZ of the 50 mm plate results probably from the full penetration, ie. the whole root gap surface is available for heat transfer to the base plate. The underestimated groove filling inevitably changes the HAZ width at the top side. The simulated border between fusion zone and HAZ is closer to the weld centreline. This could probably be adjusted by the re-definition of the limit temperature between the two zones in the customisation.

The Figure 26 shows the filling pass weld of the 20 and 50 mm cases at t = 6 s (It should be noted that the root pass of Figure 26a is not the same as in Figure 24 but showed equal groove fill.). As compared to the root pass welds, the difference between plate widths is negligible. Even the fusion zone shapes and dimensions are more or less equal for both cases.

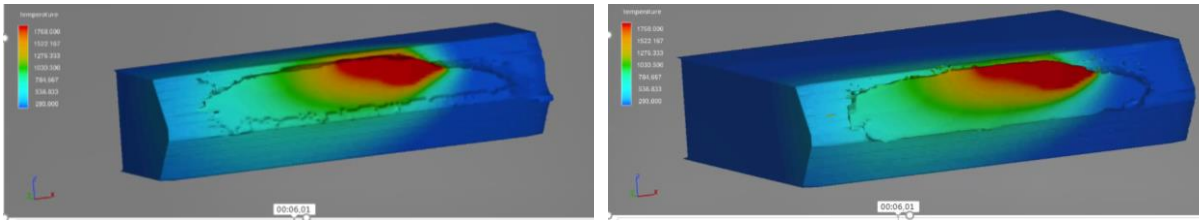

a) b)

Figure 26. The basic case filling pass with a) "standard" 20 mm and b) wide 50 mm plate width. The heat input Q = 0.82 kJ/mm (cf. Figure 23 and Figure 24).

However, as was already noted in the first pass cross-sections of Figure 25, the simulations appear to underestimate the groove filling. The true welds were filled to the top surface level with two passes - no reinforcement though - but the simulation show clear underfilling with both plate widths. The reason for this remained unclear, but one explanation could be the indications of material loss in simulations for some cases. However, this phenomenon could not be studied systematically and in detail within this project frame.

Simulation results: wire feed rate (heat input) effect

The simulation programme was continued by studying the sensitivity of the customisation to the heat input. In practise, this was realised by altering the wire feed speed, which affects the welding current directly. The arc voltage is changed, too, but relatively less as compared to the current. The parameters used for the comparison of heat input Q = 0.82 to 1.20 kJ/mm are listed in Table 7 and the simulation results with different heat inputs can be seen in the following Figure 27. The results presented here focus on the root pass results because of its higher importance with respect to achieving a successful weld.

Table 7. The heat input cases used in the simulations. IP = incomplete penetration, BT = burn through

Case	Wire feed rate (m/min)	Current (A)	Voltage (V)	Heat input (kJ/mm)	Remarks
Wire feed 1	7.5	170	21.5	0.58	IP
Wire feed 2	8.5	183	22.3	0.65	IP
Wire feed B	9.6	200	25.6	0.82	basic case root
Wire feed 3	10.5	229	29.2	1.07	sagging
Wire feed 4	11.5	240	31.3	1.20	sagging, BT?
Wire feed 5	12.5	245	32.0	1.25	sagging, BT?

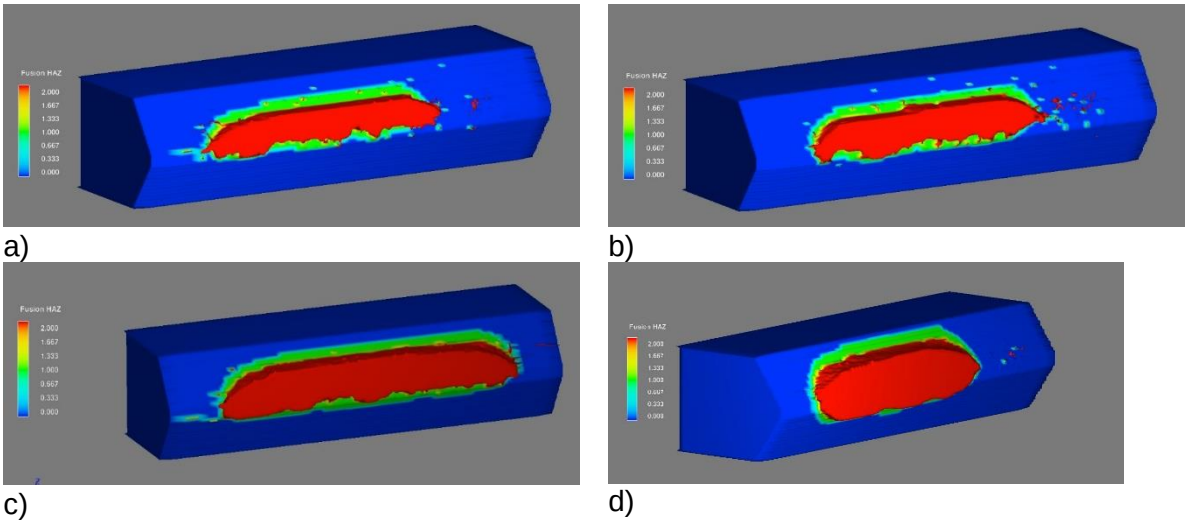

Figure 27. a) XMAG-2_4: Q = 0.58 kJ/mm, b) XMAG-2_5: Q = 0.65 kJ/mm, c) XMAG-2_1: Q = 0.82 kJ/mm and d) XMAG-2_7_10.5: Q = 1.07 kJ/mm. Red = fusion zone, green = HAZ.

As can be seen in Figure 27, the heat input values lower than the basic case, ie. 0.58 and 0.65 kJ/mm, result in incomplete penetration and very irregular root quality. This could be expected, because the basic case values were defined experimentally. Furthermore, it can be concluded that the basic case parameters are very close to the optimum feasible heat input range. Increasing the heat input to 1.07 kJ/mm leads inevitably in complete penetration and root sagging: in reality, this would be very close to a burnthrough situation. The two largest heat inputs led to even more pronounced sagging, ie. in reality a certain burnthrough.

When comparing the fusion zone and HAZ dimensions in the simulation cross sections of Figure 28, the results follow logically the above 3D images of Figure 27. The lowest heat input of 0.58 kJ/mm results in practically no penetration in the air gap. On the other hand, the highest heat input case was not taken into comparison because of the burnthrough, ie. an unacceptable weld.

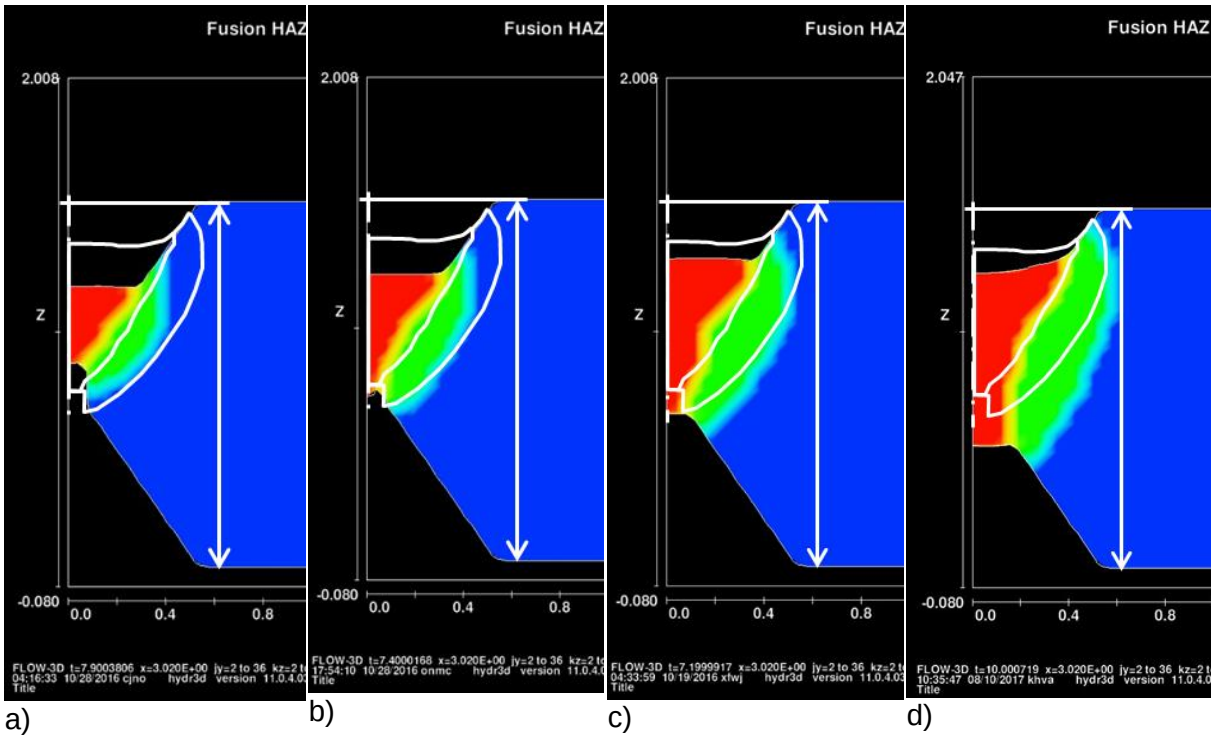

Figure 28. Fusion zone and HAZ: a) Q = 0.58 kJ/mm, b) Q = 0.65 kJ/mm, c) Q = 0.82 kJ/mm and d) Q = 1.07 kJ/mm. Red = fusion zone, green = HAZ and white = macrograph borders.

In the intermediate cases both the penetration, fill height and HAZ width and overall geometry follow logically the applied heat input and wire feed rate. However, as was already noted the simulation tends to overestimate both the penetration and HAZ width of the reference weld root pass.

Simulation results: thermal efficiency effect

It was noticed already in the very first TIG weld simulation results that the thermal efficiency value used in the customisation may have a marked effect on the agreement between the simulation and the validation test results. Therefore, a comparison was made between the thermal efficiency value k = 0.8, which is the most commonly used single value and also specified in the relevant welding standards, and a slightly higher k = 0.85. The latter is commonly used as a practical maximum value and also well in line with the arc efficiency range of 0.84 ± 0.04 defined by DuPont and Marder (1995). A comparison of thermal efficiencies 0.80 and 0.85 kJ/mm is presented in Figure 29.

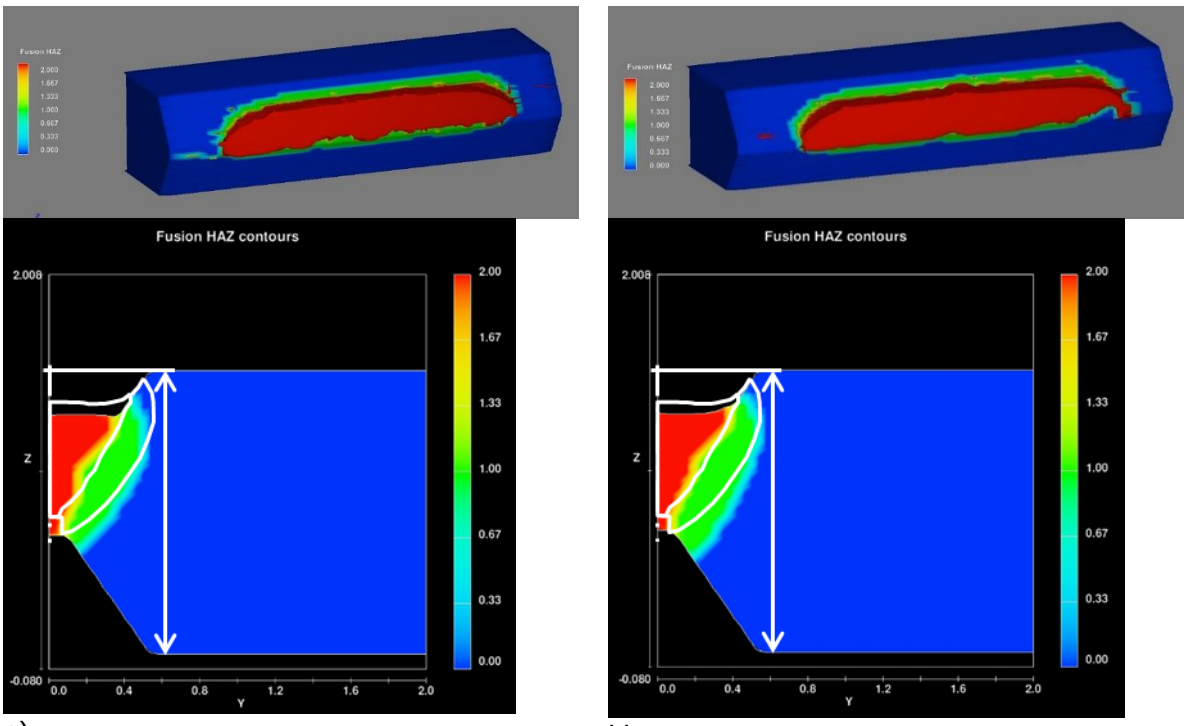

a) b)

Figure 29. a) XMAG-2_1 root: k = 0.80 and b) XMAG-2_8 root: k = 0.85. Red = fusion zone, green = HAZ and white = macrograph borders.

The simulations show clearly that in the case of MAG welding the thermal efficiency effect is not very pronounced. The main effect is the evenness of the weld root with the higher efficiency k = 0.85 as compared to the reference case value k = 0.8. Also the HAZ is slightly wider but the penetration and fill height are more or less the same in both the cases.

Simulation results: torch angle effect

In practical welding cases a key parameter is the torch angle with respect to the traverse direction. Therefore a comparison was made with the basic case torch angle α = 0° and a pushing α = +10°, Figure 30.

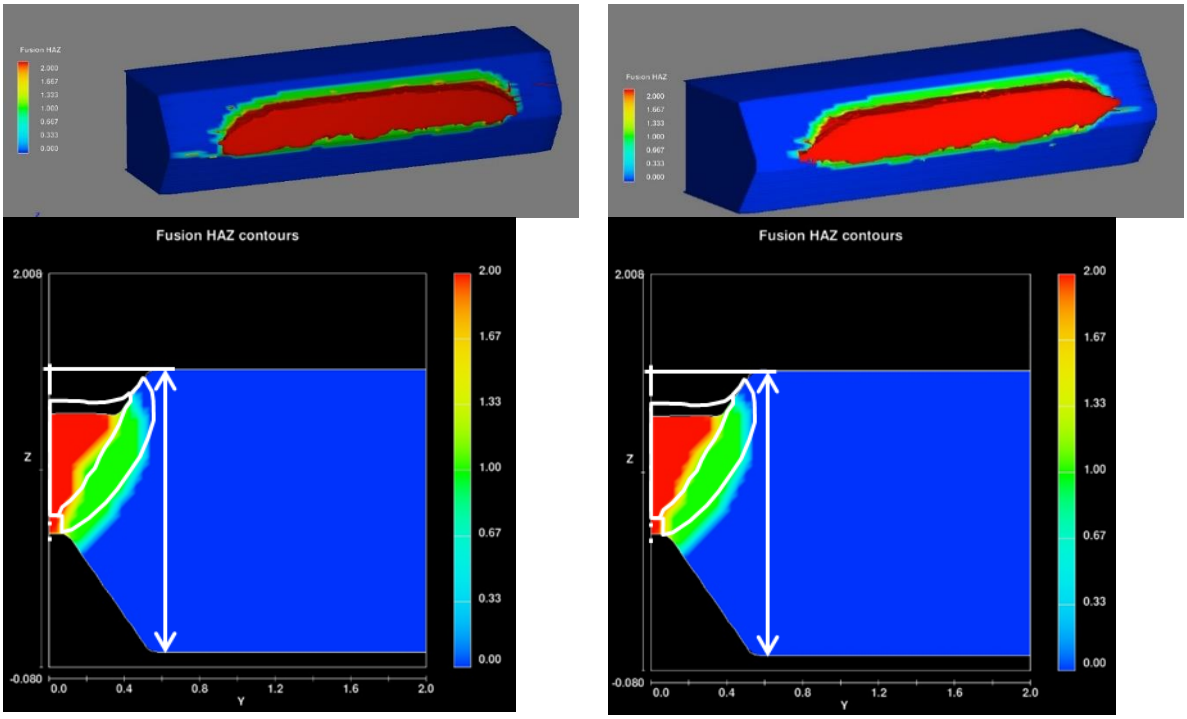

a) b)

Figure 30. a) XMAG-2_1 root: α = 0° and b) XMAG-2_10 root: α = +10° (pushing). Red = fusion zone, green = HAZ and white = macrograph borders.

It can be clearly seen in Figure 30 that there is practically no effect of the torch angle seen in the simulation results. The penetration, fill height and HAZ are more or less the same in both simulation cases.

Simulation results: droplet velocity effect

As stated earlier, the initial Flow 3D simulation conditions, including the arc parameters (pressure, EMF, heat flux) and material data, were used from the KAIST customisation as such. However, since the originating case for this data was not known, it was decided that rough sensitivity check should be made. Due to practical reasons, the deposited weld metal droplet vertical speed was selected for this purpose, mainly because it is described in the customisation as a single numerical value. Thus, a comparison was made between the droplet Z direction velocity component of the basic case v_{dropZ} = -50 m/s and a 20% increased value of v_{dropZ} = -60 m/s, Figure 31.

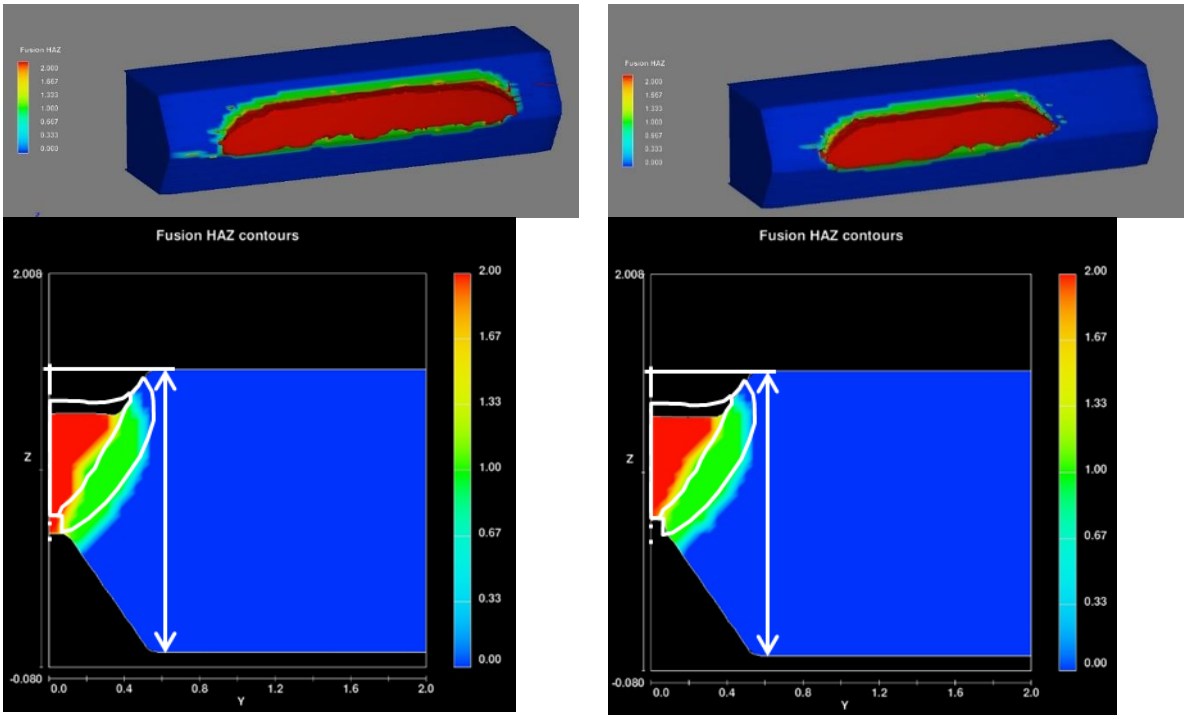

a) b)

Figure 31. a) XMAG-2_1 root: v_{dropZ} = -50 m/s and b) XMAG-2_9 root: v_{dropZ} = -60 m/s. Red = fusion zone, green = HAZ and white = macrograph borders.

As was the case with the torch angle effect of Figure 30, the difference between the two different velocity value was marginal in both cases. Although Figure 31b shows incomplete penetration in the air gap with the higher velocity, a more detailed examination revealed that it was a local disturbance that can be seen with both cases in the top 3D images of Figure 31a and b. The HAZ appearance and the fill height are in practise equal with both velocities.

Simulation results for FE deformation analysis source data

One of the key goals of the project was to utilise the Flow 3D CFD simulation results as a key data for consequent FE analyses to be further used for the definition of the deformation and residual stress evolution during the weld cooling after solidification. For this purpose, the data transfer from Flow 3D to Sysweld FE software was demonstrated, Figure 32.

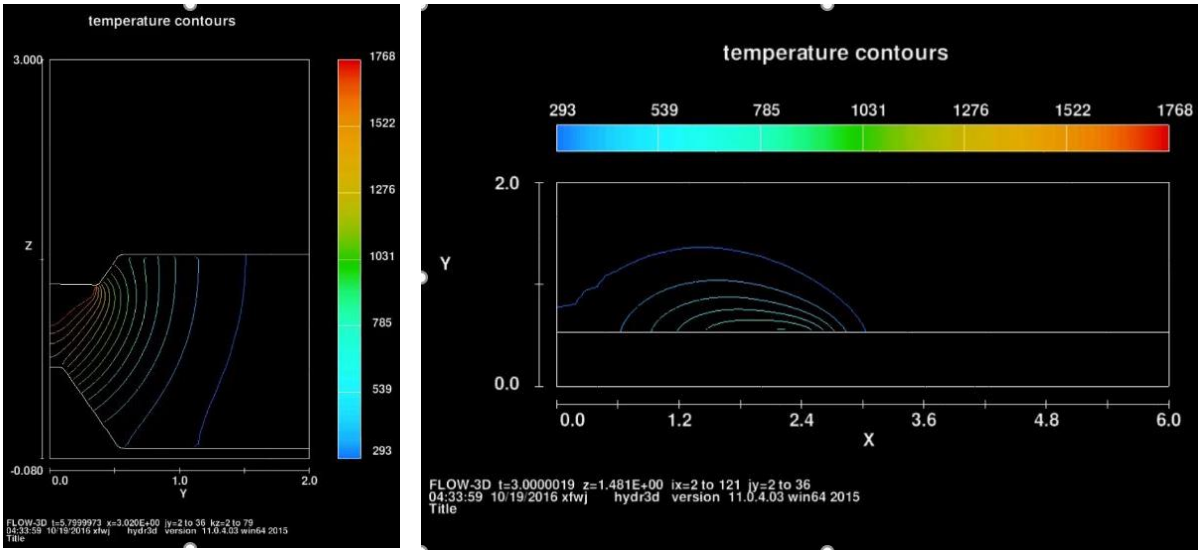

a) b)

Figure 32. The basic case XMAG-2_1 root weld temperature contours. a) YZ view: X = 30 mm = 20 mm from weld start, t = 5.8 s, and b) XY view: Z = 15 mm = top surface, t = 3 s.

Flow 3D allows the examination of eg. the temperature distribution in 1D (point), 2D (cross section) or 3D views as a function of time. Figure 32 shows the visualisation of the isotherms in two 2D configurations and thermal histories of single point were utilised in the $t_{8/5}$ analyses, as described in chapter 5.2.2 Reference case simulation results, Table 5. However, all this data can also be exported in numerical ASCII form that can be read into a FEA package relatively easily, see also the following chapter 6 Thermo-mechanical FE analyses using Sysweld software.

Summary on simulation results vs. validation weld

Generally, it can be concluded that the Flow 3D simulation with the KAIST customisation tend to typically overestimate the HAZ width as compared to validation in the reference case. Furthermore, the penetration in the air gap is typically overestimated, too, although variation in penetration, ie. the location of the studied cross section, also plays a role.

The plate width has no marked effect on simulated final fusion zone or HAZ geometry, but it does have an effect on temperature distribution during welding. As could be expected, the wire feed rate, i.e. heat input, has a crucial effect on penetration. However, excessive sagging at the root occurring in some simulation cases is unrealistic, but higher heat inputs would in reality lead into burn through.

The thermal efficiency effect is logical: increasing the *k* value smoothens the root penetration, i.e. removes the occasional defects. In practise, the thermal efficiency can be affected eg. the choice of shielding gas, and particularly the CO_2 content. The torch angle has marginal effect on penetration or HAZ width. The simulation results have also been reported in Sirén and Martikainen (2016).

5.5.5 Mild steel arc welding case residual stress measurements

Contour method is relatively new method for measuring two-dimensional residual stress contours destructively. The method is based on measuring displacement caused by relaxation of residual stresses on a cut surface. For the measurement, the sample to be studied is cut in two pieces. If the studied sample was free from residual stresses, the cut surfaces will retain their planeness. However, if residual stresses existed in the cut surface, those stresses are now relaxed by the cutting process and cause deviations from planeness on the cut surface.

These deviations resulting from relaxation of residual stresses can be measured, e.g., by co-ordinate measurement machine and analyzed to reveal the residual stress contours. The main advantages of this method are the attainable 2-dimensional stress contour and the robustness of solving residual stresses from the measured surface displacements.

The method assumes, as with all relaxation techniques for residual stress measurement, that the relaxation of residual stresses occurs elastically and that the cutting does not induce stresses. In addition, because the displacements are measured directly from the cut surface, it is assumed, that the cut occurs along a plane that was flat when the cutting started. This assumption requires, that the sample is constrained from both sides, when the cut is made. The main error sources for this method are inadequate constraint during cutting and possible stresses caused by the cutting. A more detailed description of the contour method can be found online from Los Alamos National Laboratory´s web pages by Prime & DeWald (2013).

In this project, contour measurement was performed to three welded joints provided by VTT. The samples were carbon steel welds; two butt-welds of 25 mm AH420(sample 1) and 15 mm S355 (sample 2) plates, and one fillet welded T-section of 15 to 25 mm AH420 plates (sample 3).

For the contour measurement, the samples were cut with electric discharge machining (EDM) at Aalto university. The cut surfaces were measured by 3D measurement system by VTT and white light interferometry by Aalto university. The resulting measurement data were analyzed by Aalto in-house developed code and, finally, residual stresses solved by open-source Elmer finite element code.

All the measured welds show high residual stresses due to weld process, as expected. The residual stresses are highest in the 25 mm butt-weld sample. The location of the highest tensile stress is well within the weld. Sample 2 showed lower stresses and also displayed two separate stress concentrations one below the top bead of the weld and another below the bottom bead of the weld. The T-junction showed asymmetric residual stress distribution with highest stresses located near the weld presumably welded last.

More detailed contour measurement results can be found in the full Aalto University report in Appendix 2. A comparison of the contour measurement results to the FE analysis is being done in the following chapter 6 Thermo-mechanical FE analyses using Sysweld software.

5.6 References

Chandel, R.S., Seow, H.P., Cheong, F.L. 1997. Effect of increasing deposition rate on the bead geometry of submerged arc welds. Journal of Materials Processing Technology 72 (1997), 124-128

Cho, D-W, Kiran, D.V., Song, W-H. and Na, S.J. 2014. Molten pool behavior in the tandem submerged arc welding process. Journal of Materials Processing Technology 214 (2014) 2233–2247

DuPont, J. N. and Marder, A. R. 1995. Thermal efficiency of arc welding processes. Welding Journal - Including Welding Research Supplement, 74 (12), 406s.

Esab. Products and solutions. Mild steel / Low alloy Fluxes. OK Flux 10.71 documents and specs. 2017. http://www.esabna.com/us/en/products/index.cfm?fuseaction=home.product&productCode=420014&tab=2. Referred to on 5 July, 2017

García, V.G. 2004. Constitutive relations to model the hot flow of commercial purity copper. PhD thesis, Universitat Politècnica de Catalunya 2004. http://hdl.handle.net/10803/6043

Karhu, M.; Kujanpää, V.; Gumenyuk, A.; Lammers, M. 2013. Study of Filler Metal Mixing and its Implication on Weld Homogeneity of Laser-Hybrid and Laser Cold-Wire Welded Thick Austenitic Stainless Steel Joints. Proceedings of 32nd Int. Congress on Lasers and Electro-Optics (ICALEO2013), Oct. 6-10, 2013, Miami, FL, U.S.A. Laser Institute of America. Miami, Florida, U.S.A. (2013), 252-261

Kuitunen, M. 2016. Comparison of the material modelling performing characterization of weld microstructure of S355N steel and defining of residual stresses. Master´s Thesis, Aalto University School of Engineering, Department of Mechanical Engineering. 97 p. + app. http://urn.fi/URN:NBN:fi:aalto-201606172637

Lincoln Electric. Resource Center. Process and Theory. Weld fusion vs. weld penetration. 2017. http://www.lincolnelectric.com/en-us/support/process-and-theory/Pages/weld-fusion-weld-penetration.aspx. Referred to on 5 July, 2017

Prime, M. B. and DeWald, A.T. 2013. The Contour Method. Chapter 5 in Practical Residual Stress Measurement Methods, G. S. Schajer (ed.), Wiley-Blackwell, 2013, pp. 109-138 http://www.lanl.gov/contour/

Sirén, Mika and Martikainen, Hannu. 2016. CFD simulation of MAG welded mid steel joints for FEM deformation analysis. Final seminar of Fidipro Na project, DIMECC 9th Annual Seminar, 14 - 15 November 2016, Helsinki, Finland, DIMECC Oy. 18 p.

Tello K. E., Gerlich A. P., Mendez P. F. 2010. Constants for hot deformation constitutive models for recent experimental data, Science and Technology of Welding and Joining, vol. 15, no. 3, pp 260-266

TWI. Technical Knowledge. Job Knowledge. Design - Part 3. 2017. http://www.twi-global.com/technical-knowledge/job-knowledge/design-part-3-092/. Referred to on 5 July, 2017

Voß, O. 2001. Untersuchung relevanter Einflußgrößen auf die numerische Schweißsimulation. Der Fakultät für Maschinenbau und Elektrotechnik der Technischen Universität Carolo-Wilhelmina zu Braunschweig. Forschungsberichte des Instituts für Schweißtechnik. Band 3. Shaker Verlag, Aachen, 2001. ISBN 3-8365-9119-4, ISSN 1617-2248. 188 p. + 100 p. app.

6. Thermo-mechanical FE analyses using Sysweld software

6.1 Background

Numerical and analytical methods can be used for optimization of welding process parameters. The aim of the current study was to evaluate the possibilities to use numerical methods for welding process optimization. The simulations were carried out by the Sysweld-program which is based on Finite Element Method (FEM). Sysweld has several different modules. In the current study, programs of Visual Environment (pre- and post-processing programs) and Sysweld -solver were used (single CPU-version). Material data was defined on the basis of Sysweld material database that includes some of the most common materials. The thermo-mechanical simulations were carried out as uncoupled: thermal simulation is followed by mechanical one - no backward coupling.

6.2 Simulations

Butt-welding experiments simulated were carried out at Lappeenranta University of Technology with parameters presented in Table 8 and Figure 34. Simulations were made using Sysweld solver (single CPU version: Windows64 - 2015.1 (17.1)). The problem was described by means of a 2D-model, Figure 33. Two-dimensional generalized plane strain elements were used (geometry described with 20008 elements and 20599 nodes). All beads were simulated in one run, taking care that the initial temperature of the specific process stage matches the experimental measurements (time between starting times of subsequent beads adjusted on the basis of this restriction).

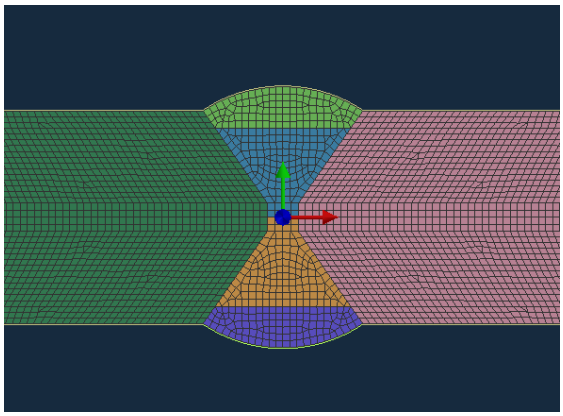

Figure 33. The mesh of the test piece (a piece of the model).

Heat input was described by Goldak's Double ellipsoidal heat source. The heat source input was adjusted by trial and error to match the experimental thermal cycles of thermocouples starting with the pool size calculated by the Flow-3D. The thermocouples on the back side of the plate and farthest from the weld were used for comparison, since it has been shown in open literature by Hansen (2003) that using thermocouples near the weld will lead to certain difficulties in validation, e.g. because of high temperature gradients present. For the first side weld, thermocouples Second_5 (18 mm from weld centerline) and Second_6 (23 mm from weld centerline), were used, Figure 34. For the second side weld, thermocouples First_5 and First_6, were used (thermocouples at equal distances as in the first side). Heat source parameters and iterated heat input parameters are presented in Figure 35 and Table 9, respectively. Default parameters were used for Power- and Length-ratio. Power-ration describes maximum front and rear -power intensities (front/rear= 1.2) and Length-ratio the Front and rear -lengths of the weld (front/rear = 0.5).

Table 8. Welding parameters (Kemppi Pro 5300).

Bead	Velocity [mm/min]	Wire feed [m/min]	Current [A]	Voltage [V]
Root W1	300	9.6	213	25.6
Surface W2	300	10.5	233	29.2
Root W3	300	9.6	212	25.7
Surface W4	300	10.5	230	29.3
Wire: ø 1 mm Aristorod 12.50 (EN ISO 14341-A: GSi3) Gas: Awomix Argon 8% CO_2; flow rate 16 l/min Weld backing: ø 7 mm Ceramic round bar,				

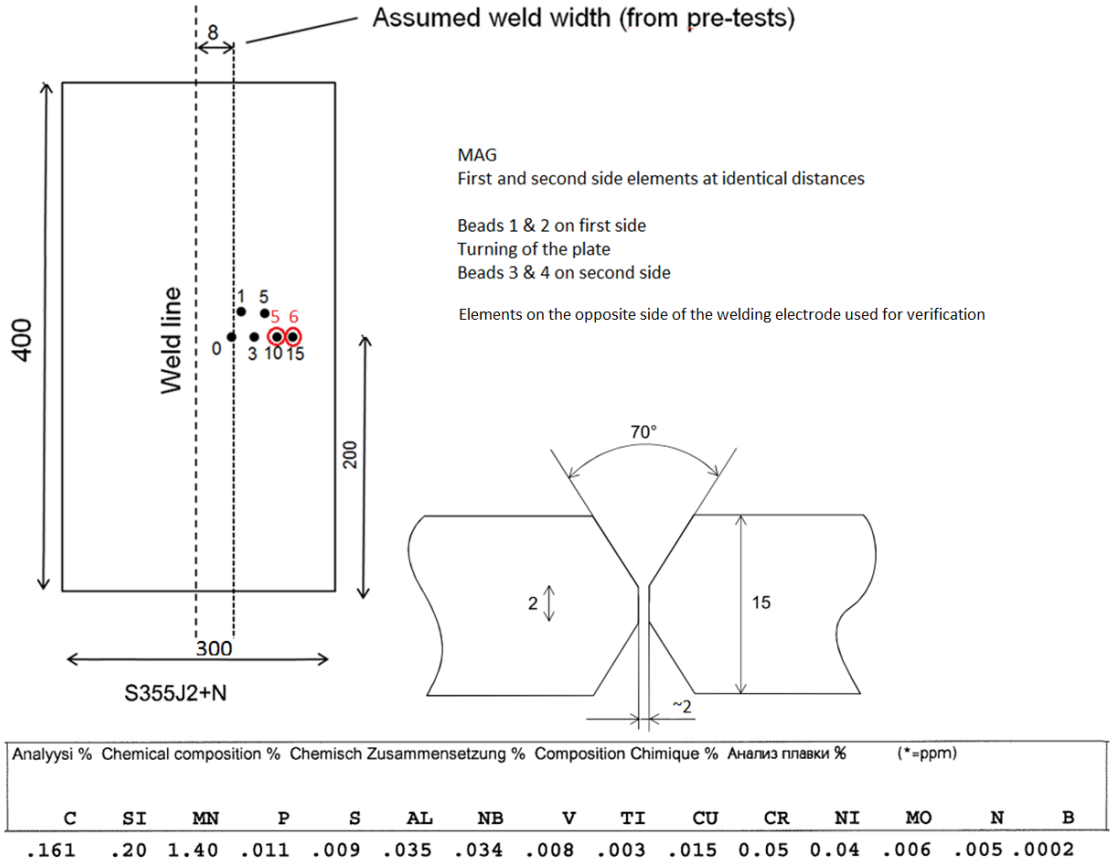

Figure 34. Butt-weld -plate and location of thermocouples. Thermocouple IDs are shown in red numbers.

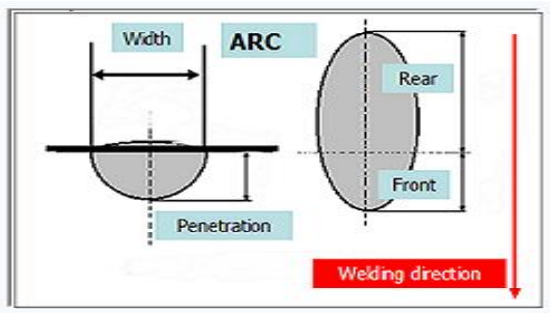

Figure 35. Heat source parameters.

Table 9. Heat input parameters for each weld.

Parameter	W1 [mm]	W2 [mm]	W3 [mm]	W4 [mm]
Length (= front + rear)	4.5	19.9	4.7	19.0
Width	4.5	13.0	4.7	14.0
Penetration	6.0	4.5	5.5	4.0
Efficiency	0.88	0.88	0.88	0.88

The emissivity and convective losses used, were calibrated on the basis of the measured cooling curve. Thermal boundary conditions used are as follows:

- emissivity 0.7
- free air cooling: convective losses 8 W/m^{2}K (for all boundaries),
- ambient temperature 22°C
- initial temperature of the plate 22°C

In terms of mechanical restraints, only rigid body motions were eliminated: a free support of the plate was used, Figure 36

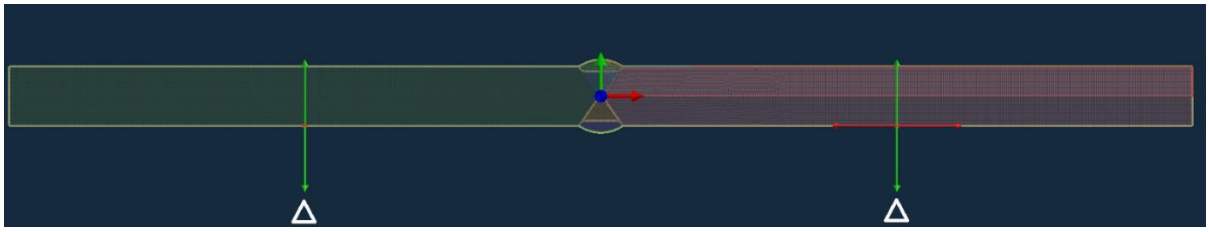

Figure 36. Mechanical restraints (fixed freedoms shown by long arrows; given using two nodes).

6.3 Material properties

For the welding tests SSAB provided plates of S355J2+N. The plates were welded by using OK Aristorod 12.50 wire with diameter 1 mm (with gas Awomix 8% CO_2). Material W_S355J2G3 of Sysweld material database was used in the simulations. The same material properties was used both the base plate and weld. The hardening law of the material model is isotropic. The model includes transformation plasticity. The composition of the material is as follows: C = 0.18, Mn = 1.6, P = 0.035, S = 0.035, Si = 0.55. It should be noted that for some material properties the Data Base uses “average values for not and low alloyed steels”. The material properties used are presented in Figure 37 though Figure 40.

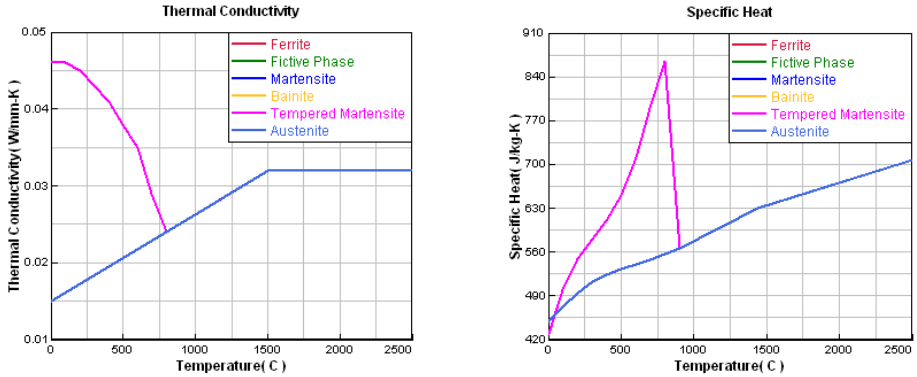

Figure 37. Thermal Conductivity and Specific Heat (W_S355J2G3). The melting and solidification enthalpy is not taken into account.

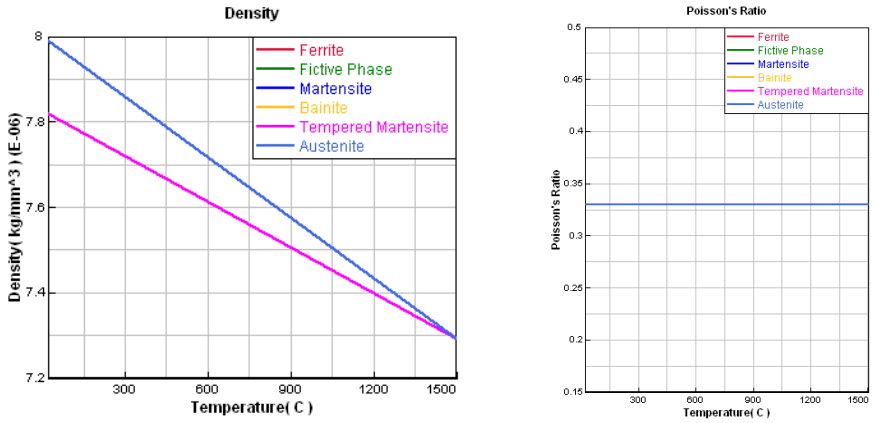

Figure 38. Density and Poisson's ration (W_S355J2G3).

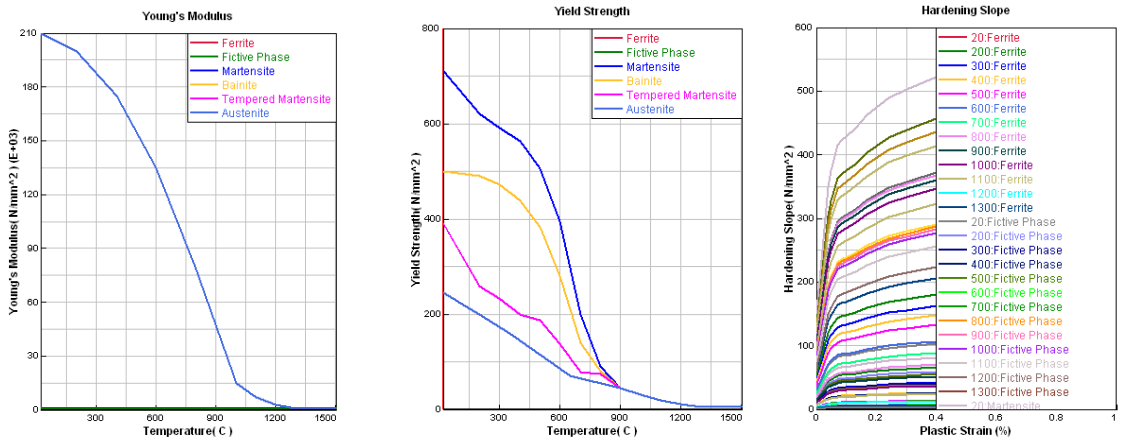

Figure 39. Young's Modulus, Yield strength and Hardening slope (W_S355J2G3).

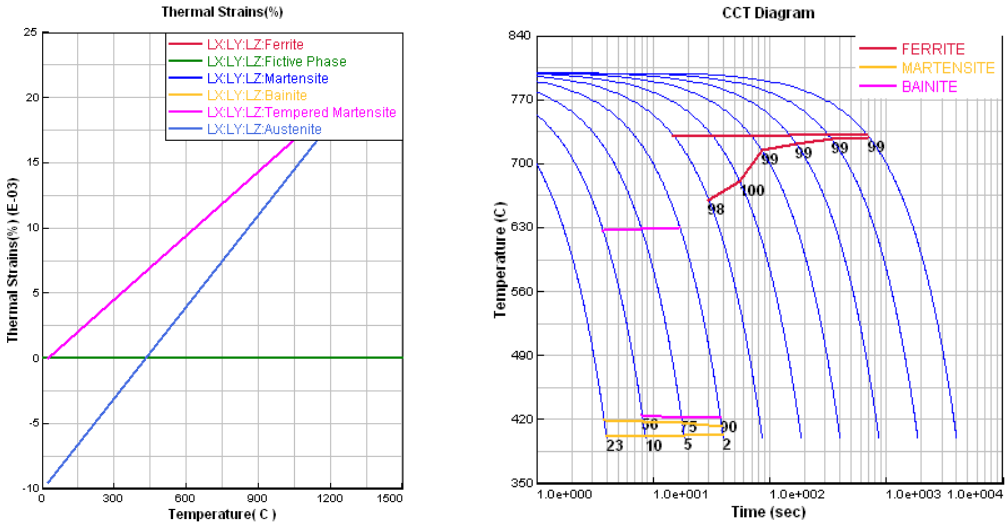

Figure 40 Thermal strains and CTT, W_S355J2G3 (diagram is not complete because of a bug in the program).

6.4 Results

Solving of the complete welding process took about 1942 CPU seconds using Dell Precision Workstation with Intel® Xeon® CPU E5-2650 v3@ 2.30GHz. Simulation results and comparison with experimental ones are presented in following chapters.

6.4.1 Thermo-metallurgical simulations

The simulated temperature field and experimental penetrations are presented in Figure 41 through Figure 43. It should be born in mind that the solidus temperature of S355 depends on the analysis and is typically around 1500 °C.

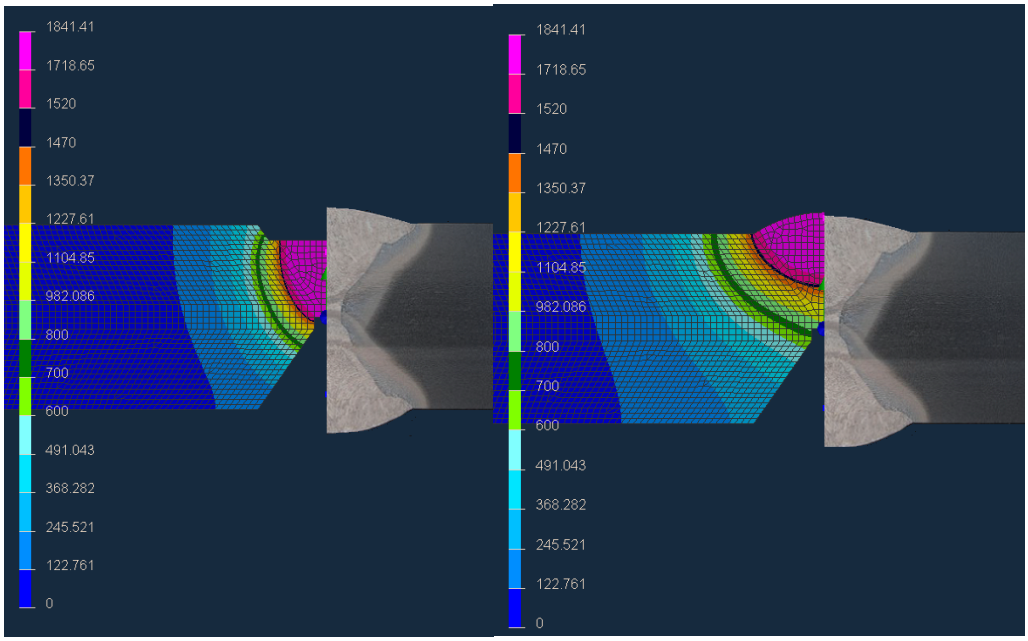

a) W1 b) W2

Figure 41. Simulated temperature and experimental penetration of beads W1 and W2.

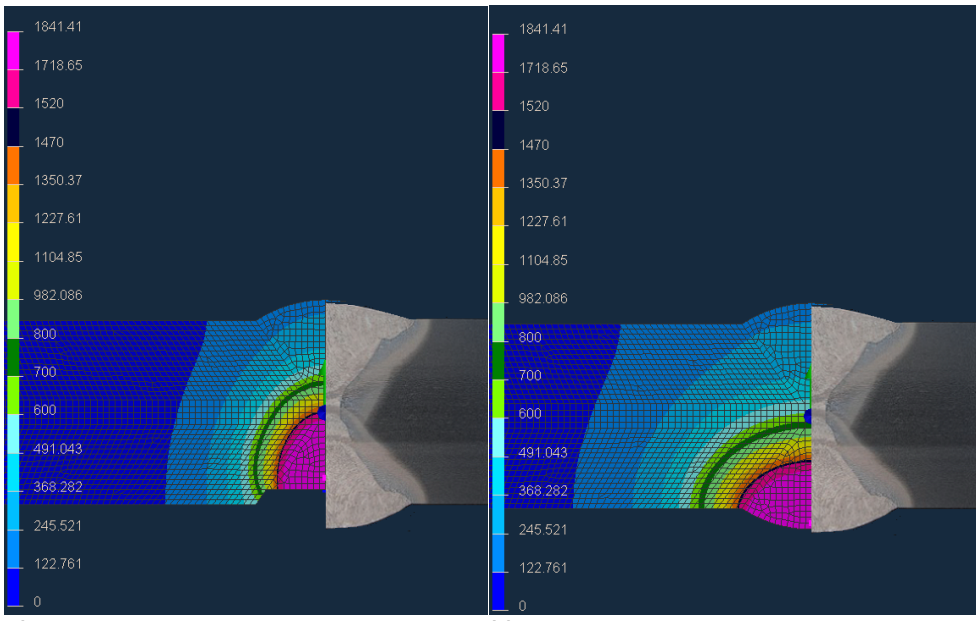

a) W3 b) W4

Figure 42. Simulated temperatures and experimental penetrations of beads W3 and W4.

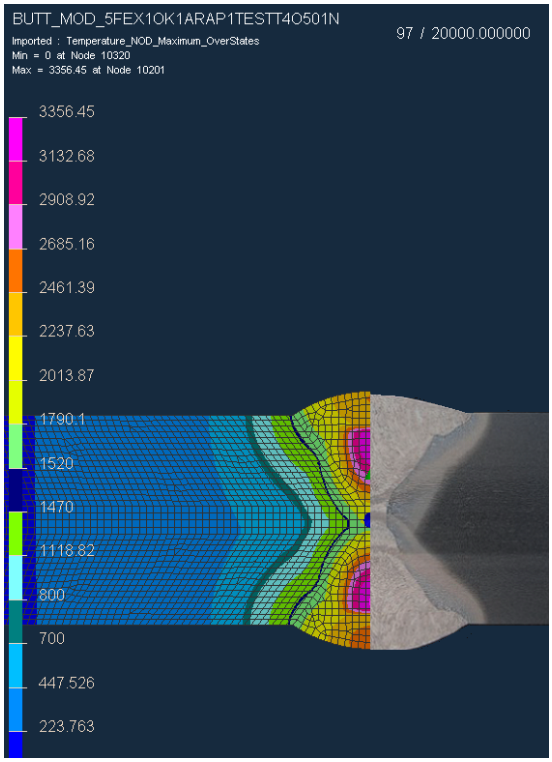

Figure 43. Multipass weld: simulated temperatures (maximum value) and experimental penetrations.

Cooling times ($t_{8/5}$) of the weld metal (around in the centre of the bead) calculated by means of numerical and analytical methods are presented in Table 10.

Table 10 Cooling time $t_{8/5}$ [s]. Analytical equation for 2D heat conduction used:
$t_{8/5} = (4300-4{,}3*T_0)*10^5*(k^2*E^2)/d^2*[1/(500-T_0)^2 - 1/(800-T_0)^2]*F_2$,with $F_2=1$;
(T_0 = starting temperature [°C], K = efficiency, E = energy [kJ/mm], d = thickness [mm])

Weld	**W1 $t_{8/5}$ [s]**	**W2 $t_{8/5}$ [s]**	**W3 $t_{8/5}$ [s]**	**W4 $t_{8/5}$ [s]**
Numerical*)	5	9.2	4.8	8.9
Analytical**)	3.9	6.5	4.1	6.5
*) Thermal efficiency K = 0.88 **) SFS-EN 1011-2: 2001; thermal efficiency K = 0.88				

Comparison of experiments and calculated temperatures on the backside of the welding: thermocouples 5 (18 mm from centreline) and 6 (23 mm from centreline), Figure 44 to Figure 47. Because of the discrete mesh, the calculated and experimental measurement points are not exactly at the same position. However the error is negligible.

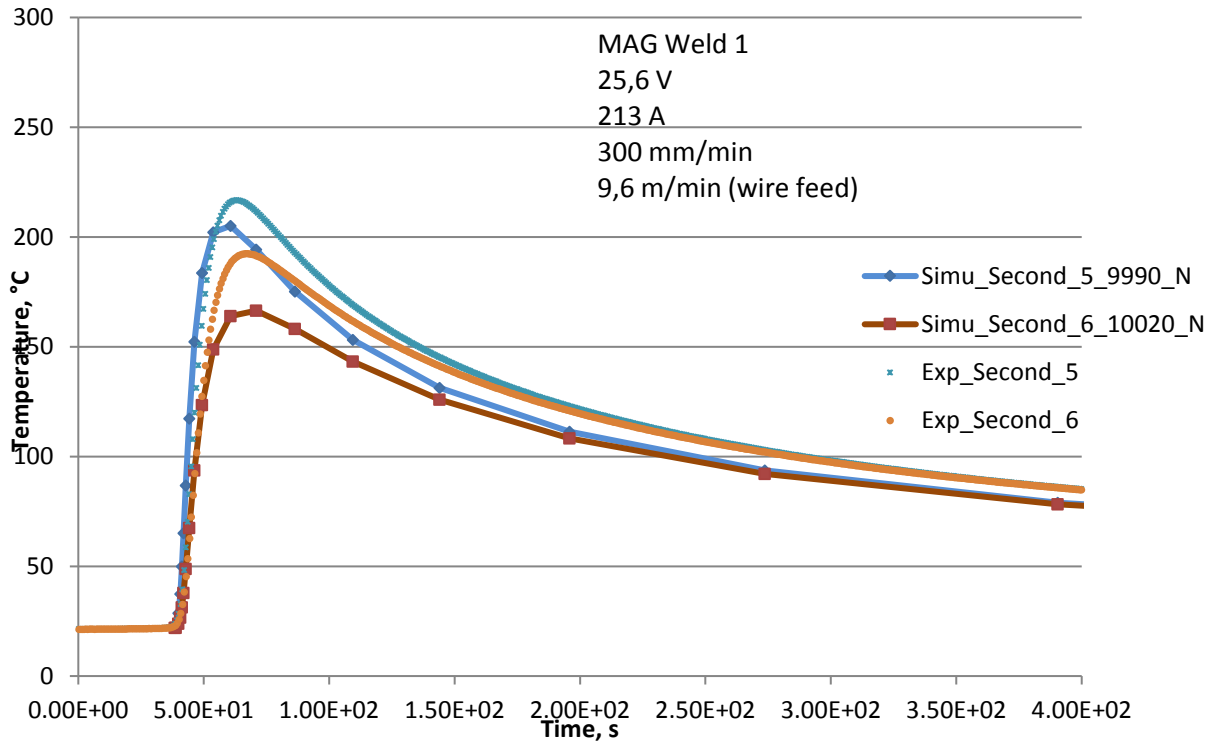

Figure 44. Simulated and experimental temperatures for the First side bead W1 with thermo-couples on the Second side.

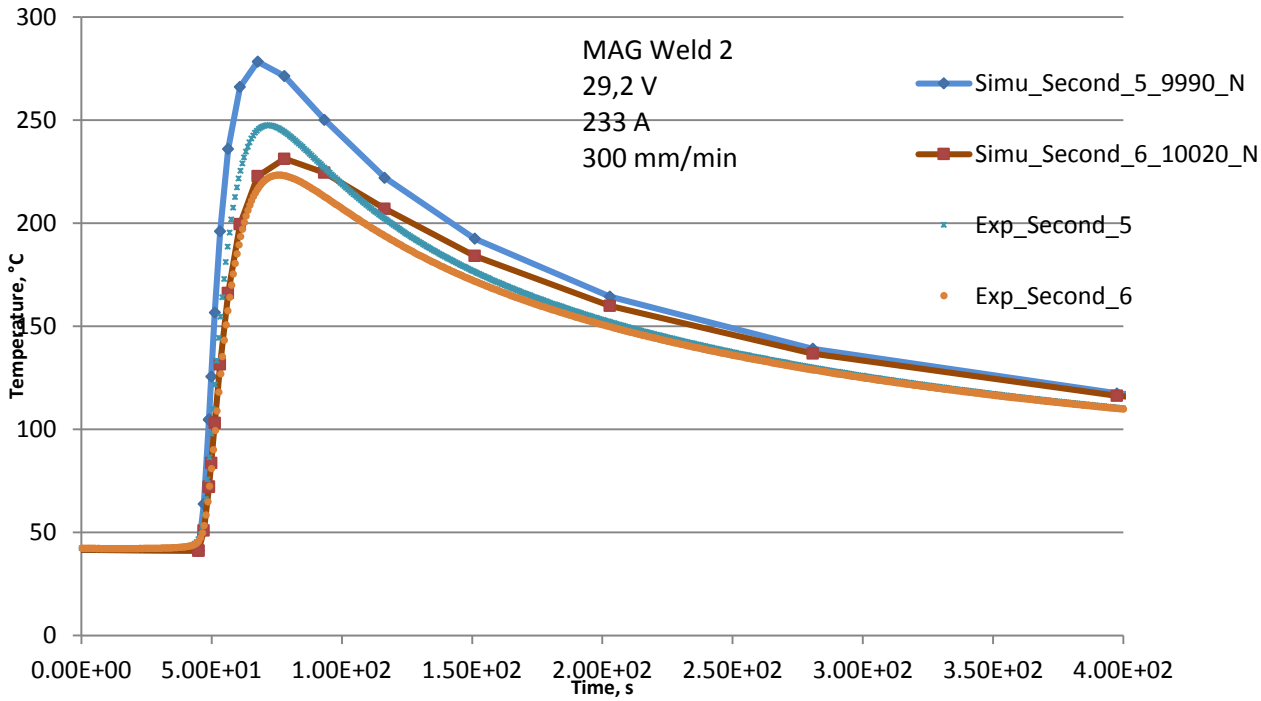

Figure 45 Simulated and experimental temperatures for the First side bead W2 with thermo-couples on the Second side.

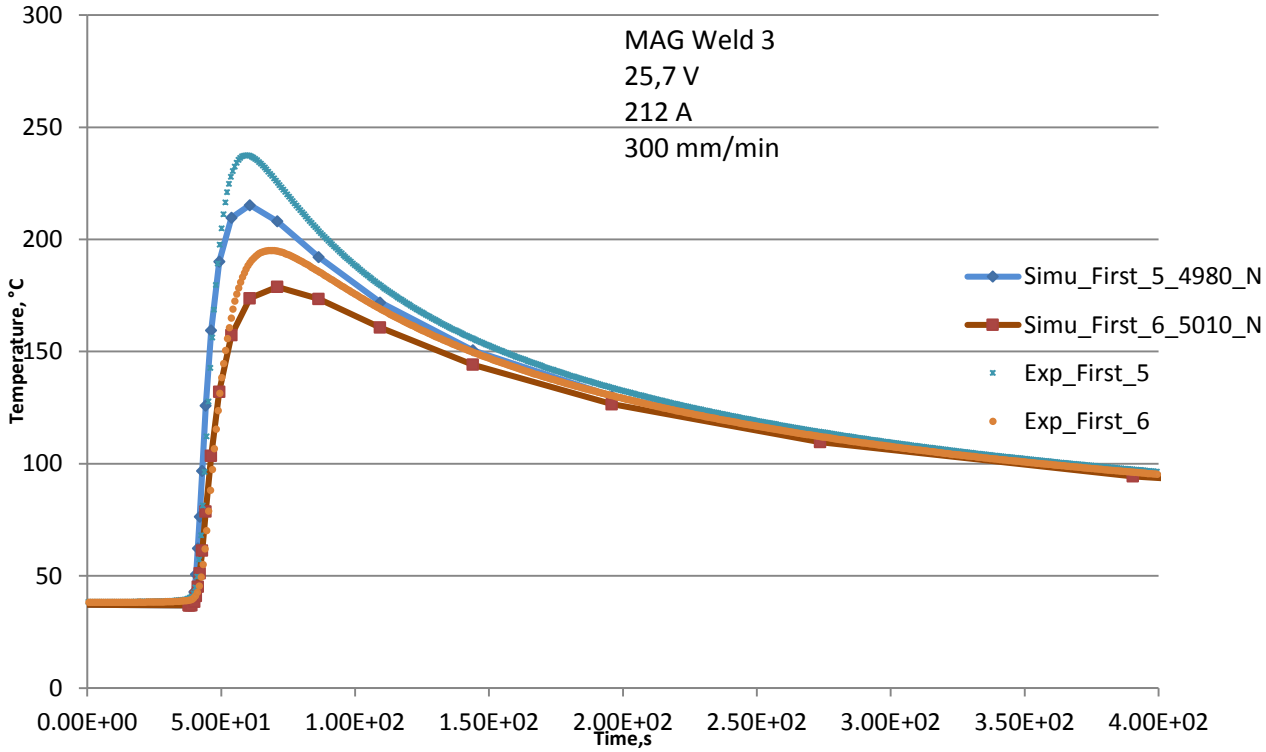

Figure 46 Simulated and experimental temperatures for the Second side bead W3 with thermocouples on the First side.

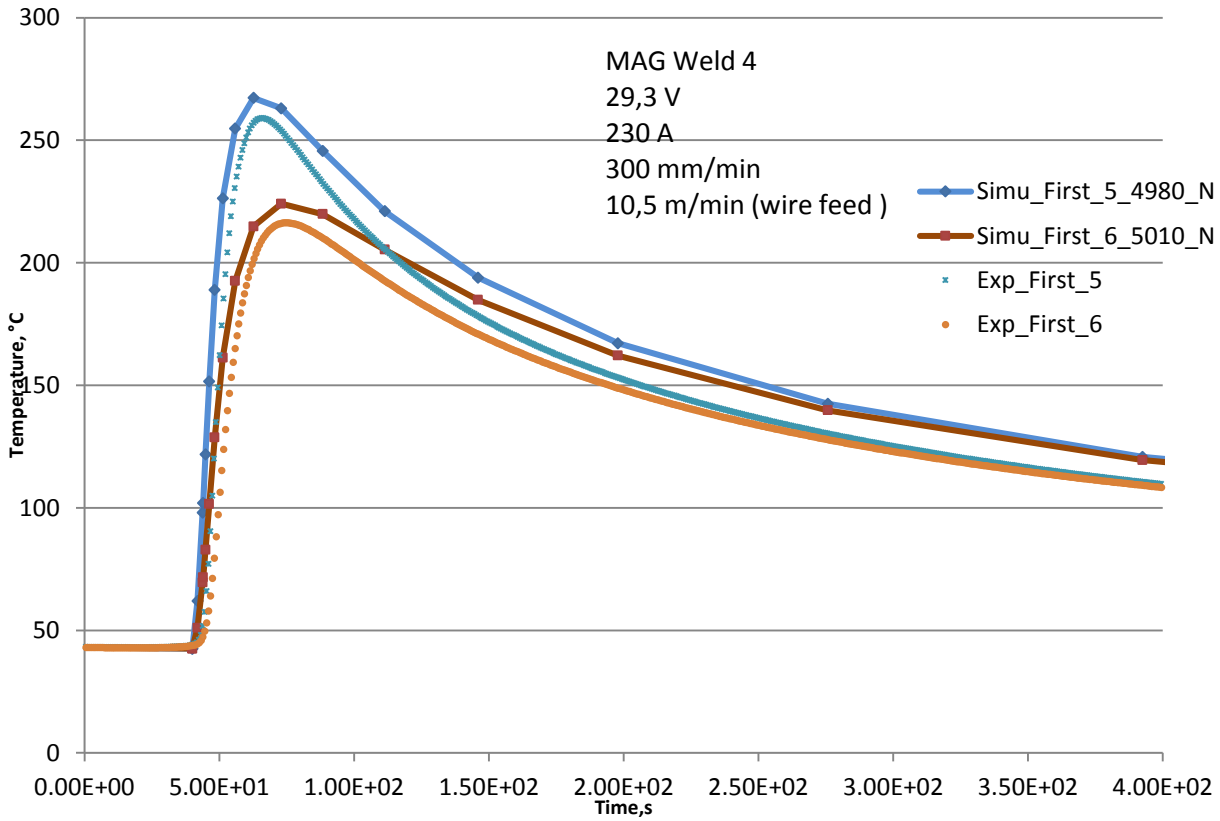

Figure 47. Simulated and experimental temperatures for the Second side bead W4 with thermocouples on the First side.

Calculated phases are presented in Figure 48 and Figure 49 (no experimental data available).

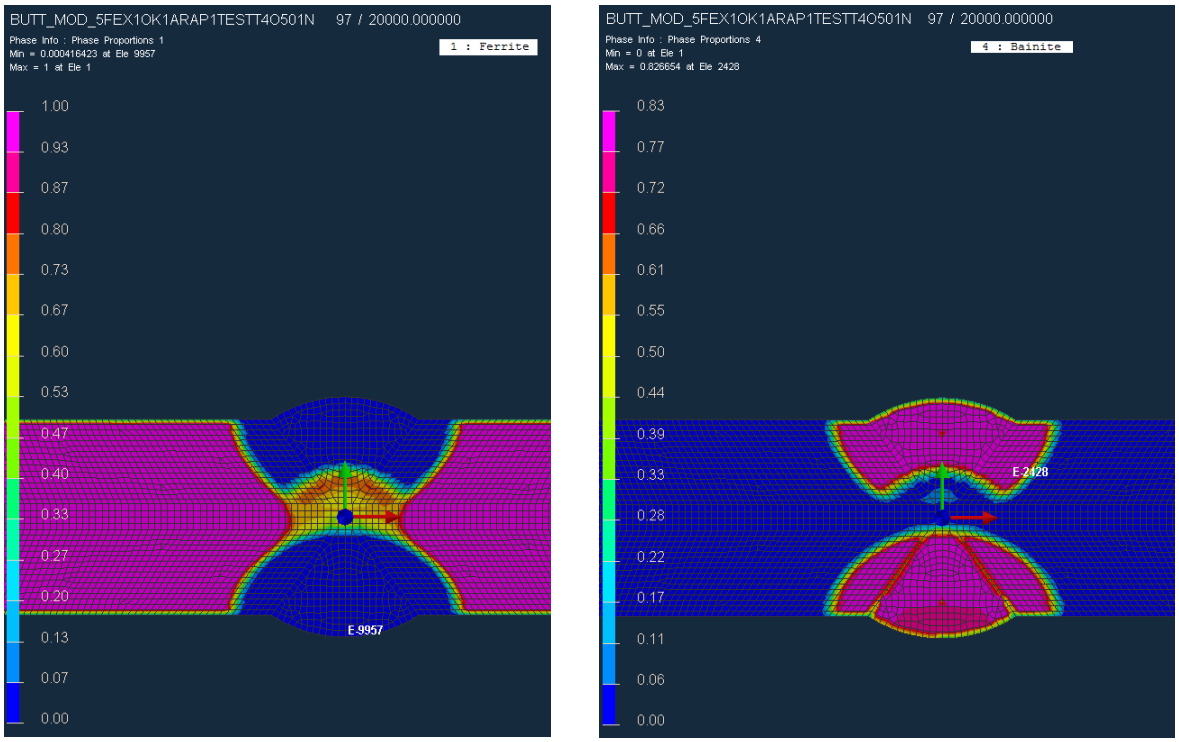

Figure 48 Ferrite and bainite [%].

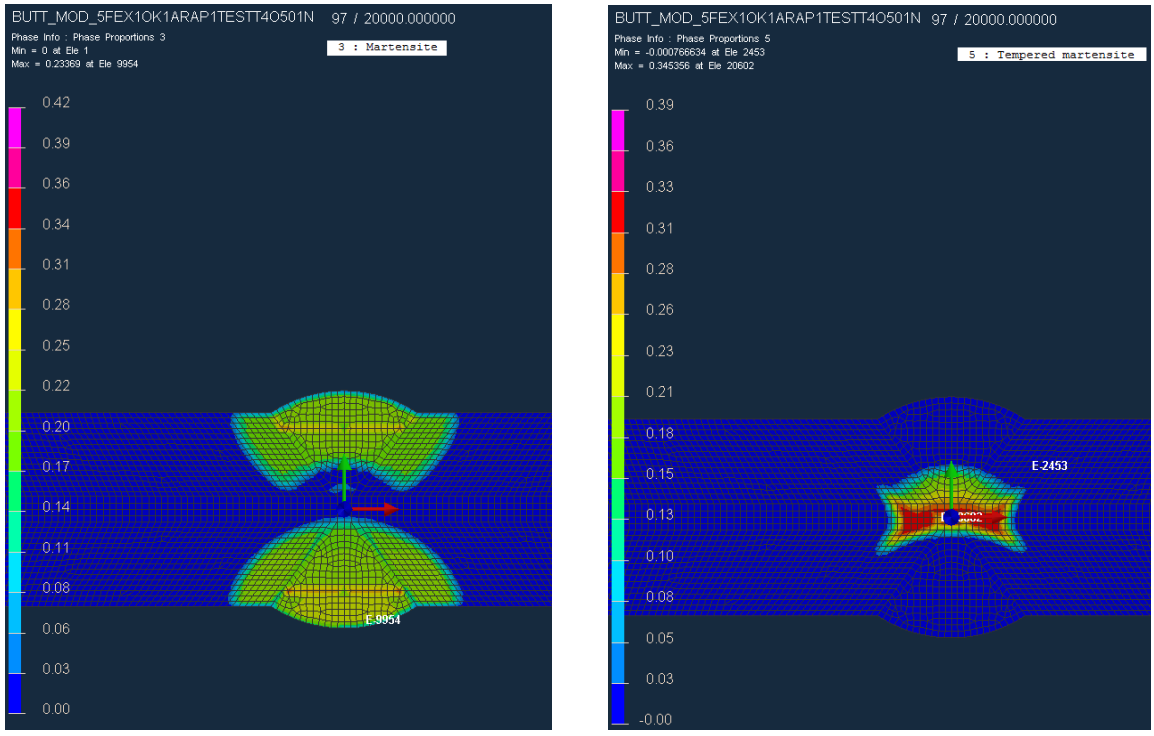

Figure 49 Martensite and Tempered martensite [%].

6.4.2 Mechanical simulations

Distortions of the plate after beads W2 and W4 are presented in Figure 50 and Figure 51, respectively. In addition to 2D-simulations preliminary computationally intensive (several days) analysis with 3D-model were tested with the same input parameters: the distortion was opposite than in tests (the plate was contracted on the final weld side after W4: the same tendency as in 2D-simulations).

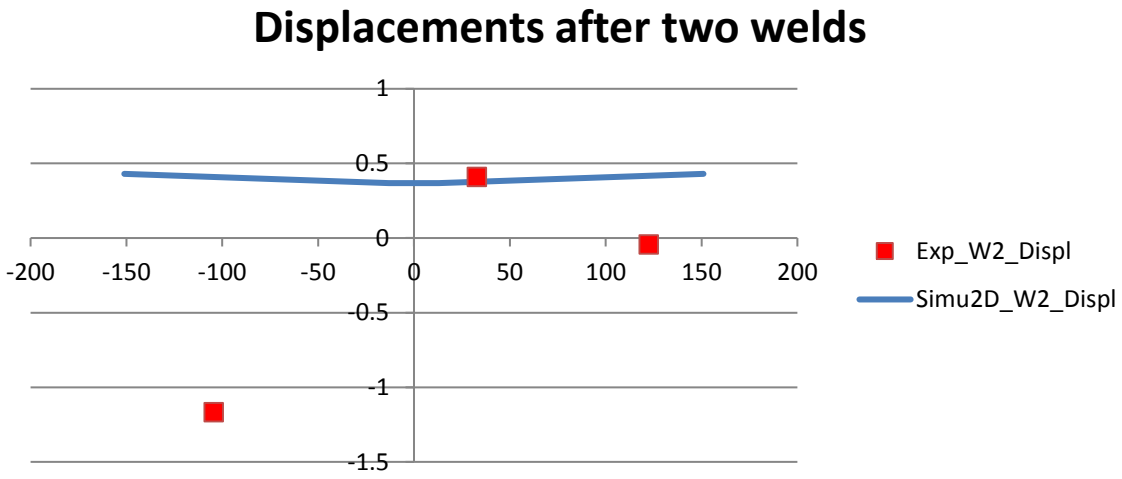

Figure 50 Experimental and simulated displacements after W2 in a transversal line around the middle of the plate [mm]. Weld line in the origin. Plate is in the measurement position: First side up.

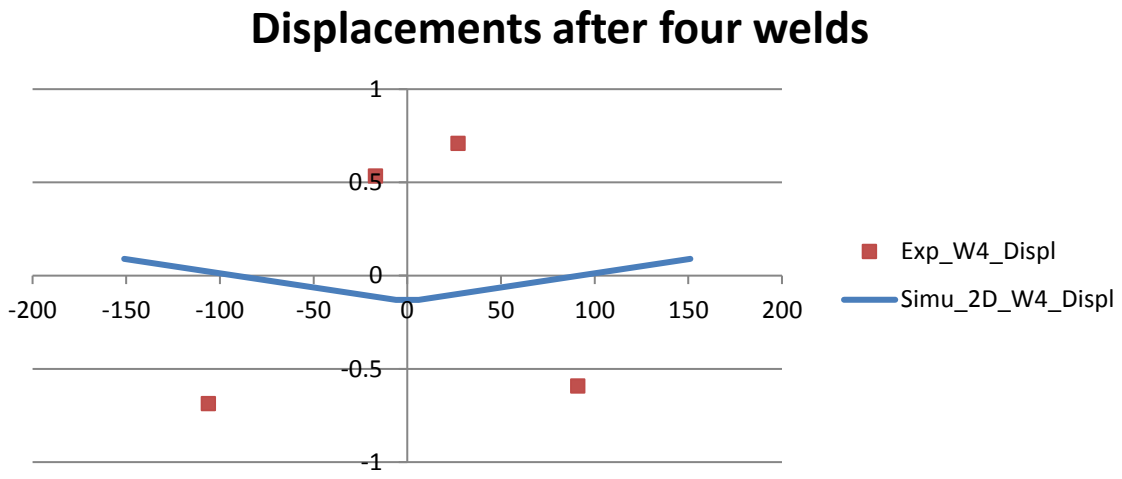

Figure 51 Experimental and simulated displacements (relative to the coordinates after W2) after W4 in a transversal line around the middle of the plate [mm]. Weld line in the origin. Plate in measurement position: Second side up.

Von Mises, transversal and perpendicular stresses are presented in Figure 52 and Figure 53, respectively.

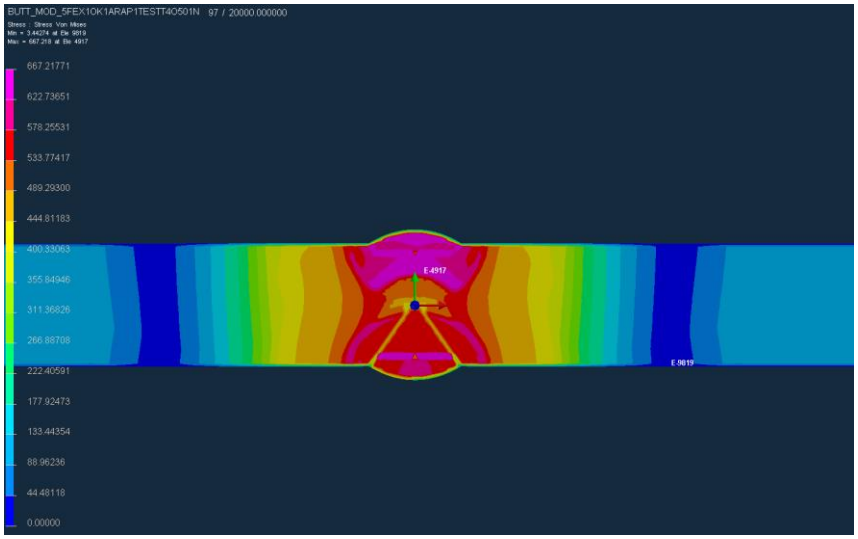

Figure 52 Von Mises stress [MPa].

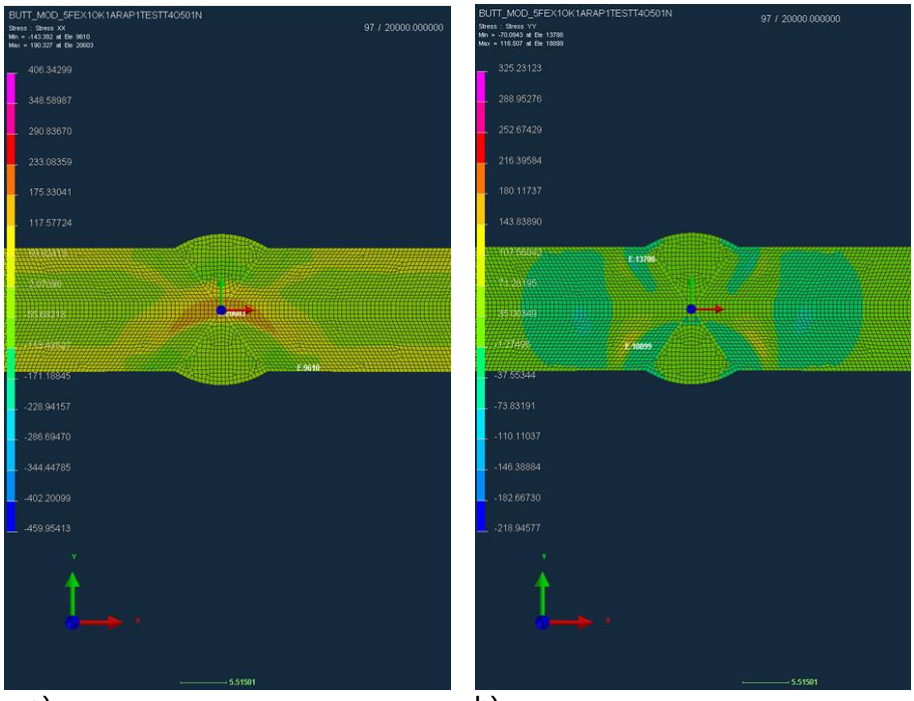

a) b)

Figure 53 a) Transversal stress, b) Perpendicular stress; [MPa].

Simulated longitudinal residual stresses and experimental ones measured by means of 3D- and white light methods as described in Virkkunen (2016) are presented in Figure 54.

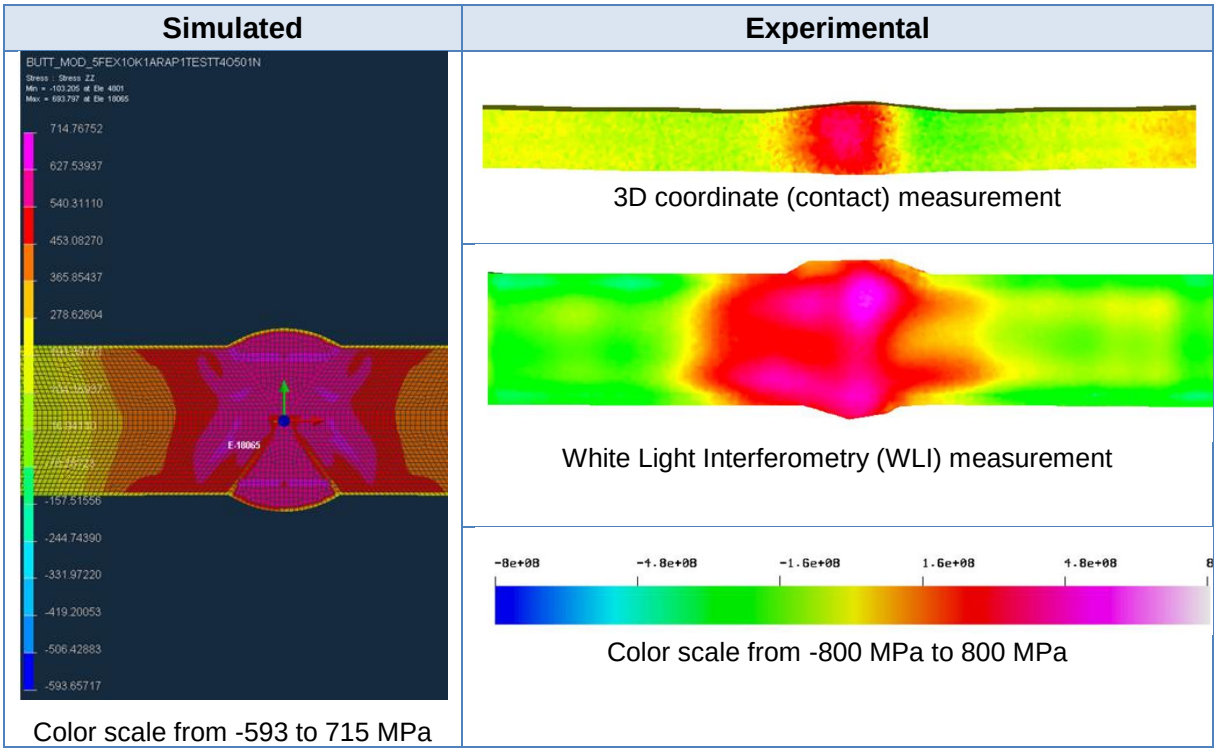

Figure 54 Longitudinal stresses (plate cut at location of about 50 mm from the weld end).

6.5 Discussion

The thermo-metallurgical simulation is followed by mechanical simulation: there are no backward couplings. In these kind of uncoupled simulations mechanics does not have any effect on metallurgy or temperature: stress induced phase transformation and heat due to mechanical work are neglected. This is one popular simplified approach and gives good results in similar welding cases as the current one, e.g. Wu et al. (2008)

Because of restricted computational resources a 2D-model was used. 2D-model does not take into account the heat transfer in the longitudinal direction of the weld: calculated temperatures are not accurate. However 2D-calculations are fine-tuned on the basis of the experimental temperature measurements, which will partly compensate this error.

Weld penetration and temperatures were iteratively adjusted on the basis of measurements, previous knowledge and in some cases penetrations calculated by means of Flow-3D (surface welds W2 and W4). The agreement of the simulated penetrations with experimental ones was satisfactory. The heat source was a simple Goldak's source and more complicated source should be used in order to get better agreement on the shape and size of the penetration. The agreement of the calculated temperatures with measurements was satisfactory with a maximum error of peak temperature of about 16%. Agreement of the $t_{8/5}$ times calculated with Sysweld and analytical equations were also satisfactory. However, because no experimental measurements of cooling rates in the welds were available no final conclusions of the true accuracy can be made.

Only one CCT curve was used to describe the different weld areas and the base metal. This was because of the lack of data in Sysweld material database. Using only one CCT is however popular simplified approach and may not lead to remarkable errors. However, because there were no experimental information of metallurgical phases, no final conclusions can be made.

The mechanical behaviour cannot be accurately simulated by means of 2D-model:

- The run-on and run-off tabs (start and end plates) of the current case cannot be modelled,
- The restraint in butt weld that originates from the deposited weld before and after the 2D-calcutation plane is not taken properly into account: this can be estimated by using artificial boundary conditions (fixing more nodes in order to restrict the nearly free movement of the plate halves when the weld is at high temperatures),
- The mechanical behaviour cannot be accurately simulated by means of 2D-model because microstructural behaviour is really a 3D-phenomenon

The comparison of the calculated longitudinal stresses to experimental ones shows that the agreement is satisfactory. However, it shall be kept in mind that standard gives wide tolerable composition range for the steel and this range affects the yield strength spread of the individual phases, as reported by Heinze et al. (2012). Additionally, it should be noticed that the experiments include an uncertainty because of the approximate nature of the measurement methods. Furthermore, only one cut was measured (50 mm form the end of the plate).

In the end of the study some 3D-simulations with the same input parameters as in 2D were made (no fine-tuning of the input-parameters on the basis of measurements were done). These preliminary simulations did not lead to remarkable change on deformations and stresses.

6.6 Conclusions

Temperatures and weld penetration can be iteratively adjusted based on previous knowledge and in some cases also utilizing CFD (Flow-3D). In the current case the agreement of calculated temperatures with experimental and analytical results was satisfactory. Also the agreement of calculated and experimental weld penetrations was satisfactory.

Calculated residual stresses gave satisfactory agreement with experiments, but because of the simplifications made in the 2D-calculations they should be considered as approximate values. The calculated bending direction of the plate did not agree with the experiments. However the measured displacements were relative small and small variations of process and material parameters may have a big effect on the result. More experimental data is needed to evaluate the reasons, e.g. measured metallurgical phases of the welds. Results of phases, deformations and stresses should be validated by means of more accurate 3D-simulations with calibrated input parameters.

6.7 References

Hansen, J. L. 2003-. Numerical modelling of welding induced residual stresses, Ph.D. Thesis, Department of Manufacturing Engineering and Management, Technical University of Denmark, 2003.

Heinze, C., Schwenk, C., Rethmeier, M. 2012. Numerical calculation of residual stress development of multi-pass gas metal arc welding under high restraint conditions, Materials and Design, Vol 35 (2012), pp. 201–209.

Virkkunen, Iikka. 2016. Contour measurement report: three welded joints, Aalto University, School of Engineering, Revision 2, 2016-12-19, Otaniemi, Espoo, Finland.

Wu, T. , Coret, M., Combescure, A. 2008. Numerical simulation of welding induced damage and residual stress of martensitic steel 15-5PH, International Journal of Solids and Structures, Vol 45, Issues 18–19, September 2008, pp. 4973-4989.

7. Summary and conclusions

The scientific and the technical goals for the project were set as:

- To develop weld simulation skills, collect source data, validate the simulation procedure and demonstrate the simulation of chosen industrial structures and details
- To develop modelling and simulation techniques for optimisation of weld geometrical and metallurgical quality according to the practical industrial demands
- To develop modelling and simulation techniques of welding procedure and solidification process

The key project action to reach the above goals was co-operation with the top Korean technical university, the Korea Advanced Institute of Science and Technology KAIST, realised by inviting professor Suck-Joo Na of KAIST, Division of Mechanical Engineering, for a visiting professorship of three years to VTT. Professor Na is one of the leading scientists in the field of process simulation of arc and laser beam welding, most notably of laser hybrid welding.

According to the original goals of the project, the simulation work was heavily concentrated on CFD based simulations for GMAW and FSW, in order to adopt both the simulation approach and the tools for work at VTT. Furthermore, FE based simulation was conducted for evaluation of GMAW butt weld deformations and residual stresses. It should be noted that the KAIST customisation for Flow-3D was used as such for the reference case simulations. More detailed simulation information can be found in the appropriate simulation case descriptions, as well as in the project scientific publication in the attachments.

Numerical and analytical methods can be used for optimization of welding process parameters. The aim of the studies in this project was to evaluate the possibilities to use numerical methods for welding process optimization. The simulations were carried out by the FEM based Sysweld program. Material data was defined on the basis of Sysweld material database that includes some of the most common materials. The thermo-mechanical simulations were carried out as uncoupled: thermal simulation is followed by mechanical one with no backward coupling. Finite element analyses (FEA) were carried out for double side butt-welded GMAW experiments simulated using Sysweld solver. The problem was described by means of a 2D-model and two-dimensional generalized plane strain elements were used. Heat input was described by Goldak's Double ellipsoidal heat source.

Stainless steel weld simulation

The conclusions from the simulation results and corresponding experimental validation tests of the stainless steel and their characterization can be summarised as follows:

- Experimental results of full penetration hybrid welding show the bead shape for two configurations, MAG leading and trailing, is quite different. The same cases are simulated in order to study the mixing behaviour and flow characteristics.
- In laser-MAG hybrid welding the laser is dominant in defining flow pattern. Two recirculating flows are found, one on top surface and another on root surface. The molten pool is longer in bottom surface as compared to top surface, this is also a characteristic of full penetration laser welding.
- The filler wire used in MAG contains an additional amount of Cr to compensate for the Cr loss during high temperature processing. It was found that MAG leading configuration is showing more concentration of Cr in upper half of bead while in MAG trailing comparatively uniform mixing is observed.

- Tungsten particles were introduced in simulation to study the flow behaviour, which reveals that in MAG leading configuration, once the particles reach the bottom recirculation they are unable to return back to the upper one. In MAG trailing configuration the particles introduced in upper part were able to reach the bottom recirculation and then return towards the upper recirculation; this phenomenon helps in mixing of Cr in MAG trailing configuration.

Copper FSW simulation

The simulation of FSW process was a difficult topic due to high strain rates and high temperature viscoplastic flow with frictional and plastic heat generation involved. In this project, CFD approach was used, for it has the advantage of being able to naturally handle the high strain rates present in FSW. Generally, there were several challenges present in CFD simulation.

- Firstly, accurate simulations also require accurate models for flow stress/viscosity of the base material. However, experimental data for stress/strain relation under high temperature, high strain rate conditions is not abundant, and the flow stress is usually only a function of temperature and strain rate because dynamic effects and strain state are ignored.

- Secondly, modelling of friction and frictional/plastic heating is challenging because no universal consensus exists on the importance of frictional vs. plastic heating. Therefore, calibration of the models would be required since the models are not fully predictive.

- Thirdly, modelling of complex tool shapes is challenging. Cylindrically symmetric tools are easy to model but real tools usually have threads, flutes and other small details that require a very fine mesh to be resolved. On the other hand, simulation of a non-axisymmetric rotating tool is complicated: transient simulation with sliding mesh is computationally expensive, therefore simplifications, such as Multiple Reference Frame (MRF) approach were needed.

The aim of the project was to test methods presented in literature and estimate their feasibility for copper FSW by implementing in OpenFOAM, which is a free, open source code. This means it is easily extendable and modifiable and the full source code is available, ie. there is no ”black box” between customization and results

The simulation framework implemented in OpenFOAM platform was tested. Qualitatively reasonable results were obtained considering the simplifications used. However, the results are quite sensitive to modelling assumptions. In order to progress further with the CFD simulation of the FSW process, comprehensive experimental validation would be needed ideally starting with simple tool shapes and progressing towards more realistic and detailed tools.

Mild steel arc welding simulation

The Technip SAW fillet weld company case was simulated at KAIST and the work concentrated on the double-sided fillet weld. It can be concluded from these initial simulations that full penetration may be possible because the thickness of the vertical plate is only 14 mm, and the welding was performed from both sides of the joint using high welding current.

Based on the MAG weld simulation case results, it can be generally concluded that the Flow 3D simulation with the KAIST customisation tend to typically overestimate the HAZ width as compared to validation in the reference case. Furthermore, the penetration in the air gap is typically overestimated, too, although variation in penetration, ie. the location of the studied cross section, also plays a role.

The plate width has no marked effect on simulated final fusion zone or HAZ geometry, but it does have an effect on temperature distribution during welding. As could be expected, the wire feed rate, ie. heat input, has a crucial effect on penetration. However, excessive sagging at the

root occurring in some simulation cases is unrealistic, but higher heat inputs would in reality lead into burn through.

The thermal efficiency effect is logical: increasing the *k* value smoothens the root penetration, i.e. removes the occasional defects. In practise, the thermal efficiency can be affected eg. the choice of shielding gas, and particularly the CO_2 content. The torch angle has marginal effect on penetration or HAZ width.

Simulation results for FE deformation analysis source data

One of the key goals of the project was to utilise the Flow 3D CFD simulation results as a key data for consequent FE analyses to be further used for the definition of the deformation and residual stress evolution during the weld cooling after solidification. For this purpose, the data transfer from Flow 3D to Sysweld FE software was demonstrated. Flow 3D allows the examination of eg. the temperature distribution in 1D (point), 2D (cross section) or 3D views as a function of time. All this data can also be exported in numerical ASCII form that can be read into a FEA package relatively easily.

Temperatures and weld penetration can be iteratively adjusted based on previous knowledge and also utilizing CFD, in this case Flow3D. In the case of a MAG weld in an X groove in 15 mm S355 steel, the agreement of calculated temperatures with experimental and analytical results was satisfactory. Also the agreement of calculated and experimental weld penetrations was satisfactory.

Calculated residual stresses gave satisfactory agreement with experiments, but because of the simplifications made in the 2D-calculations they should be considered as approximate values. The calculated bending direction of the plate did not agree with the experiments. However, the measured displacements were relative small and small variations of process and material parameters may have a big effect on the result. More experimental data is needed to evaluate the reasons, e.g. measured metallurgical phases of the welds. Results of phases, deformations and stresses should be validated by means of more accurate 3D simulations with calibrated input parameters.

Project publications

1. Sohail, Muhammad; Na, Suck-Joo; Han, Sang-Woo; Karhu, Miikka; Kujanpää, Veli. 2017. Effect of leading and trailing torch configuration on mixing and fluid behavior of laser-GMA hybrid welding. Accepted for publication in Journal of Laser Applications.

2. Na, Suck Joo. 2016. Thermal, Metallurgical and Mechanical Behavior of Welded Structures based on CFD Process Simulations. Final seminar of Fidipro Na project, 9th annual seminar, DIMECC, 14 November 2016, Helsinki, Finland, DIMECC Oy. 72 p.

3. Kujanpää, Veli; Na, Suck Joo. 2016. Simulation of laser-arc hybrid welding of stainless steel. Structures for extreme - Cutting edge in welding simulation. Final seminar of Fidipro Na project, 9th annual seminar, DIMECC, 14 November 2016, Helsinki, Finland, DIMECC Oy. 29 p.

4. Niemi, Timo. 2016. Simulation of Friction Stir Welding of Copper. Final seminar of Fidipro Na project, DIMECC 9th Annual Seminar, 14 - 15 November 2016, Helsinki, Finland, DIMECC Oy. 19 p.

5. Sirén, Mika; Martikainen, Hannu. 2016. CFD simulation of MAG welded mid steel joints for FEM deformation analysis. Final seminar of Fidipro Na project, DIMECC 9th Annual Seminar, 14 - 15 November 2016, Helsinki, Finland, DIMECC Oy. 18 p.

6. Kujanpää, Veli. 2016. Introduction to Finnish laser processing activity (invited paper). 9th International Conference on Photonic Technologies LANE2016, 19 - 22 September 2016, Furth, Germany. Proceedings. Bayerisches Laserzentrum GmbH (2016), 4 p. http://lane-conference.org/downloads/IndustrialContributions/LANE2016_1289_Kujanpaeae_IC_endformat.pdf

7. Karhu, Miikka; Kujanpää, Veli; Romu, Jyrki; Sarikka, Teemu. 2016. Metallurgical response of weld metal to different filler metal and joint design combinations of laser-arc hybrid welded lean duplex and novel ferritic stainless steels. Journal of Laser Applications . American Institute of Physics; Laser Institute of America. Vol. 26 (2016) No: 2, 022422, 9 p. doi: 10.2351/1.4944094

8. Karhu, Miikka; Kujanpää, Veli; Romu, Jyrki; Sarikka, Teemu. 2015. Metallurgical response of weld metal to different filler metal and joint design combinations of laser-arc hybrid welded lean duplex and novel ferritic stainless steels. 34th International Congress on Applications of Lasers and Electro-Optics, ICALEO 2015, 18 - 22 October 2015, Atlanta, GA, USA. Proceedings. Laser Institute of America (2015), 465-474

9. Kujanpää, Veli. 2015. FIDIPRO-NA project in CFD modelling for optimisation of welding. FIMECC BSA+HYBRIDS Annual Forum 2015, 8.10.2015 , Helsinki. FIMECC (2015)

10. Karhu, Miikka; Kujanpää, Veli. 2015. Defocusing techniques for multi-pass laser welding of austenitic stainless steel. 15th Nordic Laser Materials Processing Conference, NOLAMP 2015, 25 - 27 August 2015, Lappeenranta, Finland. Physics Procedia. Elsevier. Vol. 78 (2015), 53-64. doi: 10.1016/j.phpro.2015.11.017

11. Na, Suck-Joo; Muhammad, Sohail; Han Sangwoo; Karhu, Miikka and Kujanpää, Veli. 2015. Flow and element mixing characteristics in laser GMA hybrid welding. 15th Nordic Laser Materials Processing Conference, NOLAMP 2015, 25 - 27 August 2015, Lappeenranta, Finland.

12. Sohail, Mohammed; Na, Suck-Joo; Karhu, Miikka; Kujanpää, Veli. 2015. Numerical study on effect of laser position and joint gap on full penetration Laser-GMAW-P hybrid welding. 7th International Congress on Laser Advanced Materials Processing, LAMP 2015, 26 - 29 May 2015, Fukuoka, Japan. Proceedings. Japan Laser Processing Society JLPS (2015), 1-5

13. Sirén, Mika. 2015. Finnish welding R&D projects supported by public funds. Welding Technology Exchange Event between Finland and Japan (in connection to 68th IIW Annual Assembly and Conference, Helsinki). Espoo 26 June, 2015. Welding Society of Finland (2015)

14. Sirén, Mika. 2015. Finnish welding R&D projects supported by public funds. VTT-Korea mini symposium on welding research collaboration (in connection to 68th IIW Annual Assembly and Conference, Helsinki). Helsinki 2 July, 2015. VTT (2015)

15. Kujanpää, Veli. 2015. Laser and hybrid laser welding of thick stainless steels. VTT-Korea Symposium, 2.7.2015, Helsinki, Finland. VTT (2015). http://www.vtt.fi/inf/julkaisut/muut/2015/OA-Laser-and -hybrid-laser-welding.pdf

16. Kujanpää, Veli. 2015. Laser and hybrid laser welding of thick stainless steels. Technological Exchange Event between Finland and Japan, 26.6.2015, Espoo, Finland. Welding Society of Finland (2015). http://www.vtt.fi/inf/julkaisut/muut/2015/OA-Laser-and-hybrid-laser.pdf

17. Na, Suck-Joo; Han, Sang-Woo; Muhammad, Sohail; Zhang, Linjie; Gumenyuk, Andrey; Rethmeier Michael; Karhu, Miikka and Kujanpää, Veli. 2015. Flow and Bead Formation

Characteristics in High Power Laser Welding at Different Positions (Invited). Lasers in Manufacturing LiM 2015, 22 - 25.6.2015, München, Germany. Wissenschaftliche Gesellschaft Lasertechnik e.V. http://www.wlt.de/lim/Proceedings/Stick/1.html

18. Karhu, Miikka; Kujanpää, Veli. 2014. Thick-section laser multi pass welding of austenitic stainless steel joints using defocusing technique. 33rd International Congress on Applications of Lasers & Electro-Optics (ICALEO 2014), Oct. 19-23, 2014, San Diego, CA, U.S.A., Paper#609. Laser Institute of America, ss. 472-481

19. Kujanpää, Veli. 2014. Thick section laser and hybrid laser welding of austenitic stainless steels. Physics Procedia. Vol. 56 (2014), 630 - 636. doi: 10.1016/j.phpro.2014.08.056

Appendices

1. A summary of Mr Ligang Wu´s MSc. thesis work

2. Virkkunen, I. 2016. Contour measurement report: three welded joints. Aalto University, School of Engineering. Rev. 2, 19.12.2016. 9 p.

Appendix 1. A summary of Mr Ligang Wu´s MSc. thesis work

Details of SAW welding simulation

1. The value of each parameter was taken as the average of the maximum and the minimum in the WPS;

Hitsausprosessi Welding process		1) SAW TWIN	2)		3)		4)			
Palko no. Pass no.	Hitsaus asento/ suunta Welding pos./ dir	Lisäainetyyppi Wire/rod type	Halkaisija Dia mm	Jayhe Flux	AC DC- DC+	Virta Current A	Jännite Voltage V	Hitsausnopues Welding speed mm/min	Lämmöntuonti Heat input KJ/mm	Vapaalanka Stick-out mm
1 - n	2F	OK AUTROD 13.27	2 x 2.0	OK 10.71	DC+	600 - 750	26 - 32	700 - 850	1.1 - 1.7	25 - 30

675A 29V 1.3cm/s

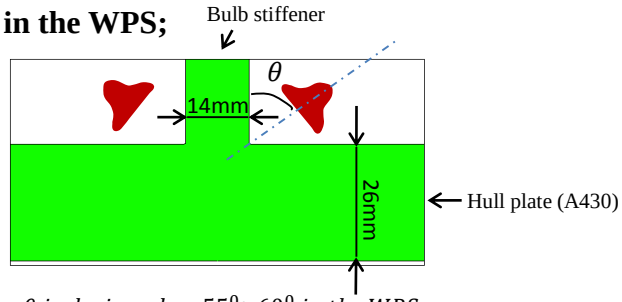

θ *is designed as* 55^0~ 60^0 *in the WPS,*
In simulation, θ= 60^0 was used.

2. The wire feeding rate was approximated by fitting Chandel's data

Table 1
Welding parameters and features

No.	Polarity	Current (A)	Electrode diameter (mm)	Electrode extension (mm)	Melting rate (kg h^{-1})	Bead height (mm)	Bead width (mm)	Penetration (mm)
1	DCEP	400	3.2	25.4	4.58	3.54	16.95	5.52
2	DCEP	500	3.2	25.4	6.11	4.15	16.11	7.54
3	DCEP	600	3.2	25.4	7.76	4.75	15.26	9.73
4	DCEP	700	3.2	25.4	9.52	5.36	14.41	12.08
5	DCEN	400	3.2	25.4	6.66	4.58	15.45	3.31
6	DCEN	500	3.2	25.4	8.74	5.29	14.50	5.47
7	DCEN	600	3.2	25.4	10.93	6.01	13.56	8.23
8	DCEN	700	3.2	25.4	13.22	6.73	12.62	11.63
9	DCEP	300	2.4	25.4	3.54	3.48	17.54	4.70
10	DCEP	400	2.4	25.4	5.27	4.09	16.69	7.04
11	DCEP	500	2.4	25.4	7.20	4.70	15.85	9.61
12	DCEP	600	2.4	25.4	9.32	5.31	15.00	12.41
13	DCEP	400	3.2	50	5.44	4.37	16.29	5.90
14	DCEP	500	3.2	50	7.46	4.98	15.44	8.06
15	DCEP	600	3.2	50	9.70	5.59	14.60	10.41
16	DCEP	700	3.2	50	12.16	6.20	13.75	12.91

***Reference: R.S. Chandel et al. : Journal of Materials Processing Technology* 72 (1997) 124–128**

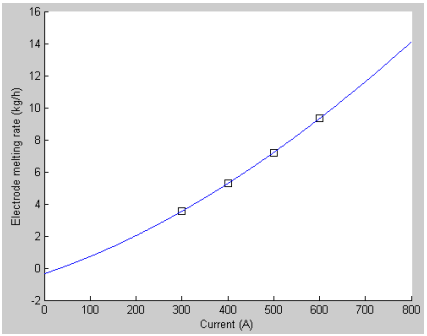

Melting rate was fitted as a function of current:

$$MR = -1.667 * 10^{-9} * I^3 + 1.25 * 10^{-5} * I^2 + 0.009517 * I - 0.35 \ \text{(kg/h)}$$

$$\pi r^2 * \text{WFR} * \rho = MR$$

$$WFR = \frac{MR}{\pi r^2 \rho} = \textbf{1.88m/min}$$

*the density of the wire is approximated as the density of steel (7.8g/cms)

3. The effective radius was calculated by the equations available in Dr.Cho's paper;

The following equation was for AC:

$$I(t) = \begin{cases} |1270\sin(2\pi ft)| + 1.3\,\text{A}, & \text{if } \sin(2\pi ft) > 0 \\ |1274\sin(2\pi ft)| + 1.3\,\text{A}, & \text{if } \sin(2\pi ft) < 0 \end{cases}$$

$$\sigma_{qL}(t) = \begin{cases} |0.94\sin(2\pi ft)| + 1.2\,\text{mm}, & \text{if } \sin(2\pi ft) > 0 \\ |1.45\sin(2\pi ft)| + 1.2\,\text{mm}, & \text{if } \sin(2\pi ft) < 0 \end{cases}$$

$$\sigma_{qR}(t) = \begin{cases} |1.25\sin(2\pi ft)| + 1.2\,\text{mm}, & \text{if } \sin(2\pi ft) > 0 \\ |1.60\sin(2\pi ft)| + 1.2\,\text{mm}, & \text{if } \sin(2\pi ft) < 0 \end{cases}$$

With the welding current being I=675A, the following effective radii can be calculated:

$$\begin{cases} |\sin(2\pi ft)| = 0.5305, if\ \sin(2\pi ft) > 0 \\ |\sin(2\pi ft)| = 0.5288, if\ \sin(2\pi ft) < 0 \end{cases}$$

$$\begin{cases} \sigma_{ql}(t) = 1.6986mm, if\ \sin(2\pi ft) > 0 \\ \sigma_{ql}(t) = 1.966, mm\ if\ \sin(2\pi ft) < 0 \end{cases}$$

average value

$$\begin{cases} \sigma_{qr}(t) = 1.8631mm, if\ \sin(2\pi ft) > 0 \\ \sigma_{qr}(t) = 2.0461mm, if\ \sin(2\pi ft) < 0 \end{cases}$$

Axisymmetric shape:

σ_r=1.8936mm

(The surface heat flux model, arc pressure model , and EMF model were assumed to be axisymmetric)

4. The flux consumption rate for the slag heat flux model was fitted with the data available from ESAB Solid wire brochure;

Flux type: OK flux 10.71

Flux consumption, kg flux/kg wire

Voltage	DC+	AC
26	0.6	0.5
30	0.85	0.7
34	1.15	0.95
38	1.35	1.15

Reference. ESAB solid wire brochure

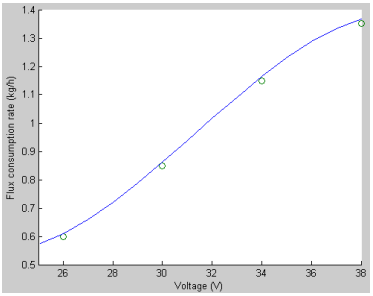

Flux consumption rate was fitted as a function of voltage:

$$FC = -0.0003906 * V^3 + * 0.03672 * V^2 \text{ -1.073} * V - 10.55 \text{ (kg/h)}$$

V= 29*v* ⇒ *FC* =0.7882 kg flux/ kg wire
= 2.41g/s

Slag heat flux model:

Slag efficiency: $\eta_s = \dfrac{\dot{m}_f C_{pf}(T_{m.flux} - T_0)}{VI}$

where: $\dot{m}_f$: flux consumption rate
C_{pf} :Specific heat of flux
$T_{m.flux}$:melting temperature of flux

If $R_a < r_e < R_b$ then

$q_s = \dfrac{\eta_s VI}{\pi(R_b^2 - R_a^2)}$, where $Ra = 3\sigma_r$, $R_b = R_a + 0.3cm$

Assumed to be same with the slag thickness in Dr. Cho's paper

5. The following parameters were assumed:

1) Total arc efficiency was assumed to be 0.95;
2) The droplet radius was assumed to be same with the welding wire radius (0.2cm);
3) The droplet speed was assumed to be 100cm/s;
4) The slag thickness for modeling the slag heat flux was assumed to be 0.3cm (same with Dr. Cho's case);

6. Due to the difficulty to find the material properties of A430 (this material is rarely used for welding simulation research), the simulation is currently using the material properties of AH36;

7. Since the flux (OK Flux 10.71) indicated in WPS belongs to the same classification (AWS A5.17) as the flux used in Dr. Cho's paper, so that same material properties of the flux were used;

8. Drag force is a shear stress induced by the shielding gas, but flux is used instead of shielding gas in submerged arc welding, therefore, the drag force model is not used in the current simulation.

SAW welding simulation result

Click to watch video

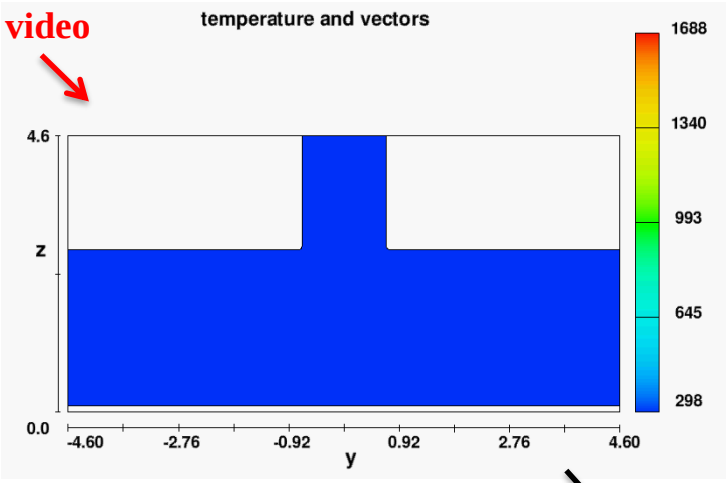

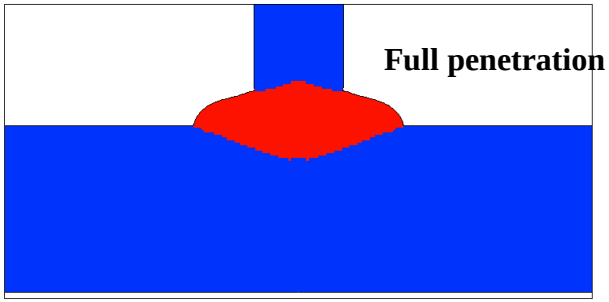

Full penetration was achieved in the double sided T-butt welding

Comments:

1. **Full penetration may be possible because the thickness of the vertical plate is only 14mm, and the welding was performed from both sides of the joint with high welding current.**

2. **Full penetration welding from both sides of T-butt joint is an economical way used to improve the joint strength (See the two references in Slide 4).**

Reference 1: http://www.twi-global.com/technical-knowledge/job-knowledge/design-part-3-092/

As mentioned in Job knowledge 91, the fillet weld requires no weld preparation, is easy to deposit and is often regarded as the cheapest weld of all to make. However cross sectional area, and therefore cost, increases as a function of the square of the leg length. Assuming the same strength requirements from the fillet welds as for the T-butt welds it becomes more economical to use a double sided full penetration T-butt joint at a plate thickness of around 30mm. The accuracy of this figure should be treated with caution as it is dependent on many factors such as the weld preparation costs and included angle.

Welding position is an additional factor. It may be more economical to deposit a butt weld in the flat position, where large diameter electrodes and high welding currents can be used, rather than a double sided fillet weld where one weld must be made in the overhead position (*Fig.1*).

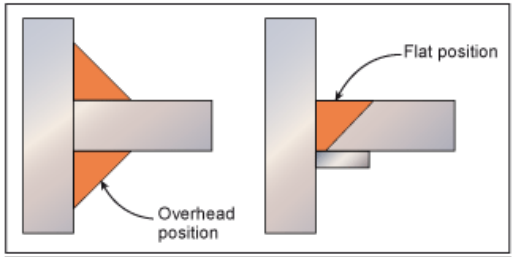

Fig.1. Flat position T-butt weld vs overhead fillet weld

Reference 2: http://www.lincolnelectric.com/en-us/support/process-and-theory/Pages/weld-fusion-weld-penetration.aspx

As an example, refer to the T joint and fillet weld in **Figure 3**. The required weld strength is achieved by having complete fusion and by producing the proper fillet weld size (measured by either the leg length or theoretical throat length) for a given weldment. The appropriate weld size needed to achieve adequate weld strength is determined by the design engineer during the design stage. How this is determined is beyond the scope of this article. However, as the fabricator, as long as you make the proper sized weld per the design specification and achieve complete fusion between the filler metal and base plates, including the root, you have produced a weld of sufficient strength. Weld strength is not determined by the level of penetration into the base plates.

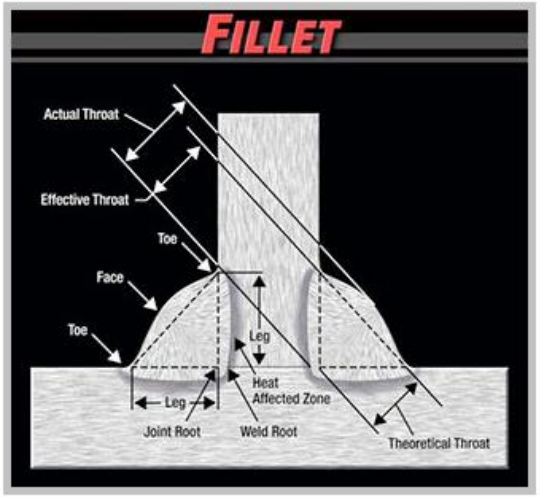

Figure 3: Parts of a Fillet Weld

Appendix 2. Virkkunen, I. 2016. Contour measurement report: three welded joints. Aalto University, School of Engineering. Rev. 2

Aalto University
School of Engineering

Contour measurement report: three welded joints

Iikka Virkkunen, Professor (adjunct), Dr. Sc. (Tech.)

2016-12-19
Revision 2
Otaniemi, Espoo, Finland

Executive summary

Contour measurement was performed to three welded joints provided by VTT. The samples were carbon steel welds; two butt-welds (25 mm (sample 1) and 15 mm (sample 2) plate) and one T-section weld (15 to 25 mm plate (sample 3)).

For the contour measurement, the samples were cut with electric discharge machining (EDM) at Aalto university. The cut surfaces were measured by 3D -measuremen system by VTT and white light interferometry by Aalto university. The resulting measurement data were analyzed by Aalto in-house developed code and, finally, residual stresses solved by open-source Elmer finite element code.

All the measured welds show high residual stresses due to weld process, as expected. The residual stresses are highest in the 25 mm butt-weld sample. The location of the highest tensile stress is well within the weld. Sample 2 showed lower stresses and also displayed two separate stress concentrations one below the top bead of the weld and another below the bottom bead of the weld. The T-junction showed asymmetric residual stress distribution with highest stresses located near the other weld (presumably the one welded last).

Table of Contents

1. Introduction

Residual stress measurement of three weld samples by contour method was commissioned from Aalto university by VTT.

Contour method is relatively new method for measuring two-dimensional residual stress contours destructively. The method is based on measuring displacement caused by relaxation of residual stresses on a cut surface. For the measurement, the sample to be studied is cut in two pieces. If the studied sample was free from residual stresses, the cut surfaces will retain their planeness. However, if residual stresses existed in the cut surface, those stresses are now relaxed by the cutting process and cause deviations from planeness on the cut surface. These deviations resulting from relaxation of residual stresses can be measured, e.g., by coordinate measurement machine and analyzed to reveal the residual stress contours. The main advantages of this method are the attainable 2-dimensional stress contour and the robustness of solving residual stresses from the measured surface displacements.

The method assumes, as with all relaxation techniques for residual stress measurement, that the relaxation of residual stresses occurs elastically and that the cutting does not induce stresses. In addition, because the displacements are measured directly from the cut surface, it is assumed, that the cut occurs along a plane that was flat when the cutting started. This assumption requires, that the sample is constrained from both sides, when the cut is made. The main error sources for this method are inadequate constraint during cutting and possible stresses caused by the cutting.

A more detailed description of the contour method can be found online from (http://www.lanl.gov/contour/).

2. Materials and methods

For the contour measurement, the samples were cut with electric discharge machining (EDM) at Aalto university. The cut surfaces were measured by 3D -measurement system by VTT and white light interferometry by Aalto university. The resulting measurement data were analyzed by Aalto in-house developed code and, finally, residual stresses solved by open-source Elmer finite element code.

The measurement cut was performed perpendicular to the weld direction and thus the measured stresses are axial stresses (stresses in the welding direction). The cut was made ≈ 50 mm from the weld end.

The 3D-measurement represents a more traditional application of the contour method with limited spatial resolution due to the limitations of the used measurement system. The data files were obtained with 0.5 x 0.5 mm measurement grid on the interesting area and 1.0 x 1.0 mm grid in

areas away from the most interesting locations. Altogether, some 23 thousand points were included in typical measurement file. For the white light interferometry, the spatial resolution is much better with effective measurement grid of 0.014 x 0.014 mm and measurement files containing some 9 million measurement points. The white light measurement was limited to the interesting area around the weld.

Three samples were provided for measurement, as designated in Table 1.

Table 1. Samples for residual stress measurement.

#	Designation	Description
1	Sample 1	25 mm butt weld sample
2	Sample 2	15 mm butt weld sample
3	Sample 3	15 to 25 mm T-joint

3. Results

For each sample, two analyses were completed: one with the 3D-measurement data and one with the white light interferometer data. Both analyses are based on the same cut surface and the only difference is in the method used to measure displacements on the cut surface.

Figures 1 – 6 show the resolved residual stress contours for each of the performed measurements.

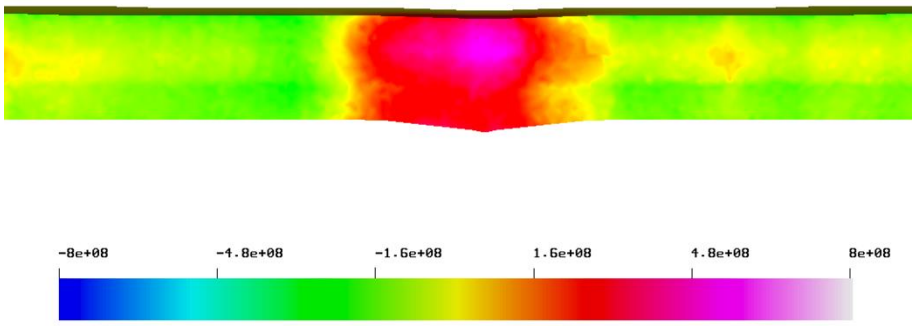

Figure 1. Residual stress contour of sample 1, resolved from 3D-measurement data. The results are shown in Pa (color scale from -800 MPa to 800 MPa)

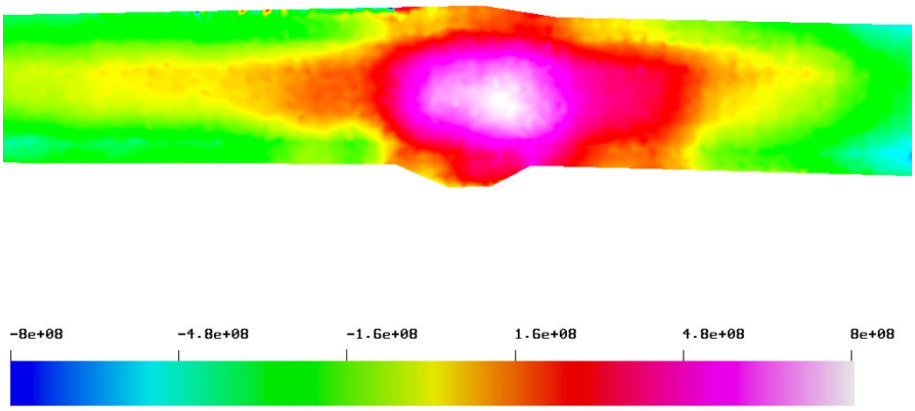

Figure 2. Residual stress contour of sample 1, resolved from white light - measurement data. The results are shown in Pa (color scale from -800 MPa to 800 MPa)

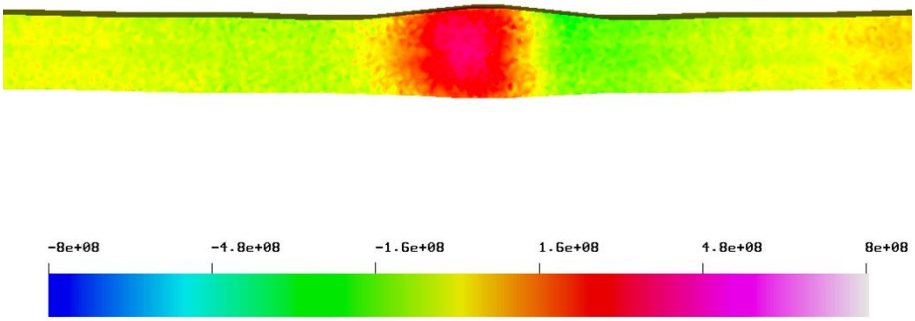

Figure 3. Residual stress contour of sample 2, resolved from 3D-measurement data. The results are shown in Pa (color scale from -800 MPa to 800 MPa)

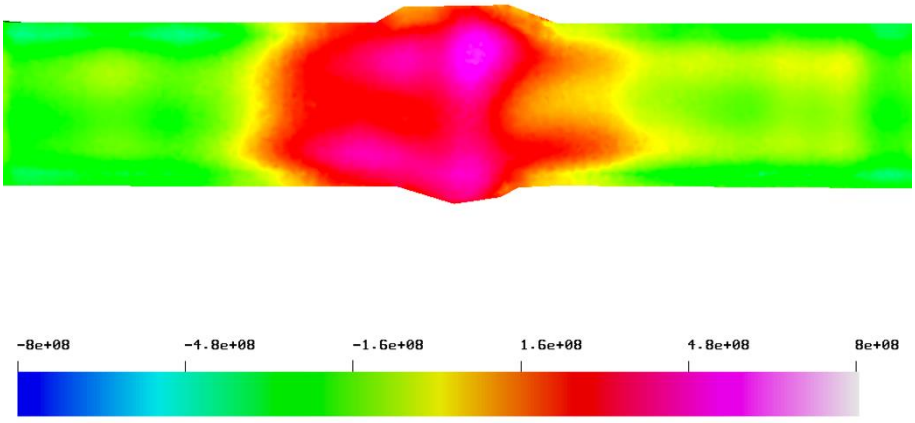

Figure 4. Residual stress contour of sample 2, resolved from white light - measurement. The results are shown in Pa (color scale from -800 MPa to 800 MPa) data.

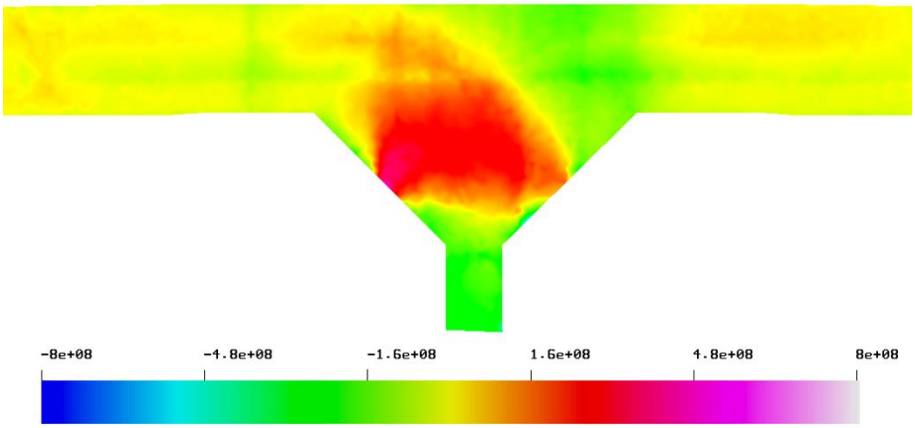

Figure 5. Residual stress contour of sample 3, resolved from 3D-measurement data. The results are shown in Pa (color scale from -800 MPa to 800 MPa)

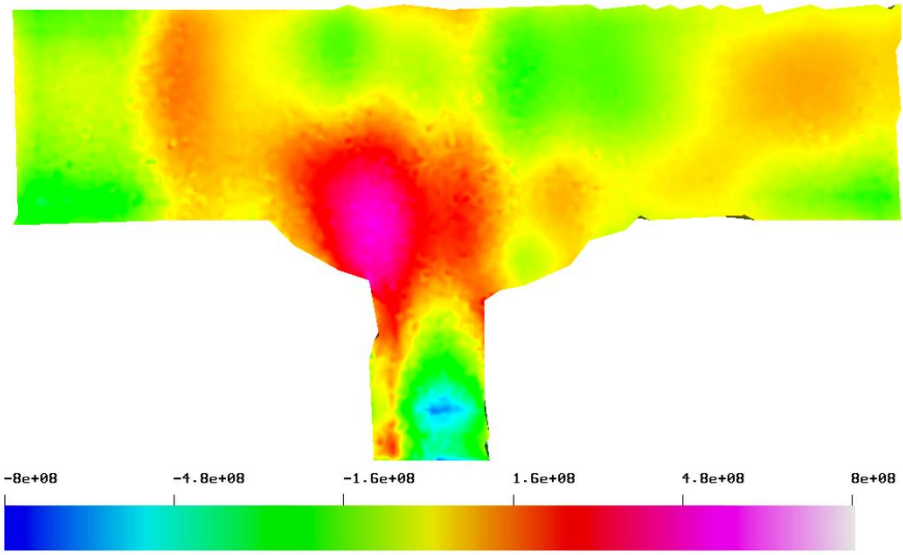

Figure 6. Residual stress contour of sample 3, resolved from white light - measurement data. The results are shown in Pa (color scale from -800 MPa to 800 MPa)

4. Discussion

All the measured welds show high residual stresses due to weld process, as expected. The residual stresses are highest in the 25 mm butt-weld sample. The white light interferometry show higher spatial resolution than the more traditional measurements. In particular, for sample 1 (figure 1, 2) the high but local residual stress peak inside the weld is missed by the 3D-measurement, but shown clearly by the white light interferometer measurements. Likewise, the two-hot-spot structure of sample 2 (figure 5) is shown with better precision. For the sample 3 (figure 6), the measurements clearly show asymmetric residual stress hot-spot on the left weld. Presumably this is the weld made last and it has relieved stresses of the previously made weld quite significantly.

Iikka Virkkunen, Professor (adjunct), Dr. Sc. (Tech.)